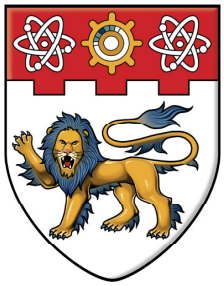

NANYANG TECHNOLOGICAL UNIVERSITY

Solution structure of the stalk subunits E and G of the vacuolar ATPase from yeast and interaction studies of subunits E and G with the neighboring subunits

SANKARANARAYANAN RISHIKESAN

SCHOOL OF BIOLOGICAL SCIENCE

2011

Solution structure of the stalk subunits E and G of the vacuolar ATPase from yeast and interaction studies of subunits E and G with the neighbouring subunits

Sankaranarayanan Rishikesan

SCHOOL OF BIOLOGICAL SCIENCES

A thesis submitted to the Nanyang Technological University
in fulfillment of the requirement for the degree of
Doctor of Philosophy

2011

Acknowledgements

Life would not start without the blessings of the parents and my life in this world has also been the same. The blessings of my mother and father have always driven the wind of success towards me. Today this is the moment of truth that I can makes me parents to be proud of me. My hearty thanks to you, “Mom and Dad”.

Guru is on par to parents and on this context I am so thankful to my PhD father, Prof. Gerhard, Grüber. He has trusted on me to succeed in the path of this study. His belief, knowledge, guidance, suggestions, advice and many more has groomed me throughout the course of my study. It is beyond an immense pleasure to stand at this juncture where I ve created a good piece of research on the V_1V_O ATPase. His hard efforts to buy research grants from various research organizations, out of sleepless nights, have fulfilled all the dreams that we had on this journey. I am so so thankful to you “Boss”.

Ardina Grüber has been a good colleague, friend, advisor and many more. The balance between work and life has been enlightened to me through her day to day life. The couple, Mrs. and Mr. Grüber was so near to my parents, that the official days were so homely filled with love and affection. I am so proud to say that I have been educated by this family.

Every success needs a beginning and so my research was kick-started by Dr. Youg Raj Thaker. The amount of time and knowledge he has shared with me has been the climbing steps on my research. Few words of thanks are less worthy for his efforts on me. My delightful thanks to you Raj.

Steps ahead in my research were enriched by few fellow mates. Dr. Goran Biuković, who has helpd me in numerous occasions during the lab work. Dr. Vivekanandan, an approachable soul for anything. The knowledge that he showered to me on protein NMR has made me to work comfortably on this field. Dr. Shovanlal Gayen, a soft character with hard entrance. But nevertheless, he has walked with me in the streets of NMR on numerous occasions. Dr. Cornelia Hunke, a person who can be approached at any point of time for anything. Dr. Asha Balakrishnan, a helpful friend many a times. Dr. Malathy Sony has taken a bit from all the chapters on my research. The more she came in to my pictures, the beauty the subject appeared. Dr. Neelakandan, “my very good friend”. If I can sit on a table and cheers a glass, then he is it. “He is my fourth friend”. Dr. Yew kwang has appeared to me as a nice chap from Singapore. I extend my gratitude to all of them with whole heart.

My days in the laboratory have been so lively with a good pool of friends with whom I ve shared a nice bit of social life. And in context, I would like to express my thanks to Dr. Anil kumar, Mr. Vikeramjeet Tadwal, Mrs. Jubi Kurup, Mrs Hema Priya, Mr. Phat Vinh Dip, Mr. Basak Sandip, and Ms. Lavanya. Thanks would not end without placing my fellow friends and other colleagues from SBS and NTU into it. I extend the same gratitude to all my known and unknown friends who have been with me during this study.

At last this piece of work is dedicated to my hearty wife and my lovely son who are the two people, to whom I owe tonnes and tonnes of love. It can just be better said that without whom, I stand nowhere in these four years.

To my beloved wife and son

Table of contents

Acknowledgements *v*

Table of contents *ix*

List of figures *xiii*

List of tables *xvi*

Abbrevations *xvii*

Abstract *xix*

1. Introduction 1

1.1 Eukaryotic V-ATPases 3

1.2 Arrangements of subunits on V_1 ATPases and/or V_1V_O ATPases 6

1.3 V-ATPases in disease and as potential drug targets 7

1.4 Regulation of V-ATPase activity 9

1.4.1 Reversible dissociation 9

1.4.2 Control of reversible dissociation in yeast 10

1.5 Isoforms of V-ATPases 12

1.6 Structural features of the yeast V_1V_O ATPase 12

1.7 Comparison of V-ATPase with A- and F-ATP synthases 19

1.8 Outline of the thesis 21

2. Materials and methods

2.1 Materials

2.1.1 Chemicals 23

2.1.2 Molecular biology materials 23

2.1.3 Chromatography 24

2.1.3.1 Ion exchange 24

2.1.3.2 Gel filtration 24

2.1.3.3 Instruments and accessories 24

2.1.3.4 Protein concentration and estimation 24

2.1.4 Other instrumentation 24

2.1.5 Computer software 25

2.2 Methods

2.2.1 Vector preparation 27

2.2.2 Cloning of yeast subunit G and E constructs from yeast V-ATPase 28

2.2.2.1 PCR amplification of the DNA fragments 28

2.2.2.2 Restriction of the DNA fragments 29
2.2.2.3 Ligation of DNA fragments and vector 30
2.2.2.4 Electroporation transformation 30
2.2.3 Protein production and purification of truncated subunits G and E 31
2.2.3.1 Induction test 31
2.2.3.2 Solubility test of recombinant proteins 32
2.2.4 Protein quantification by bicinchonic acid method 33
2.2.5 Circular dichroism spectroscopy 33
2.2.6 Production and purification of subunit G mutants 34
2.2.7 Disulphide bond formation analysis in subunit G using $CuCl_2$ 35
2.2.8 Dimer model of G_{61-101} 35
2.2.9 Peptide synthesis 36
2.2.10 Nuclear magnetic resonance (NMR) spectroscopy 36
2.2.10.1 Isotopic labeling (^{15}N, ^{13}C) of proteins 37
2.2.10.2 One dimensional (1D) NMR spectroscopy 37
2.2.10.3 Two dimensional (2D) NMR spectroscopy 38
2.2.10.4 Three dimensional (3D) NMR spectroscopy 38
2.2.10.5 Resonance assignment 39
2.2.10.6 Binding studies with NMR 42
2.2.10.7 Diffusion coefficient measurements 43

3. Results

3.1 Structural characterization of subunit G of V-ATPase from *S. cerevisiae*

3.1.1 Introduction 45
3.1.2 Expression and purification of subunit G (G_{1-59}, G_{61-114}, G_{61-101}, G_{1-77} and G_{1-101}) 46
3.1.3 Approach to study the structure of subunit G through NMR spectroscopy 49
3.1.4 Structural characterization of G_{1-59} through nuclear magnetic resonance spectroscopy 49
3.1.4.1 Backbone assignments of G_{1-59} 50
3.1.4.2 Side chain and ^{1}H ^{15}N NOESY-HSQC assignment 52
3.1.4.3 Structure calculation of G_{1-59} 52

3.1.4.4 Solution structure of G_{1-59} 54
3.1.5 Structural characterization of G_{61-101} through NMR spectroscopy 56
3.1.5.1 Effect of temperature and TFE on G_{61-101} 56
3.1.5.2 Solution structure of G_{61-101} 58
3.1.5.3 Translational diffusion rates of G_{61-101} 61
3.1.5.4 Examination of disulfide bond formation by cross linking and mutagenesis of subunit G from *S. cerevisiae* 61
3.1.5.5 Expression and purification of subunit G mutants 62
3.1.5.6 Crosslink formation in cysteine mutants of subunit G 63

3.2 Interaction studies of subunit G with the stalk subunits E and *d* of V-ATPase

3.2.1 Interaction studies of subunit G and E 65
3.2.1.1 G_{1-59} and E_{18-38} binding characterized through NMR spectroscopy 65
3.2.1.2 G_{1-59} and E_{18-38} binding characterized by FCS 68
3.2.1.3 Model for the Interface of G_{1-59} and E_{18-38} complex 68
3.2.2 Interactions Studies of Subunit G and *d* 70
3.2.2.1 Residues involved in G_{1-58} and *d* assembly 70
3.2.2.2 Interaction of G_{61-114} with the *d* subunit 71

3.3 Structural characterization of stalk subunit E of V-ATPase from *S. cerevisiae*

3.3.1 Introduction 73
3.3.2 Purification of E_{1-69} and production and purification of $E_{133-222}$ 73
3.3.3 Circular dichroism spectra of E_{1-69} 75
3.3.4 Structural characterization of E_{1-69} by NMR spectroscopy 76
3.3.4.1 NMR Solution structure of E_{1-69} 77
3.3.5 Structural characterization of $E_{133-222}$ 80
3.3.5.1 Circular dichroism analysis of $E_{133-222}$ 80
3.3.5.2 One dimensional NMR analysis of $E_{133-222}$ 80
3.3.5.3 NMR solution structure analysis of $E_{133-222}$ 81

4. Discussion

4.1 Stalks of the yeast V-type ATPases 85

4.2	Stoichiometry and importance of subunit G in V_1V_O ATPase	85
4.3	Putative Role of subunit G in V_1 ATPase	87
4.4	Arrangement of subunit G in the V_1 -ATPase	88
4.5	Dimeric model of subunit G	89
4.6	Comparison of the peripheral stalk subunits	90
4.7	Structure and arrangement(s) of the subunit E in V_1V_O ATPase	92
4.8	Structural position of subunit E with respect to subunit B	95
4.9	Subunit E and G with RAVE and aldolase on V-ATPase assembly	97

5. Conclusion 99

6. References 103

Author's publications 117

Posters presented 118

List of figures

Introduction

Figure 1.1: Role of intracellular V-ATPases in normal and disease processes 2
Figure 1.2: Topological model of V_1V_O ATPase 5
Figure 1.3: Function of plasma membrane V-ATPase 8
Figure 1.4: Regulation of V-ATPase activity 10
Figure 1.5: Ribbon diagram of the crystal structure of subunit C from yeast 13
Figure 1.6: Low resolution model of subunit F obtained from the SAXS data 15
Figure 1.7: Crystal structure of yeast V-ATPase subunit H 16
Figure 1.8: Low resolution structure of subunit *d* from yeast V-ATPase 18

Materials and methods

Figure 2.2.1: Vector Map of modified pET9d1
27
Figure 2.2.2: Flow chart of site directed mutagenesis 34
Figure 2.2.3: Transfer of magnetization in the HNCO and HN(CA)CO experiments 40
Figure 2.2.4: Strip plots of same and previous residues carbonyl peaks in HNCACO experiment 40
Figure 2.2.5: Transfer of magnetization in the CBCA(CO)NH and HNCACB 41
Figure 2.2.6: Transfer of magnetization in the (H)CC(CO)NH-TOCSY, H(CC)(CO)NH-TOCSY and HCCH TOCSY 42
Figure 2.2.7: Illustration of change in peak position in ^{1}H-^{15}N HSQC spectrum 43

Results

Structural characterization of subunit G of V-ATPase from *S. cerevisiae*

Figure 3.1.1: Secondary structure prediction of subunit G of V_1V_O ATPase from *S. cerevisiae* 45
Figure 3.1.2: PCR amplification of subunit G 46
Figure 3.1.3: 17 % SDS-PAGE showing the over-expression pattern of recombinant subunit G 47
Figure 3.1.4: Ni^{2+}-NTA purification of truncated G subunit proteins 47
Figure 3.1.5: Purification of G subunit proteins by size exclusion column, Superdex HR75 48
Figure 3.1.6: Concentrated protein of G_{61-114} 49
Figure 3.1.7: Strip plots of HNCAO and HNCACB 50
Figure 3.1.8: ^{1}H ^{15}N-HSQC spectrum of G_{1-59} 51
Figure 3.1.9: Strip plots of the ^{1}H ^{15}N NOESY-HSQC
52
Figure 3.1.10: The connectivity diagram of the calculated structure for G_{1-59}. 53
Figure 3.1.11: Structure of G_{1-59} from yeast V-ATPAse 54
Figure 3.1.12: Surface charge distribution of G_{1-59} 55

Figure 3.1.13: Effect of temperature and TFE of recombinant G_{61-101} 56

Figure 3.1.14: ^{1}H ^{15}N-HSQC spectrum of G_{61-101} 57

Figure 3.1.15: The connectivity diagram of the calculated structure for G_{61-101} 58

Figure 3.1.16: The secondary structure prediction for G_{61-101} 58

Figure 3.1.17: Ribbon diagram of the NMR solution structure of G_{61-101} 59

Figure 3.1.18: Surface charge distribution of G_{61-101} 60

Figure 3.1.19: Graph showing change of diffusion coefficient versus concentration for G_{61-101} 61

Figure 3.1.20: The solution structure of G_{61-101} 62

Figure 3.1.21: Purification of subunit G mutants 63

Figure 3.1.22: Cross-linking of subunit G mutants 63

Interaction studies of subunit G with the stalk subunits E and *d* of V-ATPase

Figure 3.2.1: Super imposition of the ^{1}H ^{15}N HSQC spectra of G_{1-59} 65

Figure 3.2.2: Sections from the overlaid 2D ^{1}H-^{15}N-HSQC spectra of the G_{1-59} 66

Figure 3.2.3: Solution NMR spectrum of G_{61-114} 67

Figure 3.2.4: Binding of G_{1-59} with E_{18-38} studied by FCS. 68

Figure 3.2.5: The docked complex of the solution NMR structure of G_{1-59} (*green*) and E_{18-38} (*orange*) 69

Figure 3.2.6: The ^{1}H ^{15}N HSQC spectra of G_{1-59} 70

Figure 3.2.7: Loss of ^{1}H ^{15}N HSQC peak intensity upon titration of unlabeled *d* subunit to ^{15}N labeled G_{1-59} at a molar ratio of 0.5 71

Figure 3.2.8: Super imposition of the ^{1}H ^{15}N HSQC spectra of G_{61-114}. 72

Structural characterization of stalk subunit E of V-ATPase from *S. cerevisiae*

Figure 3.3.1: PCR amplification of $E_{133-222}$ 73

Figure 3.3.2: SDS-PAGE showing the expression of recombinant subunit E proteins 74

Figure 3.3.3: Ni^{2+}-NTA purification of truncated E subunit proteins 74

Figure 3.3.4: Purification of E subunit proteins by gel filteration 75

Figure 3.3.5: Circular dichroism of E_{1-69} 75

Figure 3.3.6: ^{1}H ^{15}N-HSQC spectrum of E_{1-69} 76

Figure 3.3.7 The connectivity diagram of the calculated structure for E_{1-69} 78

Figure 3.3.8: NMR solution structure of *S. cerevisiae* E_{1-69} 79

Figure 3.3.9: Circular dichroism of $E_{133-222}$ 80

Figure 3.3.10: One dimensional NMR spectrum of $E_{133-222}$ 80

Figure 3.3.11: ^{1}H ^{15}N-HSQC spectrum of $E_{133-222}$ 81

Figure 3.3.12 Chemical shift index (CSI, WISHART *et al.*, 1994) plot of $E_{133-222}$ 82

Figure 3.3.13: Topological model created based on the secondary structure prediction as per CSI 83

Discussion

Figure 4.1: The 18 Å structure of V_1 ATPase without subunit C from *M. sexta*. 85

Figure 4.2: The proposed model of arrangement of subunit G and *d* 86

Figure 4.3: Dimeric model of G_{61-101} based on cross linking data and diffusion coefficient measurements 90

Figure 4.4: Comparision of the structures of subunits H, G and *b* of A_1A_O ATP synthase, V_1V_O-ATPase and F_1F_O ATP synthase 91

Figure 4.5: NMR solution structure of *S. cerevisiae* E_{1-69} 94

Figure 4.6: Structural model of subunit E of yeast V-ATPase 96

List of tables

Table 1.1	Subunit compositions of the catalytic V_1 and proton translocating V_O domains of V-ATPase	4
Table 1.2	Subunits of the V-ATPase compared with A- and F-ATP synthases	20
Table 2.1	Sequences of primers used for subunit G and E constructs	28
Table 2.2.2	Subunit G cysteine mutants of V-ATPase from the yeast genome	35
Table 3.1.1	Structural statistics of 10 lowest energy structures of G_{1-59}	55
Table 3.1.1	Structural statistics of G_{61-101}	60
Table 3.3.1	Structural statistics of E_{1-69}	77

Abbreviations

1D	One-dimensional
2D	Two-dimensional
3D	Three-dimensional
Å	Angstrom
ADP	Adenosine diphosphate
ATP	Adenosine triphosphate
BMRB	Biological magnetic resonance bank
BSA	Bovine Serum Albumin
CD	Circular Dichroism
CPMG	Carr-Purcell-Meiboom-Gill spin-echo sequence
CSA	Chemical shift anisotropy
CSI	Chemical shift index
DTT	Dithiothreitol
E. coli	*Escherichia coli*
EDTA	Ethylenediaminetetraacetic acid
FPLC	Fast protein liquid chromatography
hetNOE	Heteronuclear Overhauser effect
HSQC	Heteronuclear single quantum correlation
Hz	Hertz
IPTG	Isopropyl-β-D-thiogalactoside
kDa	Kilo-Dalton
NMR	Nuclear magnetic resonance
NOE	Nuclear Overhauser effect
NOESY	Nuclear Overhauser effect spectroscopy
NTA	Nitrilotriacetic acid
ppm	parts per million
PAGE	Polyacrylamide Gel Electrophoresis
PCR	Polymerase Chain Reaction
PDB	Protein data bank
RMSD	Root mean square deviation
R_1	Longitudinal or spin-lattice relaxation rate constant
R_2	Transverse or spin-spin relaxation rate constant
SAXS	Small Angle X-ray Scattering
SDS	Sodium dodecyl sulphate

TOCSY	Total correlation spectroscopy
Tris	Tris-(hydroxymethyl) aminomethane
V-ATPase	Vacuolar ATPase

Abstract

Subunit G of the yeast V-ATPase is observed to be an elongated protein with a maximum size and the radius of gyration as 8.0 nm and 2.7 nm, respectively (ARMBRÜSTER *et al.,* 2003). Initial studies revealed that subunit G of yeast V-ATPase, could not be purified to higher concentrations, which may be significant problem for any structural studies such as crystallization and/or solution NMR spectroscopy. In order to understand the structure of subunit G and its possible orientation with respect to the other stalk subunits, two constructs $G_{1\text{-}58}$ and $G_{61\text{-}101}$, were created using the secondary structure information of subunit G (PSIPRED V2.5 by MCGUFFIN *et al.,* 2000). The structure of both the N- and C-terminal domains of subunit G, were solved by solution NMR technique. The $G_{1\text{-}58}$ possessed an extended helix from T10 to A56 measuring a length of 67.9 Å excluding the unstructured region in the N- (1-9) and C-termini (57-59) of $G_{1\text{-}58}$. The C-terminal peptide of subunit G, $G_{61\text{-}101}$, has an extended helical structure from the residues E64 to E100 measuring a length of 47.93 Å, excluding the unstructured region in the N- (residues 59-63) and C-terminus (amino acid 101), as predicted from the amino acid sequence. In addition, the possible exposure of critical amino acids in the subunit G constructs, which are proposed to be involved in its binding with the neighboring subunits, is discussed in detail. Initial studies of subunit G through solution X-ray scattering have revealed the existence of a dimeric nature (ARMBRÜSTER *et al.,* 2003). To confirm this, the dimer diffusion coeffcient of $G_{61\text{-}101}$ peptide was studied through 1D NMR spectroscopy and showed that, $G_{61\text{-}101}$ forms a dimer. The dimer dissociation constant for $G_{61\text{-}101}$ was estimated by direct fit of translation diffusion rates, as a function of concentration, to be 1.5 mM (RISHIKESAN *et al.,* 2010). Cysteine based cross linking on the mutated full length subunit G were analysed and the possible orientation of subunit G on a dimeric model is demonstrated.

Subunit G of yeast V-ATPase is observed to be essential for activity and assembly of V_1V_O ATPases (CHARSKY *et al.,* 2000). Precipitation assays have suggested the interaction of subunit G and E on the N-termini of both the subunits (JONES *et al.,* 2005). Therefore, the interaction of subunit G with its neighboring stalk subunits, including E and *d*, was studied using approaches solution NMR spectroscopy and fluorescence correlation spectroscopy (FCS) with recombinant proteins of subunit G, E, *d* and synthetic peptides of subunit E. The studies revealed that both the subunits E and G interact only with their N-terminus, and the region specific on subunit E that

participate in this binding was characterized as E_{18-38}. Titration studies of subunit G constructs with subunit *d* showed that the N-terminus of subunit G bind with *d.* The possible orientation of subunit G with respect to subunit E and *d* is also illustrated.

Subunit E is an essential component of the V_1 assembly, as disruption of the gene on the yeast (Vma4) resulted in a disassembly of the V_1V_O complex (KANE *et al.,* 2003). The N-terminal segment of subunit E, including residues 19-38 have been predicted to be important for its assembly with subunit G (JONES *et al.,* 2005, RISHIKESAN *et al.,* 2008, 2009). Subunit E is observed to be critical for its binding with most of the stalk subunits on the V-ATPase. This includes E_{1-19}, which binds with subunit C (JONES *et al.,* 2005) and E_{1-79} that is described to assemble with subunit H (LU *et al.,* 2002). Here the N-terminus of subunit E from yeast V-ATPase was segmented to first 69 residues, expressed, purified to homogeneity and the solution structure was studied through NMR spectroscopy. The structure showed an extended helix measuring a length of 83.19 Å, as predicted from the amino acid sequence and the secondary structure prediction of E_{1-69}. The peptide consists of 34.8% charged residues, 27.5% other polar residues and 37.7% non-polar residues in the sequence. The solution structure illustrates a clear amphipathic helix with a hydrophobic N-terminus on one side of the helix and a highly charged C-terminus, exposing the charged residues towards the outer surface of the structure. The C-terminus of subunit E is predicted to be globular with a mixture of α-helix and β-strands on the secondary structure (PSIPRED V2.5 by MCGUFFIN *et al.,* 2000). The proposed C-terminal globular domain of subunit E, $E_{133-222}$ from yeast V-ATPase was cloned, expressed and purified to homogeneity. The solution structure of $E_{133-222}$ was studied through NMR spectroscopy and the first secondary structure of $E_{133-222}$ was determined through these studies. The specific sequence that forms the α-helix and β-strands on the globular domain of subunit E are described. Based on the above results and biochemical evidences from the literature, the possible orientation of subunit E with respect to other stalk subunits and the catalytic head domain of the V_1V_O complex are discussed.

1. Introduction

In a biological cell, physiological conditions maintain a slightly alkaline extracellular pH and an acidic cytosolic pH (GRINSTEIN and FURUYA, 1986). The acidic cytosolic environment can be characterized by two reasons, which includes the electrical potential across the membrane that drives the uptake of positively charged protons and secondly, the net acid equivalents generated by various metabolic reactions (GRINSTEIN and FURUYA, 1986). A protonation and de-protonation activity describes the charge distribution across the membrane and facilitates various metabolic reactions (WHITTEN *et al.,* 2005). This dynamic equilibrium between proton-extruding and proton-importing process not only facilitates pH homeostasis in the cytosol, but also in other cellular compartments. The energy required for proton extrusion is accomplished by proton pumping ATPases that are present on the endo-membranes and exchanges H^+ in an electro-neutral manner. These proton extrusions from the cells against the electrochemical gradient are coupled to other substrates through exchangers (antiporters) or co-transporters (symporters) (GRINSTEIN *et al.,* 1993).

The vacuolar ATPase expressed on the plasma membrane, energizes a wide variety of epithelial transport processes in mammalian cells, leading to the secretion or absorption of fluids, mineral ions and amino acids (HARVEY and WIECZOREK, 1997; BEYENBACH 2001). The H^+ transport by the V-ATPase for intra- or extra-cellular pH is determined by the secondary transport process that couples the ATPase activity. For instance, luminal alkalinisation of the midgut of insect larvae is coupled to the apical V-ATPase activity (AZUMA *et al.,* 1995). V-ATPases in the anterior midgut of the larval mosquitoes provides energy for the absorption of dietary amino acids causing the rise of pH to ~10.5-12.0 (DADD 1975; DOW 1984). The alkalinity is contributed to aid the breakdown of dietary tannins which interfere with the nutrient absorption (BERENBAUM 1980). Studies on the *Manduca sexta* characterizes the alkalization mechanism, where the hyper-polarization of the apical membranes of specialized "globlet cells" to 240 mV by V-ATPases drives an electrophoretic exchange (antiport) of luminal H^+ for cellular K^+ (WIECZOREK *et al.,* 1986; DOW and PEACOCK 1988; SCHWEIKL *et al.,* 1989; AZUMA *et al.,* 1995).

Besides pH regulation of the intracellular compartments, V-ATPases of the plasma membrane are also involved in specialized functions that are specific to certain cell types, such as renal acidification, bone resorption, sperm maturation, etc. (FORGAC 2007). The endosomal sorting of secretory proteins in the Golgi apparatus is affected by the lack of V-ATPase activity

(NELSON and NELSON, 1989; UMEMOTO *et al.,* 1990; YAVER *et al.,* 1993). V-ATPases also show an intimate involvement in the receptor mediated endocytosis (Figure 1.1) and receptor recycling (NELSON and HARVEY, 1999). Uncoupling of ligands from the receptors, activation of the proteases, and protonation of the microbial factors are also dependent on the change in the endosomal pH (WEISZ 2003). Evidence suggests that V-ATPases are also required for the signal transduction processes that regulate the cell growth and survival (CRUCIAT *et al.,* 2010). A change in the mitochondrial pH indicates an early event in mitochondrial dependent apoptosis (MATSUYAMA *et al.,* 1998; MATSUYAMA *et al.,* 2000). Cell death due to these intracellular acidification may not be linked to caspase-dependent apoptosis, but resembles paraptosis which is an alternate form of programmed cell death, that is typical due to cytoplasmic acidification and mitochondrial swelling (SCHNEIDER 2004).

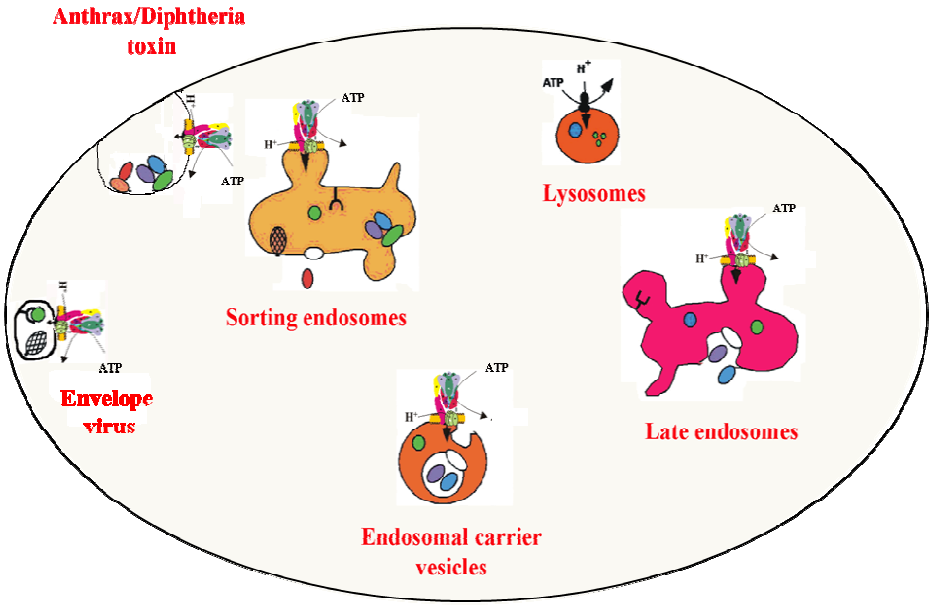

Figure 1.1: Role of intracellular V-ATPases in normal and disease processes. Internalization of ligand protein from the plasma membrane is facilitated by receptor-mediated endocytosis and trafficked to the sorting (also known as early) endosomes. Acidic environment generated by V-ATPases causes dissociation of ligand-receptor complexes, which facilitates the recycling of unoccupied receptors to cell surface. Multi-vesicular bodies (also known as endosomal carrier vesicles) target the released ligands to lysosomes for degradation which is dependent on a luminal acidic pH generated by V-ATPases. Enveloped viruses and toxins also enter cells via acidic endosomes; where in the low pH facilitates the entry of the viral mRNA or cytotoxic portions of the toxin molecules through pores that are formed in the endosomal membrane (modified from FORGAC 2003).

Evolution has channelized the intracellular compartments to spatially restrict and optimize certain biochemical reactions and pathways. Thus the lumen of different organelles has different properties in terms of ionic concentrations, redox potentials and also pH. Sub-organellar pH is

strictly regulated between neutral in endoplasmic reticulum, to slightly acidic in early endosomes and highly acidic in late endosomes and/or lysosomes (GU and GRUENBERG, 2000). Besides acidification and membrane trafficking, V-ATPases serve as pH sensors of endosomes in renal proximal tubule cells (HURTADO *et al.,* 2006). Here the release of ligands from their respective receptors in early endosomes is regulated by ADP-ribosylation factor-6 (ARF-6), ARNO (ARF-nucleotide-binding-site opener), the guanine-nucleotide-exchange factor which activates ARF-6 and thus delivers the ligand to the endocytic carrier vesicles through acidification of early endosomes (MARSHANSKY and FUTAI, 2008). ARF-6 and ARNO interact directly with V-ATPase and is pH dependent (HURTADO *et al.,* 2006). This explains the fact that movement of ligands along the endocytic pathway is pH dependent and also suggests that part of the V-ATPase itself serves as a sensor of luminal pH (HURTADO-LORENZO *et al.,* 2006). The low pH generated by V-ATPases inside the cell, triggers the formation of membrane pores through which the viral mRNA of influenza virus or the cytotoxic portions of diphtheria toxin translocate into the cytoplasm (GRUENBERG and VAN DER GOOT, 2006).

The plant V-ATPases catalyzes acidification of endo-membrane-surrounded organelles. This enzyme plays an important part in the cell expansion and stress adaptation. This is attributed through the central vacuole that occupies the symplastic cell spaces in the parenchymatic tissues (CHENG *et al.,* 2003). The vacuole function is to store the salts, metabolites, carbohydrates, amino acids, conjugates, etc. that are linked to the transport processes (MARTINOIA, 1992). The V-ATPase activity is a prerequisite for the rapid tissue expansion during etiolation in the dark (SCHUMACHER, 2006). The root meristamatic cells instigated the vacuolization upon exposure to the salt stress (NaCl) and this salt-induced vacuole volume was coupled to 2.3-fold increase in the V-ATPase activity (MIMURA *et al.,* 2003). The vacuolar ATPase is thus an enzyme that transfers the smallest ions from one compartment to another and also energizes a wide variety of eukaryotic cell organelles and bio-membranes. And therefore the structure, function and molecular mechanism of this enzyme complex is of explicit importance to researchers indeed.

1.1 Eukaryotic V-ATPases

V_1V_O-ATPases perform an exclusive proton pumping across biomembranes of eukaryotic cells. These enzymes are large multi-subunit complexes (Table 1.1) that are organized in two distinct domains, V_1 and V_O. The 650 kDa V_1 domain is a peripheral complex, which is located on the cytoplasmic side of the membrane, and hosts the ATP hydrolysis on the A_3B_3 head

domain. The 250 kDa membrane-embedded complex, V_O domain, is responsible for proton translocation from the cytoplasm to the lumen or the extracellular space (GRÜBER and MARSHANSKY, 2008).

Domain	Subunits	Yeast Gene	MW (kDa)	Subunit Function
V_1	A	*VMA1*	70	Catalytic site
	B	*VMA2*	60	Nucleotide-binding, regulatory, actin- and aldolase binding
	C	*VMA5*	40	Activity, assembly, reversible dissociation, actin binding
	D	*VMA8*	34	Assembly, activity
	E	*VMA4*	33	Activity, assembly, peripheral stalk, RAVE- and aldolase binding
	F	*VMA7*	14	Activity, assembly
	G	*VMA10*	13	Activity, assembly, peripheral stalk
	H	*VMA13*	50	Regulator subunit, assembly
V_O	*a*	*VPH1, STV1*	100	Proton pumping, targeting, assembly, peripheral stalk
	d	*VMA6*	40	Coupling, peripheral stalk, activity
	c	*VMA3*	17	Proton transport, bafilomycin binding site
	c'	*VMA11*	17	Proton transport
	c''	*VMA16*	21	Proton transport
	e	*VMA9*	9	unknown

Table 1.1 Subunit compositions of the catalytic V_1 and proton translocating V_O domains of *S. cerevisiae* V-ATPase. *S. cerevisiae* V-ATPase subunit genes are shown along with the respective molecular weight of the protein subunits. Subunit function (see text for references and detailed function of each subunit) is also shown.

The V_1 domain is composed of eight subunits, A-H (Figure 1.2), in a proposed stoichiometry of A_3:B_3:C:D:E_{2-3}:F:G_{2-3}:H_X (ARAI *et al.,* 1988; GRÜBER and MARSHANSKY, 2008). The catalytic and nucleotide binding subunits A and B, respectively, are arranged alternatively to form an A_3B_3 hexamer, where the ATP hydrolysis occurs at the interface of subunits A and B (LIU *et al.,* 1996; MACLEOD *et al.,* 1998). The other subunits of V_1 which includes C-H, form the stalk region that connects V_1 and V_O domain. Existence of one single copy of subunits C, D, F and H leaves the copy number of subunit E and G as contradictory, claiming as two (BOEKEMA *et al.,* 1997) and/or three copies (KITAGAWA *et al.,* 2007; DIEPHOLZ *et al.,* 2008) per enzyme.

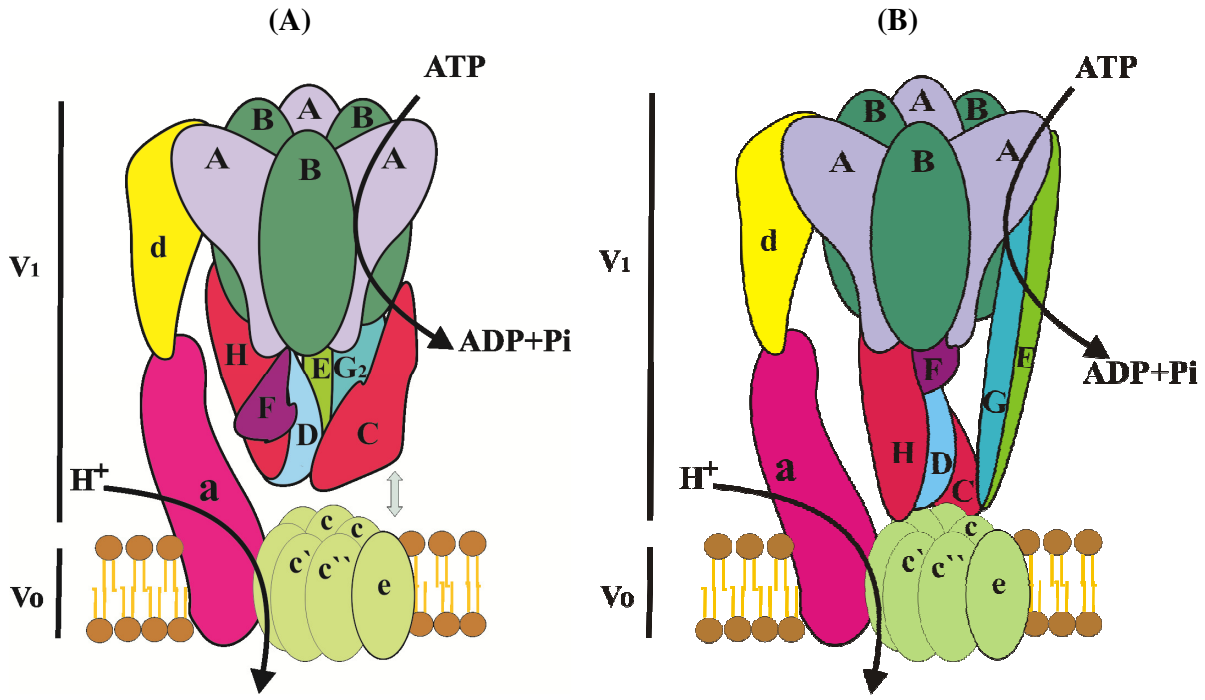

Figure 1.2 Topological model of V_1V_O ATPase. (A) Schematic diagram of the V_1V_O ATPase. V_1 domain comprising of catalytic subunits A_3B_3 and central stalk subunits C-H. The membrane embedded V_O domain consists of *a*, c *c*' *c*" and *d* subunits. The V_1 part can dissociate from the V_O part as shown by the double headed arrow. **(B)** Schematic diagram of V_1V_O ATPase showing the catalytic subunits A_3B_3, central stalk subunits C,D,F,H and peripheral stalk subunits G,E. The energy released during ATP hydrolysis on the V_1 catalytic domain of V-ATPase is used to drive the proton transport across the membrane occurring on the V_O domain, to acidify the intra-cellular compartments and generate an ion gradient potential (Modified from GRÜBER and MARSHANSKY, 2008).

The membrane embedded V_O domain consists of six different subunits including *a*, *d*, *e*, *c*, *c*' and *c*'' in yeast, whereas the higher eukaryotes lack the subunit *c*' instead contain an accessory subunit Ac45 (SUPEK *et al.,* 2004). The proteolipid subunits (*c*, *c*' and *c*'') are highly hydrophobic proteins which are arranged on a ring pattern called *c*-rings (WILKENS and FORGAC, 2001), with each proteolipid subunit containing one single buried glutamate residue located in the trans-membrane helix-4 (TM-4) of the subunits *c* and *c*' and TM-3 of subunit *c*'', where this glutamate residue undergoes the reversible protonation during the proton transport. Another crucial subunit for the proton transport across the membrane is the 100 kDa subunit *a*, which contains eight or nine TM helices at the C-terminus (NISHI and FORGAC, 2002). It has a highly hydrophilic N-terminal domain that is oriented towards the cytoplasm which interacts with the subunit A and/or B (SHAO and FORGAC, 2004) and with subunit *d* (THAKER, *et al.,* 2009).

Cross-linking studies, pull-down assays, yeast-two-hybrid screening and/or recombinant subcomplexes characterize the individual subunit composition on the stalk region (peripheral and central stalk) of V-ATPases. Zero-length cross linking studies involving cysteine mutation(s) on

the subunits, have provided evidence that subunit C, E, G, H, *d* and hydrophilic N-terminal domain of subunit *a* form the peripheral stalk and subunits D and F form the central stalk in the entire V_1V_O ATPases (ARATA *et al.,* 2002; WILKENS *et al.,* 2004; INOUNE *et al.,* 2005). Subunit F is proposed to undergo structural alterations during catalysis and is shown to interact with subunits A, D and E depending on the nucleotide occupancy on the A_3B_3 catalytic sites (GRÜBER *et al.,* 2000). Subunits C and H are described to be involved in modulating the interaction between the V_1 and V_O domain (LU *et al.,* 2002; CURTIS and KANE, 2002) and are positioned on the interface of V_1 and V_O domain (KANE, 1995; SUMNER *et al.,* 1995; ZHANG *et al.,* 2003; VENZKE *et al.,* 2005). Subunits E and G form part of the peripheral stalk in a fully assembled V_1V_O ATPases and rearrange themselves to associate as a compact central stalk in the disassembled V_1 ATPase *in vivo* (BOEKEMA *et al.,* 1999; CHARSKY *et al.,* 2000; XU *et al.,* 1999; GRÜBER *et al.,* 2003). When the copy number of subunit G and E are argued, research supports the existence of more than one copy per enzyme (OHIRA *et al.,* 2006).

1.2 Arrangements of subunits on V_1 ATPases and/or V_1V_O ATPases

In vivo, the vacuolar ATPases can dissociate into individual V_1 and V_O sub-complexes and are in a dynamic equilibrium with the fully assembled V_1V_O ATPases (BEYENBACH and WIECZOREK, 2006). This fundamental feature of the V-ATPases, as an *in vivo* regulation of ATPase activity, has been observed in *M. sexta* (SUMNER *et al.,* 1995), yeast cells (KANE, 1995) and in kidney proximal tubular cells (SAUTIN *et al*., 2005). In these cases, the V_1 sector had the same subunit composition without subunit C. Isolation of the disassembled V_1 sub-complex from the *M. sexta* elucidated the first low resolution model of the V_1 ATPase lacking subunit C (RADERMACHER *et al.,* 2001). These isolated V_1 sectors on insects and yeast cells showed a decreased Mg^{2+} dependent ATPase activity and proton pumping at the membrane and rapidly restored the activities upon reassembly of V_1 to V_O domain (SUMNER *et al.,* 1995; GRÄF *et al.,* 1996; KANE, 1995; KANE and SMARDON, 2003). The 18 Å resolution three dimensional structure of V_1 ATPase (-C), revealed the alternative arrangements of subunits A and B with a central mass located slightly offset (RADERMACHER *et al.,* 2001). The structure of A_3B_3 head domain on the 3D reconstruction showed a protuberance at its top on alternating region (RADERMACHER *et al.,* 2001), which was later characterized as the Non-Homologous-Region (NHR) of subunit A (PUOPOLO *et al.,* 1991; SHAO *et al.,* 2003). The compact central stalk formed underneath the A_3B_3 head domain of the V_1 ATPase lacking subunit C is slightly shorter when compared to the

entire and hydrated V_1 ATPase using small-angle X-ray scattering (SVERGUN *et al.,* 1998), which is mainly due to the lack of subunit C. The arrangement of the subunits D, E, F, G and H on the central stalk reveals a compact entity with no peripheral stalk region on the V_1 ATPase (RADERMACHER *et al.,* 2001).

By comparison, the negatively stained V_1V_O ATPases from *C. fervidus* showed a peripheral stalk at the side projection proposed to function as a stator (BOEKEMA *et al.,* 1998). A second (WILKENS *et al.,* 1999) and third (VENZKE *et al.,* 2005; DIEPHOLZ *et al.,* 2008) peripheral stalk was also observed on the negatively stained images of yeast V_1V_O ATPase. The stalk subunits of the V_1V_O ATPase undergo rearrangements when the V_1 ATPase reassembles with the V_O domain and forms central stalk with subunits D and F (ARATA *et al.,* 2002; WILKENS *et al.,* 2004; INOUNE *et al.,* 2005) and peripheral stalk(s) involving subunits G and/or E (BOEKEMA *et al.,* 1999; CHARSKY *et al.,* 2000; VENZKE *et al.,* 2005; DIEPHOLZ *et al.,* 2008) *in vivo* on the complex. When the central stalk serves as a rotor to couple the energy released from ATP hydrolysis to the rotation of a ring of proteolipid subunits in the V_O domain, the peripheral stalk(s) serve to prevent the rotation of A_3B_3 head region during ATP hydrolysis and therefore serve as a stator function (NISHI and FORGAC, 2002). Since subunits E and G do not have a membrane anchor to support their stator role, this may be achieved by a direct or indirect connection of the peripheral stalk subunits to static subunits of the membrane-anchored domain (BOEKEMA *et al.,* 1998).

1.3 V-ATPases in disease and as potential drug targets

Despite functioning in normal physiology at various intracellular compartments, vacuolar ATPases present in the plasma membrane are also shown to contribute to some disease aetiologies. Genetic defects in the gene encoding for a_4 or B_1 subunit isoforms of V-ATPase lead to a defective distal nephron acid secretion by renal intercalated cells in the proximal distal tubule and collecting duct (Figure 1.3A). These result in renal tubular metabolic acidosis, a condition that is characterized by a very low plasma pH and excessive urinary loss of metabolites like K^+ and Ca^{2+} (KARET *et al.,* 1999; SMITH *et al.,* 2000). Mutations on the B subunit also leads to a sensorineural deafness indicating the putative role of V-ATPases in maintaining the pH balance of the fluids surrounding the mechano-sensory hair cells (KARET *et al.,* 1999).

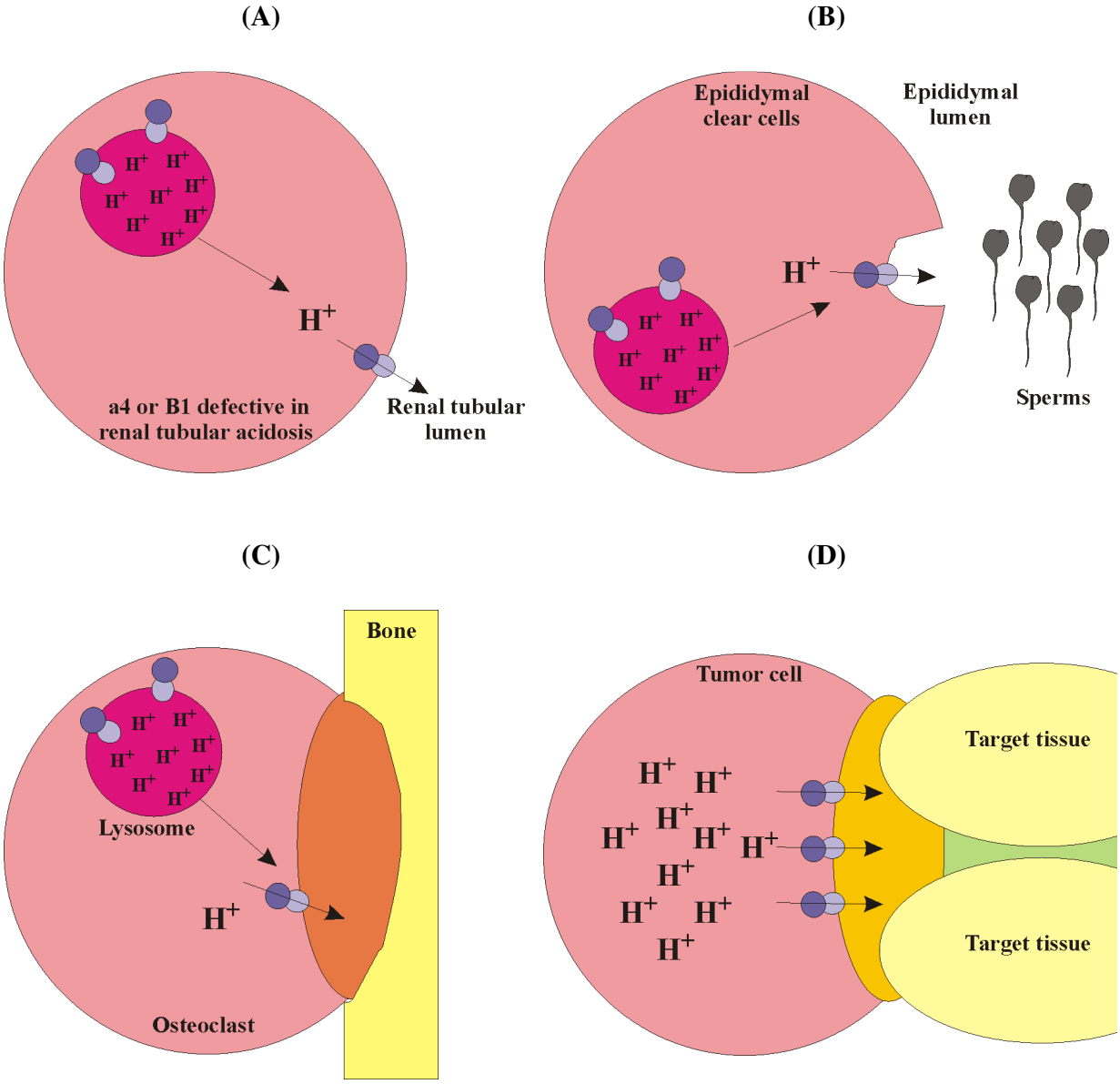

Figure 1.3: Function of plasma membrane V-ATPases. **(A)** V-ATPases pumps protons across the renal intercalated cell membranes to acidify the urine. **(B)** It also controls the pH of the sperm environment. **(C)** Bone resorption is attributed by the V-ATPases present in the osteoclasts, which requires acidification of the space that is in contact with the bone. **(D)** A similar extracellular acidification may be used in tumour cells, to promote the activity of secreted lysosomal enzymes that function in metastasis. (Modified from NISHI and FORGAC, 2002).

V-ATPases on the apical membrane of the epididymis and vas deferens control the pH of the sperm environment and are essential for sperm maturation, viability and motility, making them a prospective contraceptive target (PIETREMENT 2006, Figure 1.3B). V-ATPase with testis-specific E_1-subunit isoform is essential for its acrosome acidification which is also a potential drug target (SUN-WADA *et al.,* 2002).

Plasma membrane V-ATPases have a significant role in the bone resorption, where osteoclast attached to the surface of the bone create a concealed extracellular compartment and acidification of this space by V-ATPases, dissolve the bone matrix and increase the activity of acid hydrolases secreted by the osteoclasts (TOYOMURA *et al.,* 2000, Figure 1.3C). Genetic defects in the *a*3 isoform, which is responsible for the plasma membrane targeting of V-ATPases in osteoclasts, lead to osteophoresis where it failed to degrade bone (FRATTINI *et al.,* 2000). Subunit *a*3 could be considered as a potential drug target for the treatment of osteophoresis.

V-ATPases are found in the plasma membrane of certain tumour cells and have also been proposed to perform a similar function, where they can provide an acidic environment required to activate the secreted cathepsins that participate in metastatic invasion (SENNOUNE *et al.,* 2004) (Figure 1.3D). Because of the optimal activity of the lysosomal enzyme at low pH, V-ATPases also serves as a potential drug target to block metastasis.

1.4 Regulation of V-ATPase activity

Regulation of the V-ATPase activity is important because of its physiological relevance and this is consummated by numerous mechanisms including reversible dissociation of the V_1V_O complex, control of their cellular localization and also by the changes in the efficiency of coupling of proton transport with ATP hydrolysis.

1.4.1 Reversible dissociation

Reversible dissociation of V_1V_O-ATPase into V_1 and V_O domain (Figure 1.4), which occurs in insects during molting (SUMNER *et al.,* 1995), due to glucose depletion in yeast cells (KANE, 1995), in kidney epithelial cells (SAUTIN *et al.,* 2005), in the salivary glands of blowfly through cAMP (DAMES *et al.,* 2006) is an important mechanism of regulating the V-ATPase activity. This is a rapid process, that does not require any new protein synthesis for its re-assembly and do not involve any signal transduction pathways (PARRA and KANE, 1998) but does require an intact microtubular network (HOLIDAY *et al.,* 2000). The novel function of V-ATPase in pH-sensing mechanism and interaction with small GTPases is being suggested to be linked to the process of reversible assembly/disassembly (HURTADO-LORENZO *et al.,* 2006; MARSHANSKY and FUTAI, 2008). The function of small GTPases as "molecular switches" may be directly linked to the regulation of V-ATPase by reversible disassembly which turns this nano-machine "on/off" (MARSHANSKY and FUTAI, 2008). V-ATPases that are present in the vacuole

undergo dissociation; whereas the V-ATPase complex containing Stv1 that are localized in Golgi apparatus do not undergo dissociation (KAWASAKI-NISHI *et al.,* 2003). These results suggest that the dissociation is probably controlled by both the membrane environment and by the *a*-subunit isoform that is present in the complex. In both insects and yeasts, dissociation of the V_1V_O ATPases represents a means of preserving cellular ATP content, as the disassembly of V_1 and V_O results in a decrease in the Mg^{2+} -dependent ATPase activity and the ion pumping across the membrane (SUMNER *et al.,* 1995).

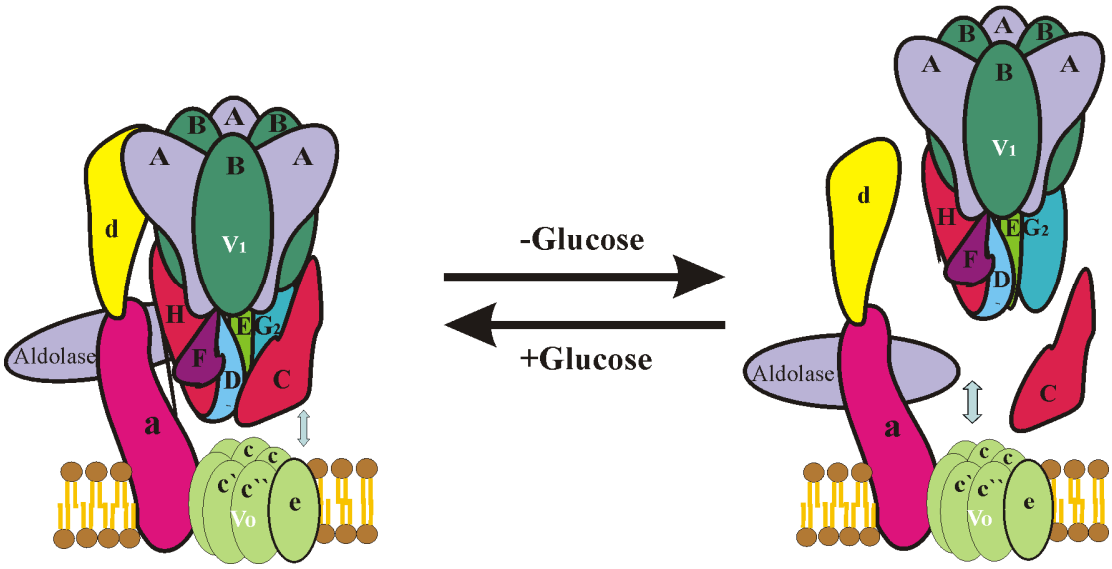

Figure 1.4: Regulation of V-ATPase activity. Reversible disassembly is observed in insects' midgut during molting (SUMNER *et al.,* 1995) in yeast cells as a response to glucose depletion which requires an intact microtubular network. V-ATPase reversible disassemble into a V_1 complex that lacks subunit C, free subunit C and V_O *in vivo*. Dissociation of V_1V_O complex may be facilitated by an altered interactions of the subunits with aldolase (LU *et al.,* 2004) and/or through altered binding of the non-homologous region of subunit A with V_O domain (SHAO *et al.,* 2004).

1.4.2 Control of reversible dissociation in yeast

Dissociation and re-association of the V_1V_O complex are two independent processes, because dissociation requires an intact microtubule (XU and FORGAC, 2001), while reassembly requires a novel protein complex called RAVE (regulator of the ATPase of vacuolar and endosomal membranes) (SEOL *et al.,* 2001). RAVE is a complex protein composed of Rav1, Rav2 and Skp1 (SMARDON *et al.,* 2002), and is proposed to interact with the V_1 sector on the G and E subunits (SMARDON *et al.,* 2002).

Another important protein that is proposed to modulate the assembly of the V_1V_O complex is the aldolase (LU *et al.,* 2004), wherein disruption of the aldolase gene causes the dissociation of the V-ATPase complex *in vivo* (in a manner that was not observed when depleting glucose-6-

phosphate isomerase). This suggests that dissociation of the V_1V_O complex is not merely a consequence of blocking glycolysis. More relevantly aldolase acts as a glucose sensor that signals for the dissociation of the V-ATPase (LU *et al.,* 2004, 2007). Subunits B, E and G in V_1 and subunit *a* in V_O domain are shown to interact with aldolase (LU *et al.,* 2004) and among these, interaction with subunit B is referred to be crucial for the assembly (LU *et al.,* 2007). Another important domain of the V-ATPase that controls the *in vivo* dissociation is the non-homologous region of the catalytic A subunit (SHAO *et al.,* 2003), where mutation in the region blocked the dissociation of V-ATPase from yeast without affecting the catalytic activity (SHAO *et al.,* 2003).

Reversible dissociation of V_1V_O complex is also shown to be regulated by the nucleotide concentration and ATP/ADP ratio (ARMBRÜSTER *et al.,* 2005). It has been hypothesized that subunit C may be the sensor of the cellular ADP:ATP ratio based on the results from photo-affinity labeling and fluorescence correlation spectroscopic (FCS) studies (ARMBRÜSTER *et al.,* 2005). The C-terminal region of subunit C, which includes residues 320-392, has been mapped to be the binding sites of nucleotides. The structural changes of subunit C due to nucleotide binding is described to be the key for reversible dissociation of both domains (WIECZOREK *et al.,* 2003), by binding of subunit C as an anchor protein to the actin-based cytoskeleton. Thus, this nucleotide binding may induce structural changes in the foot region causing a disturbance in the subunit interactions and leading to a dissociation of V_1 and V_O domain.

Protein phosphorylation, an ubiquitous mechanism known to regulate the activity of numerous proteins including ion channels and proton pumps (JOHNSON *et al.*, 2005), also participates in the regulation of reversible dissociation of V_1V_O complex. Subunits C from *Arabidopsis thaliana* and yeast undergoes major structural changes after binding of adenine nucleotides (ARMBRÜSTER *et al.*, 2005). A*t*WNK8 (*A. thaliana* With-No-lysine (K)) phosphorylates AtVHA-C (Vacuolar H^+-ATPase subunit C) at multiple sites each including two or more serine or threonine residues phosphorylated (HONG-HERMESDORF *et al.,* 2006). The importance of the foot region for the stable assembly of V_1 and V_O is significantly described by site directed mutagenesis experiments (CURTIS *et al.*, 2002). Together with the nucleotide-binding property and the phosphorylation of subunit C proves its involvement in the regulation of reversible disassociation of V_1V_O complex.

1.5 Isoforms of V-ATPases

To achieve specific target functions on the cells, various subunits of V-ATPases exhibit different isoforms, especially in higher eukaryotes and multi-cellular organisms (GOGARTEN *et al.,* 1992; KARET 2005). These includes subunit *d* (NISHI *et al.,* 2003), subunit G (SUN-WADA *et al.,* 2003), subunit C (MURATA *et al.,* 2002; SUN-WADA *et al.,* 2003), subunit *a* (KARET 2005) (NISHI 2005) and subunit E (STROMPEN *et al.,* 2005). V-ATPase subunit *a* exhibits 17 isoforms in *Paramecium tetraurelia*, representing one of the largest known isoforms of V-ATPase subunits (WASSMER *et al.,* 2006). However, in yeast all the subunits are encoded as single isoform by their respective single gene, with an exception of subunit *a*, which is produced in two different isoforms, Vph1 (vacuole specific) (MANOLSON *et al.,* 1992) and Stv1 (Golgi specific) (MANOLSON *et al.,* 1992). These two isoforms are responsible for the localisation of V_O section to vacuolar or Golgi compartments (KAWASAKI-NISHI *et al.,* 2001). An experiment conducted with a chimeric protein containing N-terminus of Golgi isoform Stv1p and C-terminus of vacuole isoform, Vph1p, when targeted to the Golgi complex did not show any reversible dissociation in response to the glucose depletion (KAWASAKI-NISHI *et al.,* 2001). This confirms that the information for correct targeting of subunit *a* is located on its N-terminus and different isoforms have varied response to physiological conditions. In addition, the C-terminus of subunit *a* has been shown to be involved in the assembly and activity of V-ATPases (LENG *et al.,* 1998). Thus, different isoforms containing V-ATPases exhibit function in the context of its location, making V-ATPase a functionally and regulatory diverse complex in the cell.

1.6 Structural features of the yeast V_1V_O ATPase

The V_1 domain consists of ATP binding sites on the interface of the alternating subunits A and B, which form the hexameric A_3B_3 headpiece. Subunit A of the yeast V-ATPase is a 68-kDa subunit that is highly conserved across organisms and shows a sequence identity of 65-75% with homologous V-ATPase subunits and nearly 25% with subunit β of F-ATP synthases (NELSON *et al.,* 1992). Subunit A contains the nucleotide-binding, glycine rich Walker sequence with two cysteine residues (MORIYAMA and NELSON, 1989). Mutagenesis studies on subunit A from yeast V-ATPase enabled to identify residues, K263 from Walker A sequence and E286, which are critical for the ATP hydrolysis. Modeling studies of subunit A have suggested the presence of aromatic residues forming an adenine-binding pocket at the catalytic sites and mutation studies have revealed their effect on the nucleotide binding (MACLEOD *et al.,* 1998, 1999).

Subunit B from yeast, a 57 kDa protein that is homologous to the subunit α of the F_1F_O-ATP synthase (BOWMAN *et al.,* 1998), lacks the nucleotide binding motifs (like the Walker sequence) that is present in the α subunit (BOWMAN *et al.,* 1998). The role of nucleotide binding sites on the B subunit is not clear, but a specific mutation leads to a time-dependent increase in the ATPase activity, indicating an important role on the regulatory mechanism of the ATPase activity (MACLEOD *et al.,* 1998). Like the F-ATP synthase, both nucleotide binding sites are located on the interface of the subunits A and B (NELSON and HARVEY, 1999). Subunit B is also observed to bind to actin (CHEN *et al.,* 2004; HOLLIDAY *et al.,* 2005) and aldolase (LU *et al.,* 2003).

Subunit C is involved in the regulation of reversible disassembly of V_1 from V_O during physiological stress such as deprivation of glucose from the media or a drop in the ATP to ADP ratio (ARMBRÜSTER *et al.,* 2005; BEYENBACH and WIECZOREK 2006; HONG-HERMESDORF *et al.,* 2006). It is also significant that subunit C is the only component of V_1V_O ATPase that is lost during this physiological regulatory process of V_1V_O disassembly (ARMBRÜSTER *et al.,* 2005; VITAVSKA *et al.,* 2005; BEYENBACH and WIECZOREK, 2006). The low resolution structure obtained from solution X-ray scattering data revealed that the hydrated subunit C from yeast has an elongated boot-shaped structure with a maximum size of 12.5 nm (ARMBRÜSTER *et al.,* 2004). The high-resolution structure of subunit C (Figure 1.5), describes a similar feature with three distinct domains, an upper head domain, an elongated neck and a large globular foot domain (DRORY *et al.,* 2004). Photoaffinity labeling and fluorescence correlation spectroscopy experiments revealed the ability of subunit C to bind ADP and ATP (ARMBRÜSTER *et al.,* 2005). The C-terminus of subunit C involving structural motif β-α-β-α which comprises residues 320-

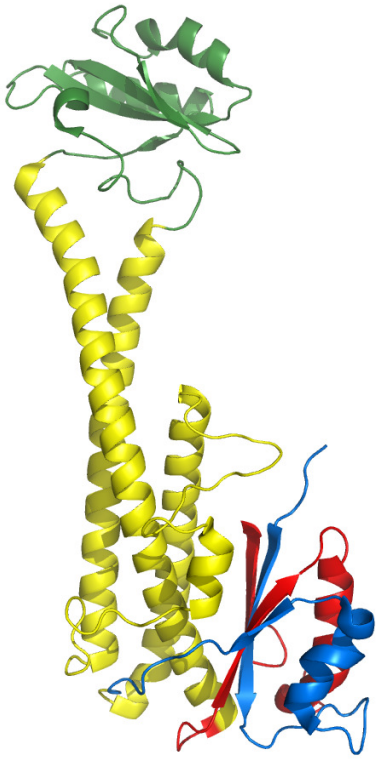

Figure 1.5: Ribbon diagram of the crystal structure of subunit C from yeast (PDB: 1U7L). A boot shaped structure with head domain (residues 167-262, green), the N-terminal (residues 1-55, blue) and C-terminal (residues 320-392, red) forming the foot region, both connected with a neck domain in yellow (DRORY *et al.,* 2004). Residues 320-392 are shown to bind the ATP molecule (ARMBRÜSTER *et al.,* 2004, 2005).

357 and 382-392 is mapped to be the nucleotide binding site (Figure 1.5, ARMBRÜSTER *et al.,* 2005). Mutational analysis of subunit C has demonstrated a critical role to balance the activities like V_1V_O assembly as well as ATPase activity (CURTIS *et al.,* 2002) by also binding to WNK kinase (With No K=Lysine domain) (XU *et al.,* 2000) and undergoing phosphorylation (HONG-HERMESDORF *et al.,* 2006). Thus, subunit C is considered as a protein that communicates with the signaling pathways and in turn contributes to the regulatory mechanism of the V-ATPase. The precise position of C subunit on the V_1V_O complex is still contradictory despite the observation of its close proximity to subunit E based on cross linking experiment (XU *et al.,* 1999; CHABAN *et al.,* 2005; JONES *et al.,* 2005).

Subunit D of V_1 domain encodes a 32 kDa protein in yeast (GRAHAM *et al.,* 1995), and its disruption resulted in the typical *vma* (Vacuolar Motor ATPase) phenotype, where mutants were unable to grow at neutral pH 7.5 and on non-fermentable carbon sources but exhibiting normal growth at pH 5.0 (GRAHAM *et al.,* 1995). Moreover, *vma8*Δ mutants failed to assemble the V_1 onto the V_O sector, besides subunit D alone was also unable to assemble with V_O in the absence of fully assembled V_1 domain (GRAHAM *et al.,* 1995). Also it has been shown that subunit D is not required for ATP hydrolytic activity in the presence of Ca^{2+} and methanol induced Mg^{2+}-dependent ATPase activity (XIE and STONE, 1988; PUOPOLO *et al.,* 1992; PENG *et al.,* 1994; GRÄF *et al.,* 1996; RIZZO *et al.,* 2003; GRÜBER *et al.,* 2000; COSKUN *et al.,* 2004). However, the detailed role(s) of subunit D is still a matter of debate. Some mutations in subunit D lower the coupling rate between proton translocation and ATP hydrolysis, and some mutations increases it (XU and FORGAC, 2000). This suggests the hypothesis that subunit D is a structural analogue of F-ATP synthase γ-subunit (XU and FORGAC, 2001).

The yeast subunit E (Vma4p), is an essential component of the V_1 assembly, as disruption of the gene on the yeast (Vma4) resulted in a disassembly of the V_1V_O complex (KANE *et al.,* 2003). Like subunit G, E is also described to be present in multiple copies per complex (OHIRA *et al.,* 2006; KITAGAWA *et al.,* 2008). Mutational analysis has demonstrated communication between subunit E and the catalytic sites at A_3B_3 hexamer and suggests potential regulatory roles for the carboxyl end of subunit E (OWEGI *et al.,* 2005). Subunit E has shown to be in a close proximity to the catalytic subunits A, B (XU *et al.,* 1999; ARATA *et al.,* 2002; RIZZO *et al.,* 2003; OWEGI *et al.,* 2005) and to subunit D (in nucleotide dependent manner, GRÜBER *et al.,* 2000) in the V_1 ATPase. It is also known to be essential for the ATPase activity (FOURY, 1990; PUOPOLO *et al.,* 1992; HO *et al.,* 1993; TOMASHEK *et al.,* 1997; XU *et al.,* 1999; CHARSKY *et al.,* 2000; LU

et al., 2001, 2002; JONES *et al.,* 2005; OWEGI *et al.,* 2005) and conformational changes on subunit E in the presence of Ca^{2+}ATP and -ADP are reported in *M. sexta* V_1 ATPase (GRÜBER *et al.,* 2000). The N-terminal segment of subunit E, that is amino acids 19-38 has been predicted to be important for its assembly with subunit G (JONES *et al.,* 2005), while the C-terminus of E is believed to have a regulatory function in V_1V_O ATPases (OWEGI *et al.,* 2005). The N-terminus of subunit E is critical for its binding with almost all the stalk subunits, including $E_{1\text{-}19}$ binding with subunit C (JONES *et al.,* 2005) and $E_{1\text{-}79}$ important for its association with subunit H (LU *et al.,* 2002). Disruption of the E-H assembly resulted in a decrease of both ATP hydrolysis and also proton transport activities of *S. cerevisiae* V-ATPase (LU *et al.,* 2002). Besides its association with the rotary subunits of V-ATPases, subunit E also interacts with the regulatory proteins like Db1, linking V-ATPases with the small G-protein Rac1 (LU *et al.,* 2001). In the human kidney, subunit E of V-ATPase assembles with the glycolytic enzyme aldolase, thereby providing a coupling mechanism with glycolysis (LU *et al.,* 2005; MIURA *et al.,* 2001). Above all, subunit E is predicted to contain an N-terminal extended structure and a globular C-terminal segment (JONES *et al.,* 2005).

Vma7p (subunit F) is a hydrophilic subunit that belongs to the V_1 domain (NELSON and HARVEY, 1999). Deficiency of subunit F on the V-ATPase affects the stability of the V_O complex, unlike the deletion of any other V_1 subunit (GRAHAM *et al.,* 1994), suggesting that this subunit would be localized in the central stalk (GRAHAM *et al.,* 2000). Cross linking experiments position subunit F in a close proximity to subunit D (TOMASHEK *et al.,* 1997) and subunit E (GRÜBER *et al.,* 2000). The loss of ATP activity by the assembled V_1V_O complex after attaching an antibody to the F subunit (AVIEZER-HAGAI, 2003), also suggest the location of subunit F on to the central stalk region. The first low resolution structure of recombinant subunit F of yeast V-ATPase, analysed through solution X-ray scattering experiment, revealed two distinct domains, a 5.5 nm long egg-like domain and a hook-like segment at the another end (BASAK *et al.,* 2011). Both the domains are connected by a linker region of about 1.5 nm long. The solution NMR

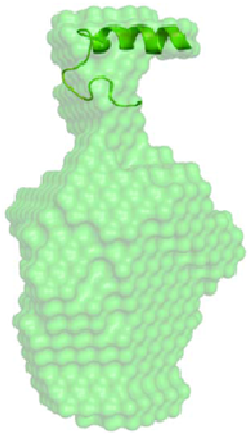

Figure 1.6: Low resolution model of subunit F of yeast V-ATPase obtained from the SAXS data. The structure represents an egg shape. The C-terminal peptide structure, determined through solution NMR (ribbon diagram), is positioned on the C-terminal end of the structure (BASAK *et al.,* 2011).

structure of $F_{90\text{-}116}$, a C-terminal synthetic peptide, displayed an α-helical region between residues 103-113 and the structure fitted well in the hook-like region (Figure 1.6) of the determined SAXS model (BASAK *et al.,* 2011).

Genetic and biochemical data reveal that subunit G is an essential component of V_1V_O ATPase in its regulation and stabilization of the complex (TOMASHEK *et al.,* 1997). The copy number of G subunit on V_1V_O complex is contradictory between two and three numbers, but recombinant subunit G forms a dimer in a gel filteration analysis and in small-angle X-ray scattering experiments (ARMBRÜSTER *et al.,* 2003) which revealed that the protein is extended with a maximum size and radius of gyration of 8.0 nm and 2.7 nm, respectively (ARMBRÜSTER *et al.,* 2003). Point mutation of subunit G on the N-terminus resulted in a complete destabilization of the V_1V_O complexes (CHARSKY *et al.,* 2000). Precipitation assays have suggested the interaction of subunit E and G on the N-termini of both the subunits (JONES *et al.,* 2005) and the interaction of subunit G with A15 and A45 of subunit B (ARATA *et al.,* 2002), which are predicted to be on the external surface of subunit B, indicates that subunit G exits as an extended protein and possibly represents a part of the peripheral stalk on V_1V_O ATPases (ARMBRÜSTER *et al.,* 2003, CHARSKY *et al.,* 2000). Requirement of subunit G for the ATPase activity, assembly of V_1V_O and inhibition of the reversible disassembly due to mutations (CHARSKY *et al.,* 2000) explains its critical role in the V_1 ATPases and V_1V_O ATPases.

Subunit H (50-kDa) is an essential component for ATPase activity but not for targeting or assembly (HO *et al.,* 1993). The crystal structure of the H-subunit showed an elongated structure consisting of two distinct segments and is primarily α-helical in nature (SAGERMANN *et al.,* 2001). The two domains of the protein are connected by a four-residue loop

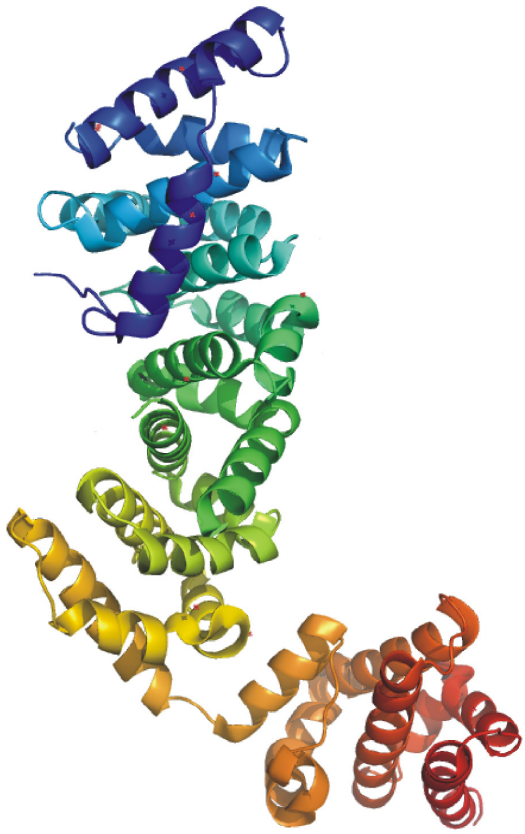

Figure 1.7: Crystal structure of the yeast V-ATPase subunit H. The structure shows an elongated feature with two distinct domains, both connected by a four residues flexible loop (SAGERMANN *et al.,* 2001).

and show a structural flexibility (Figure 1.7). Cross linking experiments showed an interaction of subunit H with subunit E (LU *et al.,* 2002). Mutation on Cys-254 of subunit A of bovine ATPase causes subunit H to dissociate from the V_1V_O complex (XU *et al.,* 1999). Cross-linking studies have also shown that subunit H and B to interact in V_1 ATPase (GRÜBER *et al.,* 2000). Subunit H is proposed to assemble with the N-terminus of subunit *a* and thus would form a stator on the V_1V_O complex (LANDOLT-MARTICORENA *et al.,* 2000).

The 250 kDa V_O domain of *S. cerevisiae* consists of four integral membrane proteins, the *c*, *c*', *c*'', and *a* subunits, and a soluble *d* subunit (POWELL *et al.,* 2000). Subunit *a* of the V_1V_O ATPase has been revealed to play an important role in the process of proton conduction (KAWASAKI-NISHI *et al.,* 2001), and its isoforms have been shown to be essential for targeting of the V-ATPase to the specific organelle (NISHI and FORGAC, 2000; KAWASAKI-NISHI *et al.,* 2001). Four isoforms of subunit *a* have been found in human and are expressed in different organelle endomembranes or plasma membrane defined by the specific function on the cell type (TOYOMURA *et al.,* 2000). Remarkably, 17 isoforms of subunit *a* are observed in *P. tetraurelia* (WASSMER *et al*., 2006*)*. The gene encoding subunit *a* on yeast was identified in the vacuolar acidification mutant, vph-1 (vacuolar pH-1) that is vacuole specific (PRESTON *et al.,* 1989). Disruption of Vph-1 is not crucial for the survival of yeast but mutants showed defects in the assembly and activity of the V-ATPase (MANOLSON *et al.,* 1992). The functional homolog of Vph-1 was identified in yeast and named as Stv-1 (Similar to Vph-1), Golgi specific, showing more than 50 % identity to the Vph-1 (MANOLSON *et al.,* 1994).

Subunit *d*, a 39 kDa protein, was observed in chromaffin granule membrane preparation (WANG *et al.,* 1988). Sequence homology amongst subunit *d* from diverse origins was observed to be conserved through evolution and suggests the essential role of this protein in the H^+-ATPase (WANG *et al.,* 1988). V_1 subunits possess the ability to assemble with V_O domain that lacks subunit *d*, and this assembly can restore the proton pumping partially (PUOPOLO *et al.,* 1992). Furthermore, it was observed that addition of subunit *d* increased the ATPase activity by two folds, indicating the putative role of the subunit in accomplishing the maximal activity of V_1V_O complex (PUOPOLO *et al.,* 1992). Disruption of the Vma6 gene from yeast genome resulted in a typical *vma* phenotype (BAUERLE *et al.,* 1993). However null mutants of Vma6p were defective in the vacuolar acidification and isolated membranes did not show detectable V-ATPase activities (BAUERLE *et al.,* 1993). Yeast cells lacking subunit *d* resulted in a condition where V_1 peripheral subunits were unable to reach and attach to the vacuolar membrane

(BAUERLE *et al.,* 1993). Considering all these facts, the position of subunit *d* on the entire V_1V_O complex is still a matter of debate. A low resolution model created from the solution X-ray scattering data (Figure 1.8), shows a boxing glove shaped molecule. The unique domain comprises of a major head part measuring 6.5 nm with a protuberance in a length of about 3.5 nm. Proteolysis of the V_1V_O ATPase from the clatherin coated vesicles resulted in a rapid cleavage of subunit *d* (ADACHI *et al.,* 1999) suggesting an exposed position on the enzyme. While the ability of subunit *a* to degrade in the absence of subunit *d* is significant on one hand (HILL and COPER, 2000), interaction of the N-terminal part of subunit *a* with the catalytic subunit A is also highlighted (LANDOLT-MARTICORENA *et al.,* 2000). This N-terminus interaction of subunit *a* to *d* may together form the peripheral stator connecting V_1 with V_O to prevent energy loss through futile rotation of V_1 with respect to V_O and reportedly suggest to interact with subunit A and subunit H (LANDOLT-MARTICORENA *et al.,* 2000; WILKENS and FORGAC 2001; THAKER *et al.,* 2007). It has also been suggested that the cavity on the boxing glove-shape structure of subunit *d* enables the *a-d* domain to bind to the non-homologous region of subunit A in the process of reversible disassembly (THAKER *et al.,* 2007; THAKER, *et al.,* 2009). These results along with the fact that subunit *a* exhibits its N- and C-terminus 18 nm and 6 nm above the membrane (RADERMACHER *et al.,* 2001), enables to suggest the model of V_1V_O ATPase with subunit *a* and *d* positioned onto the peripheral stalk.

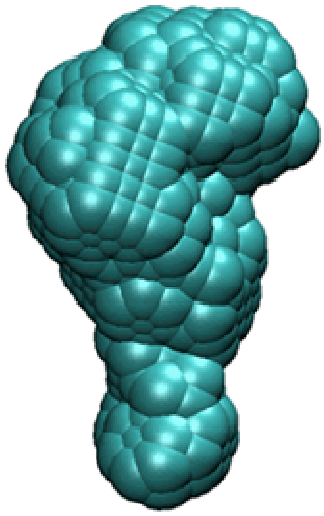

Figure 1.8: Low resolution structure of subunit *d* from yeast V-ATPase. The structure was elucidated from solution X-ray scattering (SAXS) data and shows a boxing glove shaped with a distinct head domain with protuberance and a neck domain (THAKER, YOUG R. *et al.,* 2009).

All the *c* subunits (*c*, *c*' and *c*'') are extremely hydrophobic integral membrane proteins which form an hexameric (GRAHAM *et al.,* 2003; HARRISON *et al.,* 2003) or an heptameric proteolipid ring (MURATA *et al.,* 2003). Sequence similarities suggest that the *c* and *c*' subunits have evolved by gene duplication and fusion of an ancesteral proteolipid gene resulting in a tandem repeat (NELSON and TAIZ, 1989; HIRATA *et al.,* 1997). Subunit *c* and *c*' contains four transmembrane (TM_{1-4}) helices (MANDEL *et al.,* 1988; HIRATA *et al.,* 1997; POWEL *et al.,* 2000) and subunit *c*'' has five TM helices (HIRATA *et al.,* 1997; POWEL *et al.,* 2000) with the C-

terminus exposed to the cytosolic surface (FLANNERY *et al.,* 2004). Evidence of four copies of *c* isoforms and one copy of subunits *c*' and *c*" is significant (POWELL *et al.,* 2000). Each *c* subunit contains a critical glutamate residue on the TM4 of *c* and *c*' and TM3 on *c*", that is considered to be essential for proton translocation and is accessible from the lipid phase (HIRATA *et al.,* 1997; HARRISON *et al.,* 2000; PALI *et al.,* 1995). These helices form a functional interface with subunit *a* and are involved in proton translocation (MARSHANSKY and FUTAI, 2008). The TM7 of subunit *a*, which contains a buried R735 (in yeast Vph1) is predicted to be involved in the proton translocation and is also shown to be the interface of *c* ring (MARSHANSKY and FUTAI, 2008).

1.7 Comparison of V-ATPase with A- and F-ATP synthases

Whereby the V-ATPases are called as energy transducers of the cell, A- and F- ATP synthases are energy producers. All three classes of enzymes comprise a soluble ATP hydrolyzing/synthesizing domain which is characterized as V_1, A_1 or F_1 domain that couples with the respective membrane embedded domain, characterized as V_O, A_O or F_O domain. The membrane embedded domain couples the ATP hydrolysis/synthesis occurring at the respective head domain with the ion translocation across the membrane. The details of various subunits on the three classes of enzymes are illustrated in table 1.2, where the functionally homologous subunits of respective enzymes are listed on the same row. However these similarities on the subunits may not extend to the level of sequence. Together these subunits are coupled and co-operated within the complex to produce a highly efficient energy conversion machine.

V-ATPases have subunits A_3B_3, which are homologous to A_3B_3 of A- and the $\alpha_3\beta_3$ in F-ATP synthases. Both these subunits are involved in the catalysis/regulation of the ATP hydrolysis/synthesis, respectively, in all the three classes of enzymes. V-ATPases and A-ATP synthases are closely related in terms of subunit arrangements and sequences similarities with an exception of subunits C and H that are absent on the later. One major difference of V-ATPases when compared to the A- and F-ATP synthases is the ability of V_1 head domain to reversibly dissociate from the V_O domain (SUMNER *et al.,* 1995; KANE, 1995). During this process, the stalk subunits of V-ATPases rearrange themselves to form a compact central stalk excluding subunit C and dissociate from the V_O domain to form a V_1 domain, a free subunit C and the membrane embedded V_O domain. While the number of peripheral stalks is restricted to one in F-ATP synthases, the A-ATP synthases and fully assembled V_1V_O ATPases may have a compact central stalk and one or more peripheral stalk(s). The subunits contributing to these arrangements on the

respective enzyme assembly are poorly understood. In V-ATPases and A-ATP synthases, the peripheral stalk(s) may include one or more copies of subunit(s) G and/or E, whereas F-ATP synthases include only subunits *b*. Another striking difference between the peripheral stalks of the three enzymes is that both subunit G (V-ATPase) and subunit H (A-ATP synthase) have no membrane-spanning region, when compared with the peripheral stalk subunit *b* of F-ATP synthases (HUNT and BOWMAN, 1997) and thus is assumed to interact with another subunit to fulfil this presumed role (HUNT and BOWMAN, 1997). Dimeric subunit *b* of F-ATP synthase serves to fix the F_1 domain to F_O and forms a stator through its membrane anchor, thereby preventing rotation of the F_1 domain during catalysis (HERMOLIN *et al.,* 1983; PERLIN *et al.,* 1983).

V-ATPase	**A-ATP synthases**	**F-ATP synthases**
A	A	B
B	B	α
C	-	-
-	C	-
D	D	γ
E	E	-
F	F	-
G	H	*B*
H	-	-
a (~ 100 kDa)	a (~ 100 kDa)	-
-	-	*a* (~ 28 kDa)
c, *c*', *c*'''	*c*, *c*', *c*''	*C*
d	-	-
e	-	-

Table 1.2 Subunits of the V-ATPase compared with A- and F-ATP synthases. The functionally homologous subunits of the respective three enzymes are listed on the same row.

The membrane embedded domains on the three classes of enzymes are V_O, A_O and F_O part which participate in the ion translocation through the "*c*-rings". The subunits that associate with the ion translocation includes, *c*, *c*', *c*'' and *c*''' in both V-ATPases and A-ATP synthases, where as the similar role is performed by subunit *c* in F-ATP synthases. The stoichiometry of subunit *c* is debated to be variable because of the ability of an organism to adapt to the physiological

conditions (TOMASHEK and BRUSILOW, 2000). The similarities and diversities exhibited by all the three classes of enzymes clarify the fact of an individual function on its respective location. Thus understanding the structural arrangements of various subunits on the enzyme and their possible function in the architecture, catalysis and regulation is very important.

1.8 Outline of the thesis

Chapter 1. Subunit G of the yeast V-ATPase is observed to be an elongated protein with a maximum size and the radius of gyration as 8.0 nm and 2.7 nm, respectively (ARMBRÜSTER *et al.,* 2003). Point mutation of subunit G on the N-terminus, E14A, resulted in a complete destabilization of the V_1V_O complex (CHARSKY *et al.,* 2000). Initial studies revealed that subunit G of yeast V-ATPase was not been able to be purified to high concentrations, a general requirement for any structural studies like crystallization and/or solution NMR spectroscopy. In order to understand the structure of subunit G and its possible orientation with respect to the other stalk subunits, I created the two constructs $G_{1\text{-}58}$ and $G_{61\text{-}101}$, based on the secondary structure prediction of subunit G (PSIPRED V2.5 by MCGUFFIN *et al.,* 2000). Efforts were taken to solve the structure of both, the N- and C-terminal domains of subunit G by solution NMR technique. The structures of both the constructs were well studied using molecular biology, circular dichroism and NMR spectroscopy (1D, 2D and 3D). In addition, the possible exposure of critical amino acids in subunit G constructs, which are proposed to be involved in its binding with the neighboring subunits, are discussed in detail. Earlier studies of subunit G through solution X-ray scattering have revealed the existence of a dimeric nature (ARMBRÜSTER *et al.,* 2003). To confirm this, the the diffusion coefficiency of $G_{61\text{-}101}$ peptide was studied through 1D NMR spectroscopy. Cysteine-based cross linking on the mutated full length subunit G was analysed and the possible orientation of subunit G on a dimeric model is demonstrated.

Chapter 2. Subunit G of yeast V-ATPase is observed to be essential for activity and assembly of V_1V_O-ATPases (CHARSKY *et al.,* 2000). Precipitation assays have suggested the interaction of subunit G and E on the N-termini of both subunits (JONES *et al.,* 2005). Thus the objective of this research was to study the interaction of subunit G with its neighbouring stalk subunits, including subunit E and *d*, and to characterize the epitope and residues of subunit G that contribute to the assembly. Several approaches like solution NMR spectroscopy and fluorescence correlation spectroscopy (FCS) were performed with recombinant proteins of subunit G, E, *d* and synthetic

peptides of subunit E. The epitopes of subunit G was characterized and the residues that are involved in its association with the neighbouring stalk subunits are described in details. The possible orientation of subunit G wih respect to subunits E and *d* is also illustrated.

Chapter 3. Subunit E (Vma4p) of V-ATPase from yeast is an essential component of the V_1 assembly, as disruption of the gene (Vma4) on the yeast resulted in a disassembly of the V_1V_O complex (KANE *et al.,* 2003). The N-terminal segment of subunit E, including residues 19-38 has been predicted to be important for its assembly with subunit G (JONES *et al.,* 2005, RISHIKESAN *et al.,* 2008, 2009). Subunit E is observed to be critical for its binding with almost all the stalk subunits, including $E_{1\text{-}19}$ binding with subunit C (JONES *et al.,* 2005) and $E_{1\text{-}79}$ described to assemble with subunit H (LU *et al.,* 2002). Thus, the importance of subunit E is valued and the protein was purified to homogeneity for structural studies. Unfortunately, initial studies in the laboratory resulted in the degradation of subunit E within a short period of time, which further hindered any structural studies (GRÜBER *et al.,* 2002). Therfore, the N-terminus of subunit E from yeast V-ATPase was segmented to first 69 residues, cloned, expressed, purified to homogeneity and the solution structure was studied through NMR spectroscopy involving various 1D, 2D and 3D experiments. The solution structure enabled me to understand the charge distribution across the surface of subunit E construct, $E_{1\text{-}69}$ and the exposed charged amino acids along with the conserved residues that may be predicted to interact with the neighbouring stalk subunits are described.

The C-terminus of subunit E is predicted to be globular with a mixture of α and β strands on the secondary structure (PSIPRED V2.5 by MCGUFFIN *et al.,* 2000). Recently, the C-terminus of subunit E from A_1A_O ATP synthase, a homologous region of V_1V_O ATPase, was solved through X-ray crystallography (BALAKRISHNA *et al.,* 2010). Thus, the proposed C-terminal globular domain of subunit E, $E_{133\text{-}222}$ from yeast V-ATPase, was cloned, expressed and purified to homogeneity. Efforts were also made to study the solution structure of the same through NMR spectroscopy involving 1D, 2D and 3D experiments. The first 2D structure of $E_{133\text{-}222}$ was determined through these studies which enabled me to describe the specific sequence and/or the region that forms the α-helix and β-strands on the globular domain. Based on the above results and biochemical evidences from the literature, the possible orientation of subunit E with respect to other stalk subunits and the catalytic head domain of the V_1V_O complex are discussed.

2.1 Materials

2.1.1 Chemicals

All the chemicals used in the current study were of at least analytical grade. Chemicals were purchased from the following companies:

Buffers, salts and electrophoresis chemicals	Sigma (St. Louis, MO, USA), USB (Sampscott, MA), Calbiochem (Darmstadt, Germany), Fluka (Sigma, Buchs Germany), Roth (Karlsruhe, Germany), Serva (Heidelberg, Germany)
Agarose, SDS, Glycine, APS etc.	Bio-Rad (Hercules, CA, USA)
Pefabloc^{SC}	BIOMOL (Hamburg, Germany)
PMSF	Sigma (St. Louis, MO, USA)
DTT	Hoefer (San Francisco, CA, USA)
Ni^{2+}-NTA	QIAGEN (Hilden)
$^{15}NH^4Cl$	Cambridge Isotopes Lab (USA)
^{13}C Glucose	Cambridge Isotopes Lab (USA)
LB Media	BD (Sparks, MD, USA)
Antibiotics	Calbiochem, Sigma and Gibco (Invitrogen)
IPTG	Fermentas (Glen Burnie, MD, USA)
BSA	GERBU (Heidelberg, Germany)

2.1.2 Molecular biology materials

Genomic DNA	*Saccharomyces cerevisiae* (AH104 strain)
Primers	1st Base and Research Biolabs (Singapore)
Peptides	NTU proteomics core facility (Singapore)
Pfu and T4 DNA Polymerase	Fermentas (Glen Burnie, MD, USA)
dNTP's	Fermentas (Glen Burnie, MD, USA)
*Nco*I *and Sac*I	Fermentas and New England Biolabs
T4 DNA Ligase	Fermentas and NEB
CIAP	Fermentas (Glen Burnie, MD, USA)
Miniprep Plasmid Kit	Qiagen (Hilden, Germany)

Nucleobond AX mediprep Kit	Macherey-Nagel & Co (Düren, Germany)
Escherichia coli expression strains	DH5α, BL21 (DE3) and Rosetta-gami™ 2 (DE3)
pET-9d1	(GRÜBER *et al.,* 2002) (Novagen, Germany)

2.1.3 Chromatography

2.1.3.1 Ion exchange

RESOURCE™ Q (6 ml)	GE Healthcare (Uppsala, Sweden)

2.1.3.2 Gel filtration

Superdex 75 HR (10/30)	GE Healthcare (Uppsala, Sweden)

2.1.3.3 Instruments and accessories

Akta FPLC, Akta Prime	GE Healthcare (Uppsala, Sweden)
Millex Filters (0.45 μM)	Millipore (Bradford, USA)
Syringe, needles and accessories	BD Biosceinces

2.1.3.4 Protein concentrators, estimation and dialysis

Centriprep YM3 and YM 5	Millipore (Ireland)
Amicon ulta (3-10kDa)	Millipore (Ireland)
Protein estimation: BCA Assay Kit	Pierce (Rockford, IL, USA)
Protein estimation: Bradford reagent	Bio-Rad

2.1.4 Other instrumentation

PCR Thermocycler:	
Biometra T personal	Biometra
Biometra T gradient	Biormetra
Micropulser Electroporator	Bio-Rad
Ultraspec 2100 Pro Spectrophotometer	GE Healthcare
Sonoplus Sonicator	Bendelin

2.1.5 Computer softwares

Vector NTI 10.3.0	Invitrogen
Quantity One	Bio-Rad
Topspin 1.3	Bruker
SPARKY 3.110	University of California (San Francisco, USA)
CYANA 2.1	Kimmo Paakkonen and Peter Günter (Japan)
TALOS 98.040	CORNILESCU *et al.,* 1999 (NIH, USA)
MOLMOL	KORADI *et al.,* 1996 (ETH, Zürich)
NMRpipe	DELAGLIO *et al.,*1995 (NIH, USA)
Nmr Draw	Howard Hughes Medical Institute, USA
PyMOL v0.99	DeLano Scientific LLC, USA

2.2 Methods

2.2.1 Vector preparation

Reagents

Luria-Bertani (LB) media:	*10 g/l Tryptone*
	5 g/l Yeast extract
	5 g/l NaCl
DNA Purification:	*Qiagen Kit*
Plasmid Isolation:	*Nucleobond AX Kit*
Enzymes:	*NcoI, SacI and CIAP*

pET9-d (+) (GRÜBER *et al.,* 2002) vector was prepared from a previously cloned vector on DH5α cells. A single colony containing DH5α/vector was inoculated overnight on 500 ml LB (Luria-Bertani) culture medium with kanamycin antibiotic. After 16 to 20 h of growth, the cells were harvested by centrifugation at 6,000 x *g* for 10 min at 4 °C and the plasmid DNA from the clone was isolated and purified by using the Nucleobond AX or Qiagen midi-prep kit as per the manufacturer's protocol. Isolated plasmid was checked for the quality and purity on a 1 % agarose gel and later was quantitated by UV spectrophotometer at 260 nm absorption wavelength. Plasmid was digested with respective vector specific restriction enzymes in sequential manner at 37 °C and the extent of digestion was confirmed by running 1 µl of the restricted sample on an agarose gel (1%). Upon confirmation of the successful restriction, the mixture was purified by Qiagen purification kit by the prescribed protocol. Finally the pET9-d (+) vector, with both the ends restricted with the respective restriction enzymes was dephosphorylated with CIAP (calf intestinal alkaline phosphatase) (Fermentas, MD, USA) for 20 min at 37 °C. The concentration of final product of the vector was estimated on an UV-spectrophotometer.

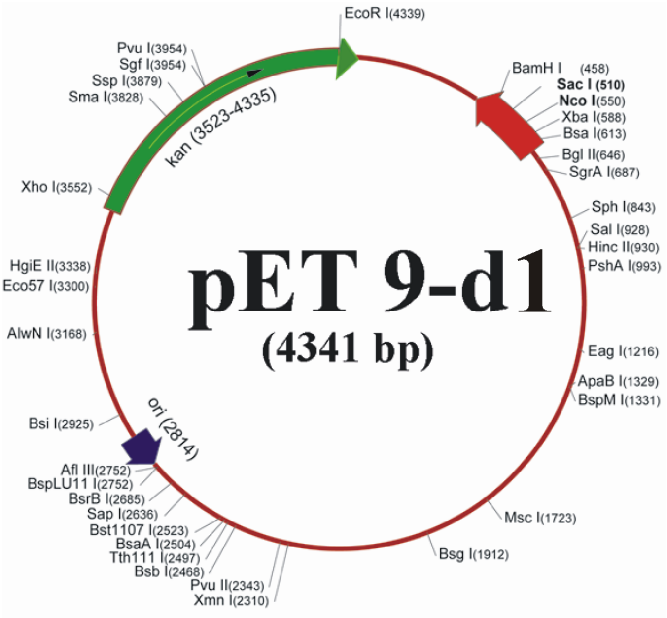

Figure 2.2.1: Vector Map of modified pET-9d1(+) (GRÜBER *et al.,* 2002). Vector shows the full map and unique multiple cloning sites (MCS) that has been used to clone various genes.

2.2.2 Cloning of yeast subunit G and E constructs from yeast V-ATPase

2.2.2.1 PCR amplification of the DNA fragments

Various constructs of subunit G and E were amplified by using the appropriate primers (as listed in table 2.1) and genomic DNA of *Saccharomyces cerevisiae* strain AH104 as template.

Constructs		Primer Sequence (5'-3')
G_{1-58}	Forward	CAT-GCC-ATG-GTA-TCC-CAA-AAA-AAC-GGA-ATT G
	Reverse	CGT-TCG-AGC-TCT-TAG-CAT-TCA-AAC-TCC-TTC-AAT-TC
G_{61-114}	Forward	TAT-GCC -ATG-GAT-AAT-GCC-GGT-GGT-GTT-G
	Reverse	CGT-TCG-AGC-TCT-TAG-CAC-AAG-GCA-TTG-ATA-TG
G_{1-77}	Forward	CAT-GCC-ATG-GTA-TCC-CAA-AAA-AAC-GGA-ATT-G
	Reverse	TTT-GAG-CTC-TTA-TTG-CAC-ACC-CGC-CTC-TG
G_{1-101}	Forward	CAT-GCC-ATG-GTA-TCC-CAA-AAA-AAC-GGA-ATT-G
	Reverse	CGT-TCG-AGC-TCC-ATA-GTC-TCG-ATC-AAG-ATC-T
G_{61-101}	Forward	TAT-GCC-ATG-GAT-AAT-GCC-GGT-GGT-GTT-G
	Reverse	CGT-TCG-AGC-TCC-ATA-GTC-TCG-ATC-AAG-ATC-T
E_{1-69}	Forward	TTT-CCA-TGG-CCT-CCG-CTA-TTA-CTG
	Reverse	CTA-TGA-GCT-CTC-ATG-CCT-TCT-TCA-ACT-TG
$E_{133-233}$	Forward	TTT-CCA-TGG-TGT-TGG-AAC-CTA-AGG-CGA-TTG
	Reverse	TTT-GAG-CTC-TCA-ATC-AAA-GAA-CTT-TCT-TG
$E_{133-222}$	Forward	TTT-CCA-TGG-TGT-TGG-AAC-CTA-AGG-CGA-TTG
	Reverse	TTG-AGC-TCT-CAC-AAT-TCC-AAT-CTG-ATG-GCG

Table 2.1: Sequences of primers used for subunit G and E constructs. The primers were synthesized either at 1st Base Pte Ltd, Singapore or at Research Biolabs Pte Ltd, Singapore.

PCR reaction was setup in a total volume of 50 µl on ice as mentioned below with the appropriate concentration of the constituents as mentioned below. All reagents were pipetted on to a PCR tube kept on ice all the time and the reagents were mixed by short centrifugation. PCR thermocycler (Biometra T personal) was preheated to 95 ºC before reaction tubes were placed inside the machine. All the constructs of subunits G and E were amplified under the same program of thermocycler program as described, with a variation in the annealing temperature. The cycle denaturation, annealing and extension steps were repeated for another 29 cycles.

Cycle steps	Temperature	Time	
Lid	99 ºC		
Initial denaturation	95 ºC	3-5 min	
Cycle denaturation	95 ºC	0.5-1 min	30 cycles
Annealing	50-68 ºC	0.5-1 min	
Extension	72 ºC	1-2 min	
Final extension	72 ºC	10 min	
End	4 ºC		

The amplified PCR products were stored at -20 °C, if the experiments were to be continued on the following day. About 5 µl of the amplified PCR products were applied onto an analytical agarose gel (1 to 2.5 %) with appropriate DNA ladder, to check the quality of the amplified products. If the products were sufficiently pure, remaining reaction mixture was applied onto the preparative agarose gel and the amplified products corresponding to the size of the DNA were excised to a clean tube. This DNA product was then purified by gel extraction kit (QIAGEN) as per manufacturer's protocol. The purified DNA may be finally eluted in 80 µl volume of water or elution buffer Tris/HCl (pH 8.0). Followed by gel extraction, purity of the PCR product was estimated on an analytical agarose gel (1 to 2.5 %) with 1 µl of the sample. The concentration of amplified DNA was estimated on an UV-spectrophotometer at 260 nm wavelength.

2.2.2.2 Restriction of the DNA fragments

Purified DNA was double digested overnight at 37 ºC by taking appropriate amount of *Nco*I and *Sac*I enzymes. After overnight digestion, the reaction mixture was again purified by enzyme reaction purification kit from QIAGEN. The purified DNA sample was finally eluted in 30 µl volume of elution buffer Tris/HCl (pH 8.0). The purity and quality of the DNA sample were checked on the respective agarose gel (1 to 2.5 %) and the quantity of the DNA was estimated on a spectrophotometer at 260 nm absorption wavelength.

2.2.2.3 Ligation of DNA fragments and vector

The pure DNA with incorporated restriction sites were ligated with the pET9-d1(+) vector and the reagents used were as follows:

Ligase buffer (10x)	1.5 µl
Vector (V)	50-100 ng
Insert (I)	Variable (1-5 times of vector)
T4 Ligase	1 µl
MilliQ water	Variable
Total	15 µl

The ligation mixture was kept at room temperature for 60 min. The reaction was terminated by precipitation of DNA from rest of the reaction mixture by adding 85 µl of Milli Q water to make a final volume of 100 µl. 1 ml of butanol was added into the mixture and mixed thoroughly. Then the mixture was centrifuged at 13,000 x *g* for 10 min at room temperature. Supernatant was discarded gently and the pellet was resuspended in 150 µl of 70% ethanol and centrifuged again for 5 min. Supernatant was removed and the pellet was re-dissolved in 10 µl of elution buffer (10 mM Tris-HCl, pH 8.5). 5 – 10 µl of ligation mixture was used for the transformation into *Escherichia coli* DH5α cells. On the next day, colonies were picked from the transformation plate and grown at 37 °C. The plasmid DNA was isolated using standard protocol (QIAGEN mini-prep kit) and subsequently double digested and applied onto a 1% agarose gel, in order to confirm the ligated insert. Size of insert and vector were compared with appropriate controls and markers. Correct plasmid with the right insert was finally transformed into *E. coli* BL21 (DE3) cells for protein production and they were grown on 30 µg/ml kanamycin-containing LB agar plates. *E. coli* BL21 (DE3) expression strains were purchased from Novagene (Darmstadt, Germany).

2.2.2.4 Electroporation transformation

Reagents

SOB media *20 g/l Tryptone*
5 g/l Yeast Extract
0.58 g/l NaCl
0.18 g/l KCl
10 ml Mg solution (1 M $MgCl_2.6H_2O$, 1 M $MgSO_4$)

SOC media: *SOC*
100 mM Glucose

Electro-competent cells were prepared as per the protocol on Current Protocols in Molecular Biology (Wiley Inter-Science) manual. Plasmid DNA (1-50 ng), which contains the vector and the amplified DNA, was added to 80 – 100 µl of the competent cells and incubated on ice for 5 – 10 min. Electroporation was done at constant voltage of 2500 V (Micropulser Electroporator, Bio-Rad) and the cuvette was immediately placed back on the ice for 1 min. Later 1 ml of pre-warmed LB or SOC (SOB + 100 mM Glucose) media was added to the mixture and was incubated at 37 °C for 1 h. Appropriate dilutions were prepared before plating out on antibiotic selection plates.

2.2.3 Protein production and purification of truncated subunits G and E

2.2.3.1 Induction test

Reagents
4x Lysis buffer: *250 mM Tris/HCl, pH 6.8*
9.2 % SDS
40 % Glycerol
0.2 % Bromophenol Blue

Upon successful cloning of the truncated subunits G (G_{1-58}, G_{61-114}, G_{61-101}, G_{1-77} and G_{1-108}) and E (E_{1-69}, E_{13-233} and $E_{133-222}$) constructs, the respective clones were checked for protein production by supplementing the culture with isopropyl-β-D-thio-galactoside (IPTG). This is achieved by picking up 5 – 10 individual colonies randomly from the respective selection plates and growing at 37 °C to an OD_{600} of 0.6 - 0.8 with constant shaking at 180 – 200 rpm on Infors HT Minitron shaker. Protein production was initiated by adding IPTG to a final concentration of 1 mM and continued to grow at 30 – 37 °C with constant shaking at 180 – 200 rpm for 3 – 4 h. Simultaneously, the respective control cultures were left un-induced under the identical conditions for comparison. After the induction period, the cells were pelleted down and re-suspended with 50 µl of 1x lysis buffer in the presence of 1 mM DTT (Dithiothreitol) as final concentration. The control cultures were also treated the same way and the re-suspended cell mass were heated at 95 ºC for 5 min. 15 – 20 µl of each sample with the respective control were loaded onto a 17 % SDS polyacrylamide gel (LAEMMLI 1970).

2.2.3.2 Solubility test of recombinant proteins

Reagents

100 mM phenylmethylsulfonyl fluoride (PMSF)
1.25 M DTT

The produced protein was tested for solubility in various buffers. 50 ml of culture was grown at 37 °C and at an OD_{600} of 0.6 - 0.8, the culture was induced with 1 mM of IPTG as final concentration. Cells were pelleted down in 5 equal fractions by centrifuging at 10,000 x g for 10 min. Cells from each centrifuged fraction was dissolved separately in 500 µl of five individual buffers as listed below:

	Buffers
Buffer 1	50 mM Tris/HCl (pH 9.0) and 200 mM NaCl
Buffer 2	50 mM Tris/HCl (pH 7.5) and 200 mM NaCl
Buffer 3	50 mM MES (pH 6.5) and 150 mM NaCl
Buffer 4	50 mM HEPES/HCl (pH 7.0) and 200 mM NaCl
Buffer 5	25 mM Na_2PO_4 (pH 6.8) and 150 mM NaCl

Freshly prepared protease inhibitor, PMSF of 1 – 2 mM (dissolved in 70% isopropanol) was added. Reducing agent, DTT, was added in all the preparations to a final concentration of 1 mM. These resuspension was sonicated at 20 % power with KE 72 tip of sonicator (Bandelin Sonoplus) three times for one min each with a cooling interval of two min between the cycles. The cells were centrifugated at 10,000 x g and the supernatant were separated and transferred to a fresh tube. The pellet was re-suspended in the same volume of the identical buffer. All the steps were carried out on ice. 10 – 15 µl of the pellet and the supernatant from each buffer sets were loaded onto a 17% SDS gel, respectively.

The *E. coli* cells having the gene of subunits G (G_{1-59}, G_{61-114}, G_{1-77}, G_{1-101} and G_{61-101}) and E (E_{1-69}, $E_{133-233}$ and $E_{133-222}$) were grown on 30 µg/ml kanamycin-containing LB agar plates. To express the truncated subunit G and E constructs, liquid cultures were shaken in LB medium containing kanamycin (30 µg/ml) for about 20 h at 30 °C until an optical density OD_{600} of 0.6-0.7 was reached. The cultures were supplemented with IPTG to a final concentration of 1 mM, in order to over express the recombinant protein. Following incubation for another 4 h at 30 °C, the cells were harvested by centrifugation at 6,000 x *g* for 20 min at 4 °C and frozen in liquid nitrogen and stored at – 80 ºC until purification. All the cells were lysed on ice by sonication for 3 x 1 min at 50% power in appropriate buffer G_{1-59}, G_{61-114}, G_{1-77}, G_{1-101}, G_{61-101}, E_{1-69}, $E_{133-233}$ and $E_{133-222}$ in buffer A (50 mM HEPES, pH 7.0, 200 mM NaCl, 2 mM PMSF). The lysate was

cleared by centrifugation at 10,000 x *g* for 35 min at 4 °C, the supernatant was passed through a filter (0.45 µm pore-size) and supplemented with Ni^{2+}-NTA resin. The His-tagged protein was allowed to bind to the matrix for 2 h at 4 °C by mixing on a sample rotator (Neolab), and eluted with an imidazole-gradient (25 mM – 250 mM) in buffer A. Fractions containing His-tagged proteins were identified by sodium dodecyl sulfate (SDS) - polyacrylamide gel electrophoresis (PAGE) (LAEMMLI, 1970) pooled and concentrated using Centriprep YM-3 (3 kDa molecular mass (MM) cut off) spin concentrators (Millipore) to a final volume of 500 µl. In order to remove the imidazole, the concentrated protein sample was injected on to a pre-equiliberated gel filtration column (Superdex 75 HR (10/30), GE Healthcare). The protein fractions were eluted on to a 1.5 ml collection tube against the same buffer A. 5 µl of the respective fractions were loaded on to an SDS gel with respective protein marker for reference. The appropriate protein fractions corresponding to the peak were pooled and were concentrated to a final volume of 300 µl. The purity and homogeneity of all the protein samples were analyzed by SDS-PAGE (LAEMMLI, 1970). SDS-gels were stained with Coomassie Brilliant Blue G250.

2.2.4 Protein quantification by bicinchoninic acid method

The bicinchoninic acid (BCA) assay is available in kit form from Pierce (Rockford, IL, USA.). The protein concentration was estimated as per the manufacturer's instructions. BSA (0 – 250 µg/ml) was used as standard. In general, two dilutions of protein samples were taken and each of them was measured in triplicate to avoid any error in the measurement. Optical density was measured at 562 nm against blank.

2.2.5 Circular dichroism spectroscopy

Circular dichroism (CD) is used to determine the secondary structure content of proteins and peptides. Steady-state CD spectra were measured in the far-UV light (185-260 nm) using a Chirascan spectropolarimeter (Applied Photophysics) under continuous purging of N_2 gas. Spectra were collected in a 60 µl quartz cell (Hellma) with a path length of 0.1 mm, at 20 °C and a step resolution of 1 nm. The readings were taken with the average of 1 sec at each wavelength, and the recorded ellipticity values were the average of three determinations for each sample at a concentration of 2 mg/ml. The spectrum for buffer was subtracted from that of the protein. CD values were converted to mean molar residue ellipticity in units of deg x $dmol^{-1}$ x aa^{-1} using the software Chirascan version 1.2 (Applied Photophysics) by giving appropriate cell path length,

molecular weight, number of amino acid residues and protein concentration values. This baseline corrected spectrum was used as input for computer methods to obtain predictions of secondary structure. Final plotting was done in MS Excel (2003).

2.2.6 Production and purification of subunit G mutants

Mutant constructs of subunit G were produced by overlap extension polymerase chain reaction (PCR) method (HO *et al.,* 1989). The single mutants A72C, A74C and A81C of entire subunit G, respectively, were generated by overlap extension polymerase chain reaction method using the *Vma10* gene as a template (ARMBRÜSTER *et al.,* 2003). In separate PCRs, two fragments of subunit G were amplified by using primers *a* and *b* and primers *c* and *d*, respectively. The amplified fragments coding the N- and C-terminal regions were fused together via a second PCR using the primers *a* and *d*. The overlap allowed one strand from each fragment to act as a primer on the other, and extension of this overlap by flanking primers (*a* and *d*) in second PCR reaction resulted in the product. Same flanking primers (*a* and *d*) were used for all the mutant constructs. The sequences of flanking primers (*a* and *d*) and internal primers (*b* and *c*) used for the mutants are enlisted in table 2.2.2. The internal primers (*b* and *c*) contain the mutation. A flow chart summarizing the procedures involved in site directed mutagenesis is given in figure 2.2.2. The above mentioned constructs were cloned, expressed, and purified as explained in section 2.2. The cells were lysed using buffer A (50 mM HEPES, pH 7.0, 200 mM NaCl, 1 mM PMSF). Imidazole was removed by gel filtration column Superdex S75 (10/30, GE Healthcare) using the same buffer as mentioned above. The purity and homogeneity of all protein samples were analyzed by SDS-PAGE (LAEMMLI 1970). SDS-gels were stained with Coomassie Brilliant Blue G250. Protein concentrations were determined by the bicinchoninic acid assay (BCA; Pierce, Rockford, IL. USA).

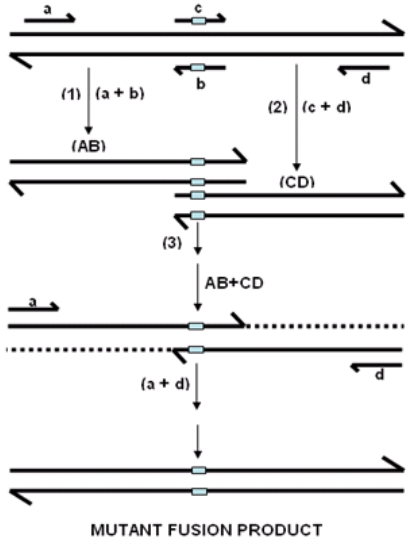

Figure 2.2.2. **A flow chart of site directed mutagenesis.** Illustration of the steps involved in site directed mutagenesis using overlap extension polymerase chain reaction (HO *et al.,* 1989).

Flanking primers		Primer sequence (5'-3')
Primer a	Forward	TTT CCA TGG CCT CCG CTA TTA CTG
Primer b	Reverse	CGT TCG AGC TCT TAG CAC AAG GCA TTG ATA TG

Mutant constructs		Primer sequence (5'-3')
A72C	Forward	GAA TTG GAA AAG AAA TGT GAG GCT GGT GTG-C
	Reverse	GCA CAC CAG CCT CAC ATT TCT TTT CCA ATT C
A74C	Forward	GAA AAG AAA GCA GAG TGT GGT GTG CAA GGT GAA
	Reverse	TTC ACC TTG CAC ACC ACA CTC TGC TTT CTT TTC
A76C	Forward	GTG CAA GGT GAA TTA TGC GAG ATT AAG AAA ATT GC
	Reverse	GCA ATT TTC TTA ATC TCG CAT AAT TCA CCT TGC AC

Table 2.2.2. Subunit G cysteine mutants of V-ATPase from the yeast genome. Sequences of flanking primers (*a* and *d)* and internal primers (*b* and *c)* used for subunit G mutant constructs. The primers were synthesized either at *1st Base Pte Ltd.,* Singapore or at *Research Biolabs Pte. Ltd.,* Singapore.

2.2.7 Disulphide bond formation analysis in subunit G using $CuCl_2$

The G subunit mutant proteins A72C, A74C and A81C (2 mg/ml each) were supplemented with 5 µM of $CuCl_2$ as a zero length cross-linker for 20 min on a sample rotator at 4 °C. The reaction was stopped by addition of 1 mM ethylenediaminetetraacetic (EDTA). Samples were dissolved in DTT-free dissociation buffer, and applied to an SDS-polyacrylamide gel as described above.

2.2.8 Dimer model of $G_{61\text{-}101}$

The average model of the NMR structure of $G_{61\text{-}101}$ was docked with itself in order to identify the dimer formation. Docking studies were performed using the web interface of the protein docking software GRAMM (TOVCHIGRECHKO *et al.,* 2006), which does a global search using the Fast Fourier Transform methodology to identify the best rigid body conformations between the two proteins. The first fifty complex configurations were analyzed, which were scored based on soft Lennard-Jones potential, evolutionary conservation of predicted interface, statistical residue–residue preference, volume of the minimum, empirical binding free energy and atomic contact energy. The best docking model was chosen from these 50 complex configurations in such a way that it should have not more than 8 Å distance for the Cα atoms of the A72 and A81 with A72' and A81', respectively, in the dimer complex. This dimer model was

then optimized using the program Swiss-PdbViewer 3.7 (GUEX and PEITSCH, 1997) by carrying out energy minimization *in vacuo* with the GROMOS96 43B1 parameter set, without reaction field as implemented in the program. For fast energy convergence, initially 200 steps of Steepest Descent protocol was carried out followed by multiple steps of Conjugate Gradient technique until the derivative convergences to 0.050 kJ/mol.

2.2.9 Peptide synthesis

The peptides from yeast V-ATPase namely, $E_{1\text{-}18}$ ($_{1}$MSSAITALTPNQVNDELN$_{18}$) and $E_{18\text{-}38}$ ($_{18}$NKMQAFIRKEAEEKAKEIQLK$_{38}$), were synthesized at the peptide core facility, School of Biological Sciences, NTU on Liberty Automatic Microwave Peptide Synthesizer (CEM, USA) using N-(9-fluorenyl) methoxycarbonyl (Fmoc) chemistry on a Rink amide MBHA resin (Novabiochem, Germany). The C-terminal amidated peptides were purified by reverse-phase high performance liquid chromatography (RP-HPLC) on a Dynamax C-18 column (Varian Inc., USA) eluted with a linear 5-100% gradient of acetonitrile in 0.04% aqueous trifluoroacetic acid. The identity of the purified peptide was confirmed by MALDI-TOF mass spectrometry (4800 MALDI TOF/TOF, AB Applied Biosystems MDS Sciex, USA). The purity of the peptides was confirmed by electrospray ionization (ESI) mass spectrometry.

2.2.10 Nuclear magnetic resonance (NMR) spectroscopy

NMR spectroscopy can be used to determine the structure of proteins in solution and to study biochemical and biophysical properties such as protein-ligand interaction, to demonstrate new binding partners as well as to map the binding regions down to single amino acid level. Specific nuclei such as hydrogen, one of the most receptive and abundant NMR active nuclei besides other isotopes such as ^{15}N, ^{13}C, ^{31}P etc. can be observed in magnetic resonance. Any nuclei having odd number of protons and neutrons, which exhibits net intrinsic magnetic momentum and angular momentum, can be defined as NMR active (WÜTHRICH *et al.,* 1982; WÜTHRICH, 1986). All the NMR experiments were collected on Bruker Avance 600 MHz machines at NTU, NMR core facility.

2.2.10.1 Isotopic labeling (^{15}N, ^{13}C) of proteins

Reagents:

Minimal Media (M9): *42 mM Na_2NPO_4*
22 mM KH_2PO_4
8.5 mM NaCl
1 g/L $^{15}NH_4Cl$
0.1 mM $CaCl_2$
2 mM $MgSO_4$
10 % D-Glucose
30 µM $FeCl_3$
5 ng/L Thiamin
Antibiotic
LB Media

For the production of uniformly labelled ^{15}N and ^{15}N- ^{13}C recombinant proteins in *E. coli* BL21 (DE3), M9 minimal media was used. All unlabeled reagents were standard laboratory reagents grade. All solutions were prepared using Milli-Q water (Millipore, Billerica, MA). 50 ml of overnight culture was grown. The cells were pelleted down by centrifugation at 5,000 x g at room temperature. Then the pellet was washed twice with LB media following a final wash in 1 x M9 media and finally resuspended in 10 ml of M9 media. 1 ml of final resuspension was inoculated per 500 ml. Cells were shaken at 37 ºC till an OD_{600} of 0.6 - 0.7 was achieved. The cultures were supplemented with IPTG to a final concentration of 1 mM and were further grown for 4 h at 37 ºC for overexpression of the respective proteins. These cells were harvested at 6,000 x *g* for 20 min at 4 °C and frozen in liquid nitrogen and stored at -80 ºC until purification.

2.2.10.2 One dimensional (1D) NMR spectroscopy

One dimensional NMR spectra of various proteins were collected in order to check the folding pattern of the proteins. Unlabeled protein sample was used to measure the 1D spectrum at various temperatures ranging from 288 K to 303 K and in 25 mM PO_4 (pH 6.8) buffer in the presence of 10 % D_2O (v/v), which is used to lock the signal. Protein concentrations varied from 100 to 500 µM. All the experiments were recorded at the core facility on the Bruker Avance 600 MHz machine. Proteins are orders of magnitude larger than the small organic molecules. Because of the increased number of each element present in a single molecule (protein), the basic 1D NMR spectra becomes packed with overlapping signals to an extent, where analysis is impossible. Therefore, multidimensional (2D and 3D) NMR experiments were carried out to resolve the overlapping region.

2.2.10.3 Two dimensional (2D) NMR spectroscopy

In order to analyze the three dimensional (3D) NMR data, it was important to get the resonance assignment for the protein (truncated subunit G and E), i.e. to find out the chemical shift in each dimension corresponding to each atom on the protein. ^{15}N Heteronuclear Single Quantum Coherence (HSQC) experiment was the frequently used NMR spectroscopy for subunit G, which has a typical two-dimensional spectrum with one axis for ^{1}H and the other for a heteronucleus (^{15}N). The spectrum contains one single peak for each amide bond on the protein. Thus the number of peaks corresponds to the number of amino acids on the protein. ^{15}N labelled proteins in 90 % H_2O and 10 % D_2O in 25 mM PO_4 (pH 6.8–7.0) buffer with/without 200 mM NaCl and 10 mM EDTA was used to collect 2D HSQC. A series of spectrum were recorded at various temperatures ranging from 288 to 303 K and with significant (100 – 500 µM) protein concentrations.

2.2.10.4 Three dimensional (3D) NMR spectroscopy

^{15}N-^{13}C labelled samples were used to record the experiments that were able to transfer magnetization over the peptide bonds and thus connect different spin systems through bonds. This was attributed through the following experiments, HNCO, HNCACO, CBCACONH and HNCACB. All the four experiments had a HSQC plane expanded with the carbon dimension. Sequential assignments were done by matching the shifts of each spin system's own and previous carbons.

The side chain proton and carbon atoms were analysed from HCCCONH and (H)CCCONH experiments, respectively. 3D ^{15}N-NOESY-HSQC spectrum was recorded using a mixing time of 200 ms, which gives the chemical shift values of all the proton atoms on the amino acids and also shows the inter-molecular and intra-molecular connectivity between the amino acids. All the two- and three-dimensional experiments made use of pulsed-field gradients for coherence selection and artifact suppression, and utilized gradient sensitivity enhancement schemes. Quadrature detection in the indirectly detected dimensions was achieved using either the States/TPPI (time-proportional phase incrementation) (MARION *et al.,* 1989) or the echo/anti-echo method (BAX *et al.,* 1980; CLARIDGE *et al.,* 1999). Baseline corrections were applied wherever necessary. The proton chemical shift was referenced to the methyl signal of DSS (2, 2-dimethyl-2-silapentane-5-sulphonate (Cambridge Isotope Laboratories) as an external reference to 0 ppm. The ^{13}C and ^{15}N chemical shifts were referenced indirectly to DSS (2, 2-dimethyl-2-

silapentane-5-sulfonate). All the NMR data were processed using Bruker Avance spectrometer in-built software Topspin and NMR pipe (DELAGLIO *et al.,* 1995). Peak-picking and data analysis of the Fourier transformed spectra were performed with the SPARKY program (KNELLER and GODDARD, 1997).

2.2.10.5 Resonance assignment

In the initial stage of any investigation of nuclear magnetic resonance data for a protein, each resonance associated with a particular nucleus in the protein molecule must be assigned. The information useful for the sequence specific assignment for a protein is of three types: via scalar couplings, via dipolar coupling and via the chemical shift. Different strategies are employed for the resonance assignments depending on the type of the sample: unlabeled proteins or isotopically labeled proteins (CAVANAGH *et al.,* 1995). Even for a small protein it is impossible to resolve all resonance lines in a one-dimensional spectrum. Assignments can be obtained using the sequential assignment approach based on homonuclear two-dimensional correlation spectroscopy (COSY) or total correlation spectroscopy (TOCSY) (BRAUNSCHWEILER and ERNST, 1983) and 2D nuclear Overhauser effect spectroscopy (NOESY). TOCSY experiment is used to identify the resonance position within each amino acid spin system and the NOESY experiment is used for the sequential assignment of the spin systems present in the amino acids. For a protein/peptide NMR spectrum, amide hydrogens are generally the best resolved set of resonances and resonate between 6-12 ppm. The side chain resonance assignments are generally done by examining the peaks in the backbone amide regions. This process is known as the sequential assignment strategy developed by Wüthrich (WÜTHRICH, 1990). The sequential assignment strategy is not useful for larger molecules (>10 kDa) because of the overlapping NMR signals that complicate the assignments. Such systems require the addition of a third dimension by the replacement of the naturally abundant isotope ^{14}N with ^{15}N and ^{12}C by ^{13}C. Here, the assignment is based on triple resonance experiments allowing further decrease in the overlap of NMR signals. There are six triple resonance experiments commonly used in chemical shift assignments of the backbone atoms of the protein: HNCO, HN(CA)CO, HNCACB, CBCA(CO)HN, HNCA and HN(CO)CA.

The HNCO experiment gives the chemical shifts of the previous amino acid's ^{13}CO, while the HN(CA)CO gives the previous amino acid's ^{13}CO and the same amino acid's ^{13}CO chemical shift values. Sequential assignment can then be undertaken by matching the shifts of each spin

system's own and previous carbons. Figure 2.2.3 shows the transfer of magnetization in the HNCO and HN(CA)CO. Figure 2.2.4 reveals ^{15}N plane of HN(CA)CO, where the peak with a stronger intensity is the amino acid's own ^{13}CO, while the weaker intensity peak belongs to the previous amino acid's ^{13}CO atom. In case of the HNCO experiment, only one peak will appear for each amide ^{13}CO shifts.

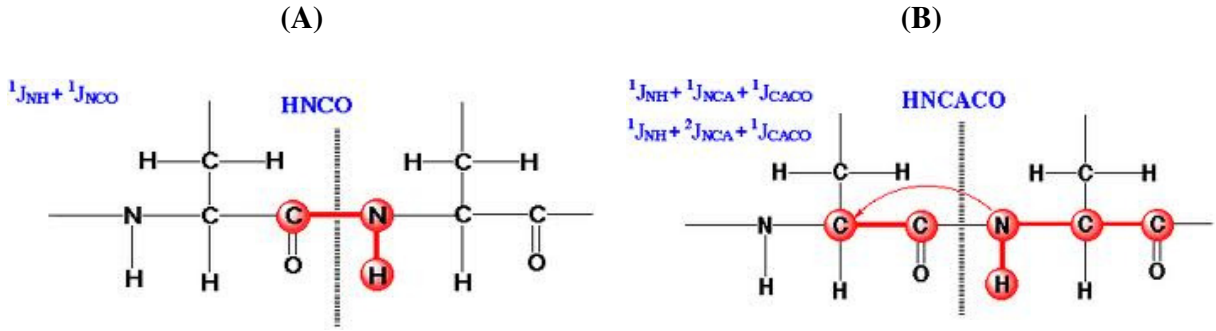

Figure 2.2.3: Transfer of magnetization in the HNCO and HN(CA)CO experiments. (A) The HNCO experiment provides sequential connectivities by making use of ^{15}N-^{13}CO J coupling (~ 15 Hz). **(B)** HN(CA)CO experiment provides sequence correlations by transferring the coherence via the intervening ^{13}CA spin (CAVANAGH *et al.*, 1995).

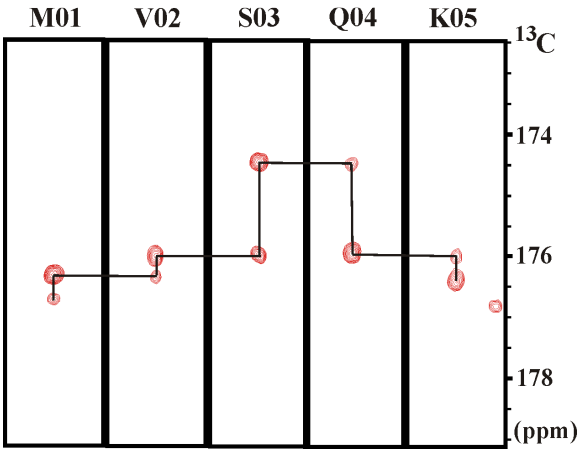

Figure 2.2.4: Strip plots of the previous and same residues carbonyl peaks obtained from the HNCACO experiments. The carbonyl peaks are obtained in the range between 174 and 178 ppm. The previous residue peaks are less intense than compared to the same residue peaks and the sequential connectivity of the previous and the same residues carbonyl peaks for the first five residues in the $G_{1\text{-}59}$ sequence are shown with the connectivity line.

The next four experiments are grouped in pairs in a similar way, providing a mean of double-checking the chemical shift data. The details of transfer of magnetization (Figure 2.2.5A and B) and an example of the assignment of five residues of truncated subunit G ($G_{1\text{-}59}$) is shown in figure 2.2.5C with respect to HNCACB and CBCA(CO)NH experiments. These two

experiments take into account both the $^{13}C^{\alpha}$ as well as $^{13}C^{\beta}$ values for the sequential assignments of residues. They are extremely useful in case of degeneracy of $^{13}C^{\alpha}$ values. In addition, $^{13}C^{\alpha}$ and $^{13}C^{\beta}$ values can provide information about the type of amino acid. In the same way, the experiments HNCA, HN(CO)CA are also used in the backbone assignment of the proteins. HNCA experiments correlates the amide ^{1}H and ^{15}N chemical shifts of one amino acid to the $^{13}C^{\alpha}$ chemical shifts of the previous residue by using ^{15}N-^{13}CO J coupling (7-11 Hz). The HN(CA)CO experiment can give correlations of ^{1}H and ^{15}N spins to the $^{13}C^{\alpha}$ chemical shifts of the previous and same residue. Thus, when the HNCA experiment is used in conjunction with HN(CO)CA experiment, it provides a method to sequentially assign the amide ^{1}H, ^{15}N and $^{13}C^{\alpha}$ resonances.

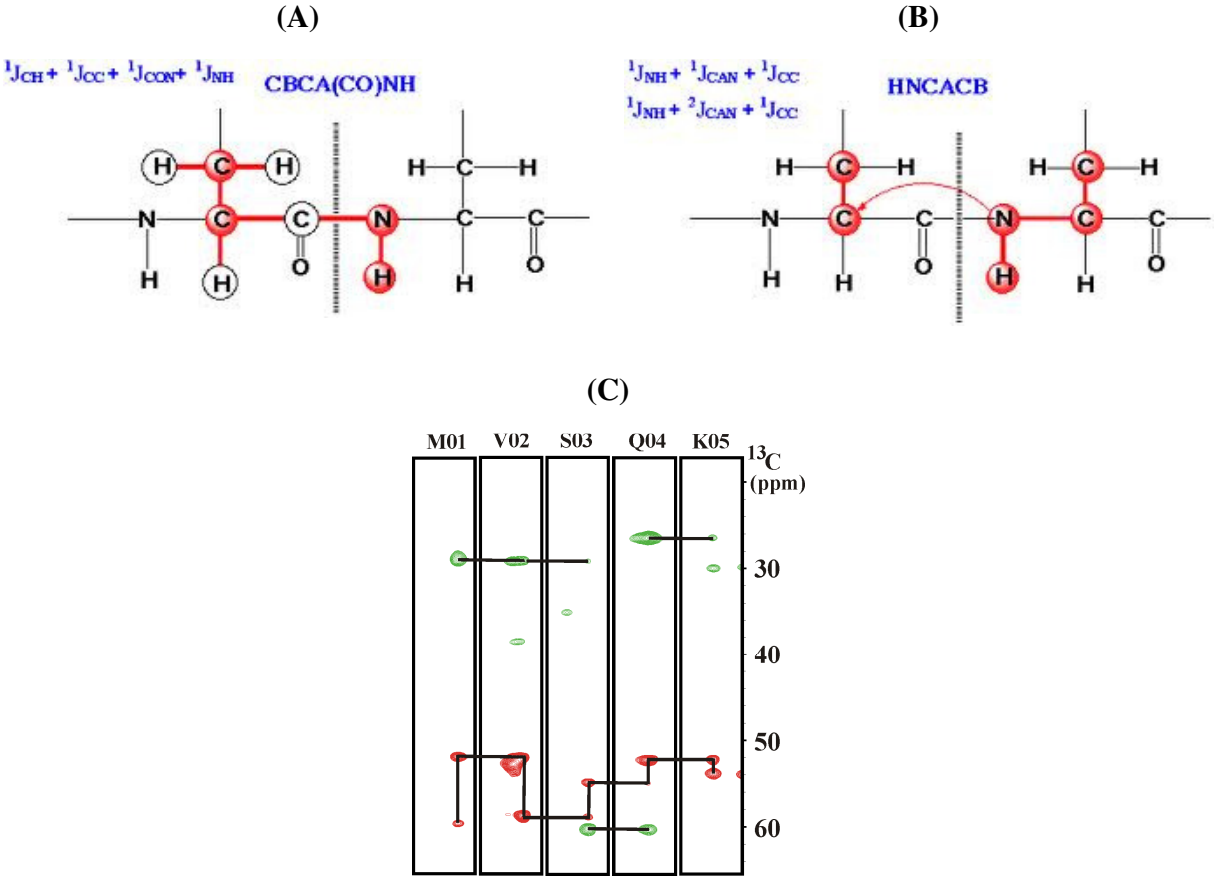

Figure 2.2.5: Transfer of magnetization in the CBCA(CO)NH and HNCACB. **(A)** CBCA(CO)NH experiment correlate the $^{13}C\alpha$ and $^{13}C\beta$ resonances with the amide 1H and 15N resonances of the previous residue whereas HNCACB **(B)** correlates the $^{13}C\alpha$ and $^{13}C\beta$ resonances with the amide ^{1}H and ^{15}N resonances of the same and the previous residue (CAVANAGH *et al.,* 1995). **(C)** An example of assignment of five residues (M01, V02, S03, Q04 and K05) by HNCACB experiment in case of subunit G ($G_{1\text{-}59}$) of V-ATPase from yeast.

After successfully assigning the backbone of residues in ^{1}H-^{15}N HSQC spectrum by using three sets of experiments (HNCA and HN(CO)CA; HNCACB and CBCA(CO)HN; HNCO and HN(CA)CO), the side chain (^{13}C and ^{1}H) chemical shifts were assigned by using mainly three experiments: (H)CC(CO)NH-TOCSY, H(CC)(CO)NH-TOCSY and HCCH-TOCSY. The first two experiments (H)CC(CO)NH-TOCSY, H(CC)(CO)NH-TOCSY provide the correlation of ^{1}H and ^{15}N amide resonances of one residue with the ^{13}C side chain and ^{1}H side chain resonances, respectively, of the previous residue (Figure 2.2.6). The 3D HCCH-TOCSY experiment is specifically designed to correlate side-chain aliphatic proton and ^{13}C resonances via ^{13}C-^{1}H and ^{13}C-^{13}C J-coupling constants (CAVANAGH *et al.,* 1995).

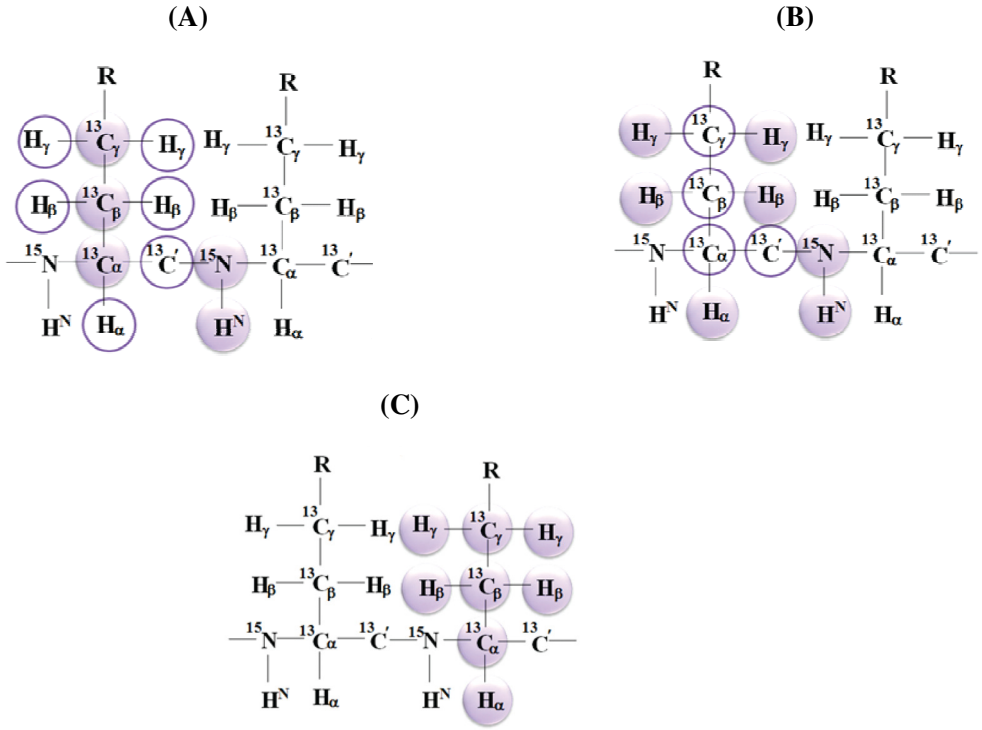

Figure 2.2.6: Transfer of magnetization in the (H)CC(CO)NH-TOCSY (A), H(CC)(CO)NH-TOCSY (B) and HCCH TOCSY (C) (CAVANAGH *et al.,* 1995).

2.2.10.6 Binding studies with NMR

NMR spectroscopy is used to identify the important residues for protein-protein interaction (TAKEUCHI and WAGNER 2006; VAYNBERG and QIN 2006). With respect to the other techniques, NMR has an advantage of monitoring the interactions at the amino acid level. ^{1}H-^{15}N heteronuclear single quantum coherence (HSQC) spectrum of labeled protein was used as starting point at optimized condition. Then the ligand protein/peptide was added in increasing amount at the same temperature and buffer conditions. A series of ^{1}H-^{15}N HSQC spectra were

recorded at each concentration of the binding partner. 100 µM - 500 µM of ^{15}N labeled protein was used for the reference spectrum. Unlabeled binding partner was added in increasing amounts to a molar ratio of 1:1 to 1:2 and chemical shift perturbations were monitored in ^{1}H ^{15}N HSQC spectrum. A typical illustration of the peak position change in the HSQC spectrum upon addition of a binding patner is shown in figure 2.2.7. Experiments were performed on a Bruker Avance 600 MHz machine using Topspin for acquisition and processing of spectra. Respective spectra were overlapped to monitor chemical shift changes, further analysis were done in SPARKY (KNELLER and GODDARD 1997).

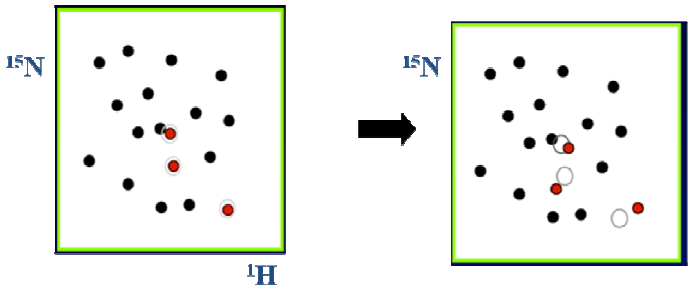

Figure 2.2.7: Illustration of change in peak position in ^{1}H-^{15}N HSQC spectrum. Upon addition of binding partner, the change in the spectrum is illustrated by red color peaks when compared to native black color spectrum (CAVANAGH *et al.,* 1995).

2.2.10.7 Diffusion coefficient measurements

The translational diffusion rates were measured by monitoring the 1D ^{1}H signal decay due to the molecular diffusion in z-direction of the sample by using PFGs (Pulsed-field gradient) at variable concentrations of $G_{61\text{-}101}$. In each experiment, the PFG strength was linearly increased from 2 to 95 G/cm, with a translational diffusion delay of 200 ms and total encoding and decoding gradient durations of 5 ms. The diffusion rates were estimated using TopSpin (Bruker BioSpin).

3.1.1 Introduction

Vacuolar ATPases (V-ATPases) are ATP-dependent proton pumps that play an important role in the pH homeostasis of various intracellular compartments to allow several cellular processes (FORGAC, 1999; FUTAI *et al.,* 2000; NELSON *et al.,* 2000). These V-ATPases are large multisubunit complexes that are organized into two domains that operate by a rotary mechanism (NISHI and FORGAC, 2002). The V_1 domain comprises of catalytic subunit A and nucleotide binding subunit B in a stoichiometry of A_3:B_3 and the so-called stalk subunits in a proposed stoichiometry of C_1:D_1:E_X:F_1:G_2:H_X (LOLKEMA *et al.,* 2003; KLUGE *et al.,* 2003). The integral and proton transducting V_O domain consists of six different subunits in a stoichiometry of a_1:d_1:c_{4-5}:c'$_1$c"$_1$:e_1 (INOUE *et al.,* 2003; MÜLLER and GRÜBER, 2003).

Physical characterization of subunit G by gel filteration and native gel electrophoresis indicated that subunit G forms a dimer in solution (XU *et al.,* 1999). Purified recombinant subunit G of V-ATPase was mono-dispersed and showed an apparent molecular mass of 28 ± 2 kDa in the solution X-ray scattering experiment (ARMBRÜSTER *et al.,* 2003). This data yielded a maximum dimension of 8.0 ± 0.3 nm and a radius of gyration of 2.7 ± 0.2 nm inferring an elongated molecule (ARMBRÜSTER *et al.,* 2003). The protein has been shown to interact with the N-terminus of subunit E (JONES *et al.,* 2005). So far, no high resolution structural knowledge is available on the stalk subunit G, which has been proposed to be essential for the assembly of V_1V_O ATPase (TOMASHEK *et al.,* 1997 and CHARSKY *et al.,* 2000) and the activity of V_1 (TOMASHEK *et al.,* 1997; GRÜBER *et al.,* 2002; RIZZO *et al.,* 2003) as well as V_1V_O ATPase (TOMASHEK *et al.,* 1997; CRIDER *et al.,* 2007). The secondary structure prediction (PSIPRED V2.5 by MCGUFFIN *et al.,* 2000) of subunit G (Figure 3.1.1) shows an extended helix from residues N_4 to V_{102}, leaving an unstructured region of four residues from N_{61} to G_{64}. The C-terminal 12 residues after the helix region are proposed to be unstructured as well. Keeping this information in mind, five constructs were created; G_{1-59}, G_{61-114}, G_{61-101}, G_{1-77} and G_{1-101}. The structural information of the N-terminal domain of G subunit could be achieved from G_{1-59} and the insight on the C-terminus could be

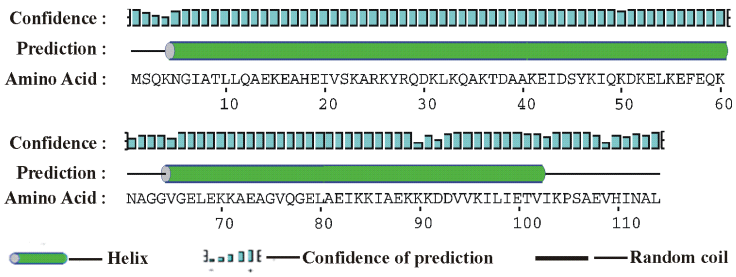

Figure 3.1.1: Secondary structure prediction of subunit G of V_1V_O ATPase from *S cerevisiae*, calculated using the program PSI-Pred (MCGUFFIN *et al.,* 2000).

obtained from $G_{61\text{-}114}$. Since the C-terminus of the subunit is unstructured and to prevent the problem of oligomerization, a shorter construct on the C-terminus was also created ($G_{61\text{-}101}$), deleting the 12 residues at the very end. An extended N-terminal construct $G_{1\text{-}77}$ will give the information on the unstructured region in between the N- and C-terminus helix. Efforts are also taken to get the full length of G subunit cloned ($G_{1\text{-}101}$).

3.1.2 Expression and purification of subunit G ($G_{1\text{-}59}$, $G_{61\text{-}114}$, $G_{61\text{-}101}$, $G_{1\text{-}77}$ and $G_{1\text{-}101}$)

Subunit G constructs, namely $G_{1\text{-}59}$, $G_{61\text{-}114}$, $G_{61\text{-}101}$, $G_{1\text{-}77}$ and $G_{1\text{-}101}$, were amplified through PCR amplification method using *Vma10* gene as a template (ARMBRÜSTER *et al.,* 2003). The amplified gene products in all the five constructs were specific and accurate with respect to the DNA marker. Figure 3.1.2 shows the amplified gene fragment of $G_{1\text{-}59}$, $G_{61\text{-}114}$, $G_{61\text{-}101}$, $G_{1\text{-}77}$ and $G_{1\text{-}101}$, respectively.

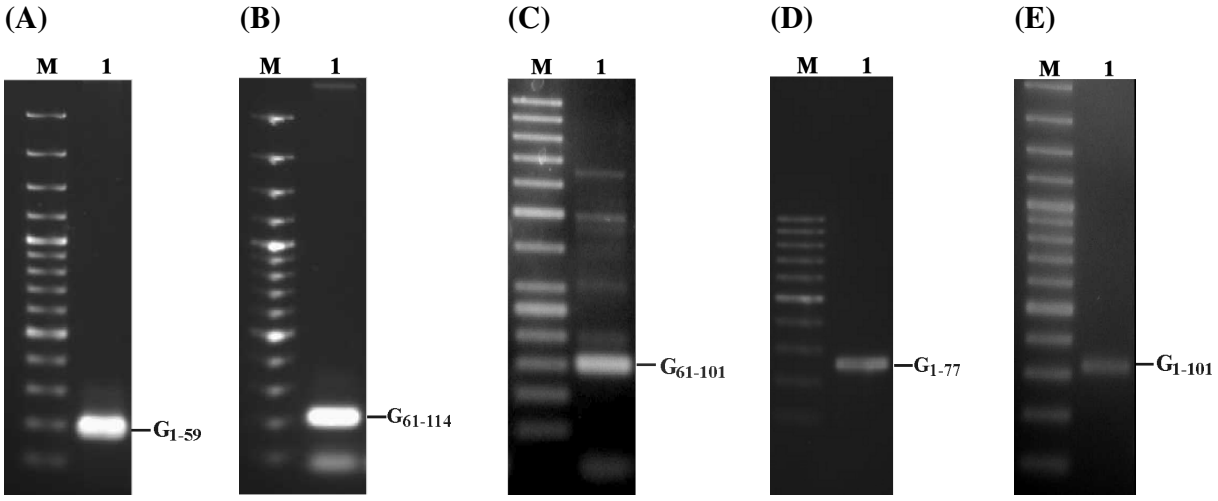

Figure 3.1.2: PCR amplification of G subunit. **(A)** $G_{1\text{-}59}$, **(B)** $G_{61\text{-}114}$, **(C)** $G_{61\text{-}101}$, **(D)** $G_{1\text{-}77}$ and **(E)** $G_{1\text{-}101}$. The amplified products were checked for its accuracy against the respective DNA markers in a 1.7 % agarose gel.

Following the amplification of the respective genes coding for $G_{1\text{-}59}$, $G_{61\text{-}114}$, $G_{61\text{-}101}$, $G_{1\text{-}77}$ and $G_{1\text{-}101}$, the PCR products were purified and incorporated with *Nco1* and *Sac1* restriction sites. These products were then ligated with pET9d1-His_3 (GRÜBER *et al.,* 2002) and the correct plasmid containing vector and the respective insert were transformed into expression cells *E. coli* BL21 (DE3). These cells were grown on 30 µg/ml kanamycin containing LB agar-plates. Random isolated colonies from these agar-plates were picked up and grown in a small volume of 4 ml to analyse the expression of the respective proteins. At an OD_{600nm} of 0.6, the cultures were supplemented with IPTG to a final concentration of 1 mM and were further grown for the over-expression of the respective proteins for 2- 3 h. Figure 3.1.3 shows the over-expression patterns

of all the five constructs, His_3-G_{1-59}, His_3-G_{61-114}, His_3-G_{61-101}, His_3-G_{1-77} and His_3-G_{1-101}. All the selected colonies from respective clones showed a good induction pattern after 4 h with more protein production in cultures supplemented with IPTG than the respective control cultures.

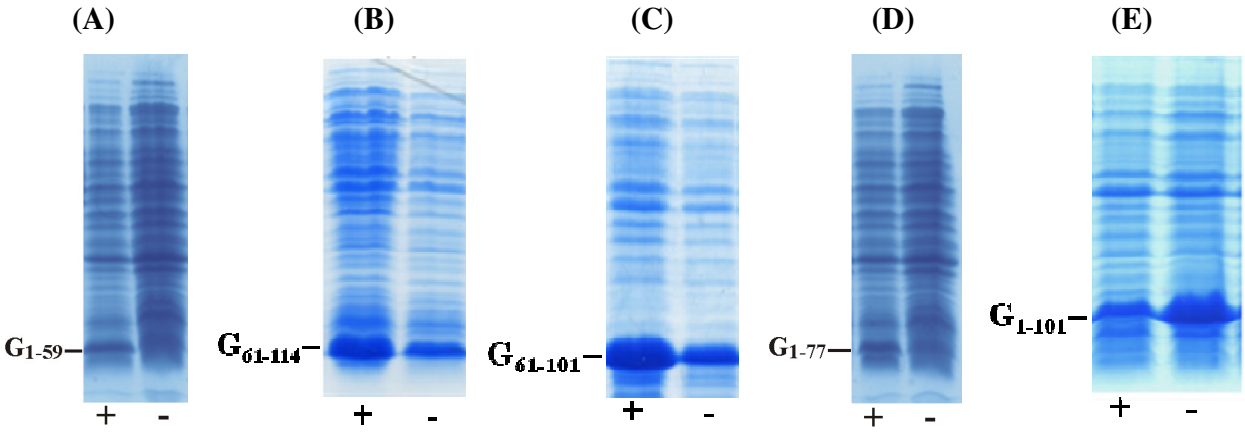

Figure 3.1.3: 17% SDS-PAGE showing over-expression pattern of recombinant subunit G. The culture containing the over-expressed protein and its respective control were lysed using the 5x-lysis buffer, heated at 95 ºC for five minutes and 15 µL was loaded on to the gel. **(A)** His_3-G_{1-59}, **(B)** His_3-G_{61-114} **(C)** His_3-G_{61-101}, **(D)** His_3-G_{1-77} and **(E)** His_3-G_{1-101} in BL21 after 4 h of induction with 1 mM of IPTG at 30 ºC. (+) and (-) are respective induced and uninduced cultures.

The produced proteins His_3-G_{1-59}, His_3-G_{61-114}, His_3-G_{61-101}, His_3-G_{1-77} and His_3-G_{1-101} were purified through affinity column, Ni^{2+}-NTA resin, against 50 mM HEPES (pH 7.0) and 150 mM NaCl buffer with 0.8 mM DTT and 1mM PMSF (Figure 3.1.4).

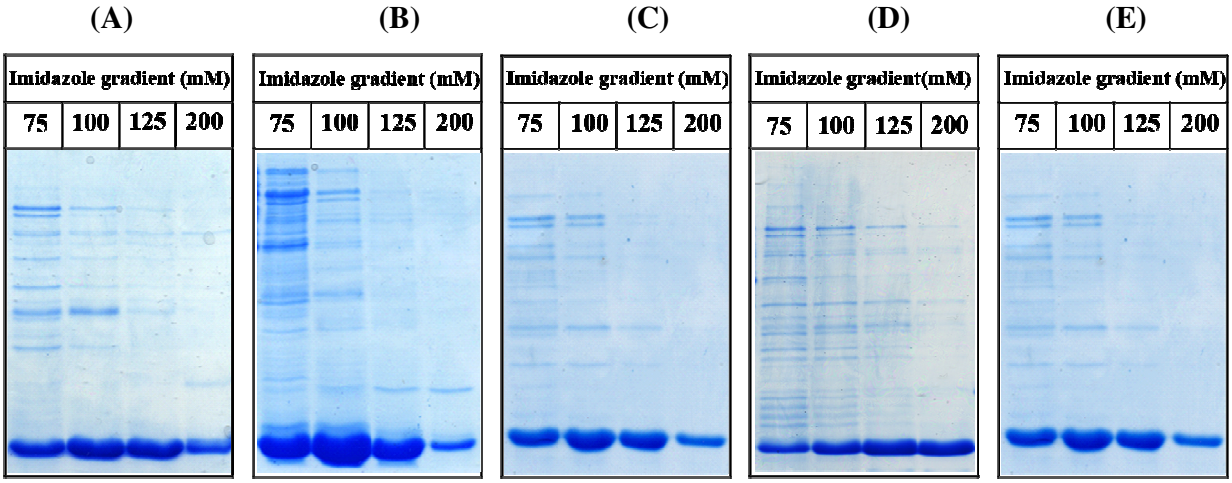

Figure 3.1.4: Ni^{2+}-NTA purification of truncated G subunit proteins. The protein bound to affinity coloumn, Ni^{2+} resin, was eluted through increasing concentrations of immidazole gradient. The fractions containing pure protein which ranges from 75 to 200 mM immidazole was loaded on a 17% SDS gel, to show the elution profile of G_{1-59} **(A)**, G_{61-114} **(B)**, G_{61-101} **(C)**, G_{1-77} **(D)** and G_{1-101} **(E)**.

The His3-tagged subunit G proteins were mostly found as the soluble fractions and were eluted between the imidazole concentrations of 75 mM to 200 mM. All fractions containing the respective His_3-tagged protein were pooled together and seperated through size exclusion

column (Superdex HR75), against the respective buffer conditions. Figure 3.1.5 shows the elution chromatogram of His_3-G_{1-59} (A), His_3-G_{61-114} (B), His_3-G_{61-101} (C), His_3-G_{1-77} (D) and His_3-G_{1-101} (E). The fractions containing the respective proteins were concentrated using Centriprep YM-3 (3 kDa molecular mass cut-off) spin concentrator and 1 µl of the respective concentrated protein sample (G_{1-59}, G_{61-114}, G_{61-101}, G_{1-77} and G_{1-101}), where loaded on to the gel and showed a high purity (insert; on Figure 3.1.5).

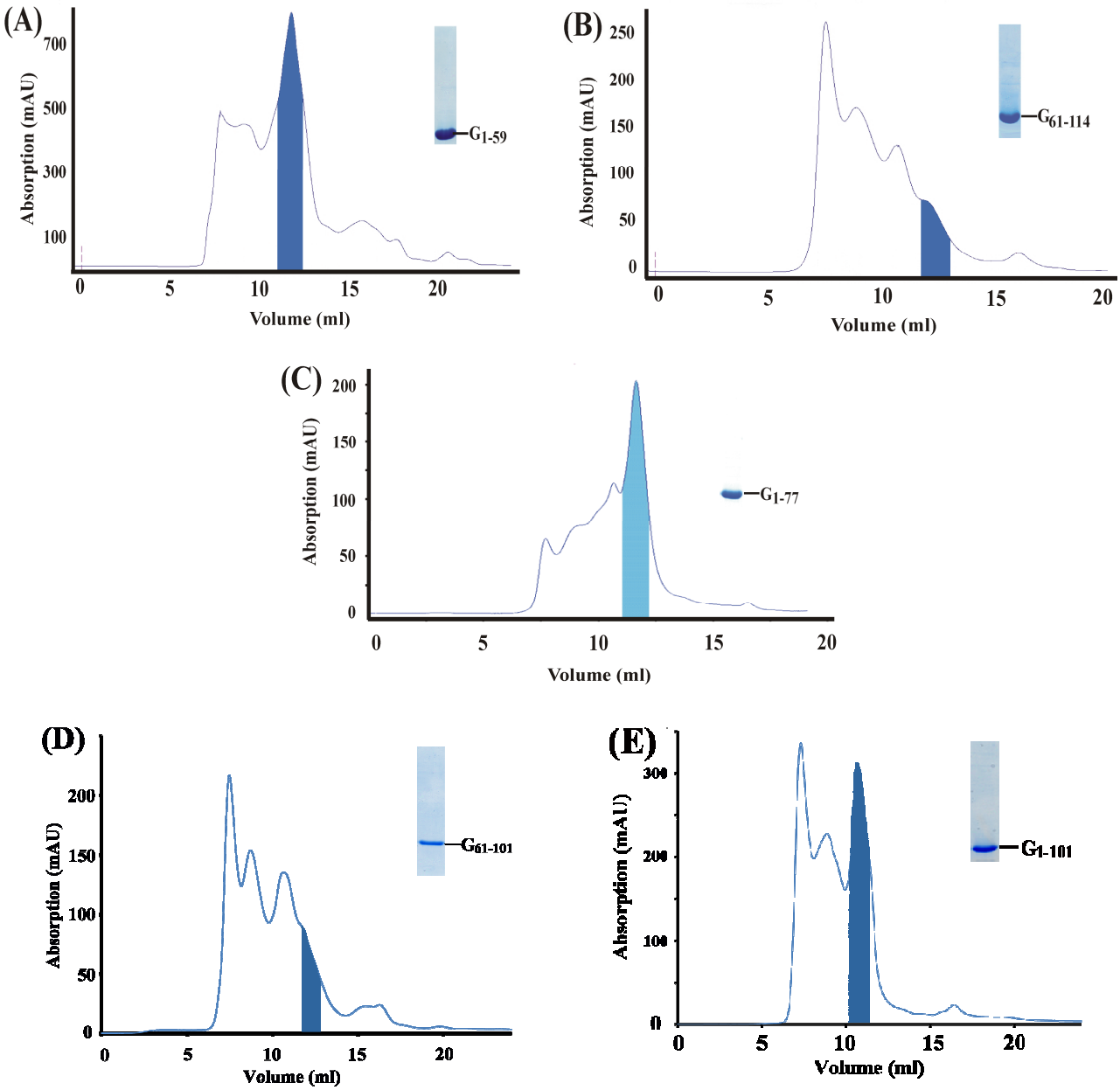

Figure 3.1.5: Purification of G subunit proteins by size exclusion column, Superdex HR75. Elution chromatogram of G_{1-59} **(A)**, G_{61-114} **(B)**, G_{1-77} **(C)**, G_{61-101} **(D)** and G_{1-101} **(E)**, where G_{1-59} and G_{1-77} was eluted in 50 mM HEPES (pH 7.0), 150 mM NaCl, 0.8 mM DTT. Truncated G subunit protein were eluted in 50 mM HEPES (pH 7.0), 150 mM NaCl, 0.8 mM DTT and 1 mM PMSF. The respective shaded peaks were concentrated with YM-3 and 1 µl was loaded on a 17% SDS gel to show the purity of the protein (top right corner of the chromatogram).

3.1.3 Approach to study the structure of subunit G through NMR spectroscopy

Based on the secondary structure prediction (Figure 3.1.1, PSIPRED V2.5 by McGuffin, 2000) of subunit G, five constructs (G_{1-59}, G_{61-114}, G_{61-101}, G_{1-77} and G_{1-101}) were cloned, expressed and purified to homogeneity. Preliminary NMR analysis of G_{1-59} (2D ^{1}H ^{15}N HSQC) gave a well dispersed spectrum with all peaks of the amide protons on the protein and also enabled to proceed further on towards the structural studies of subunit G (see section 3.1.5).

Approaches were also taken to obtain a similar result for the C-terminus of the subunit G (G_{61-114}). But the protein did oligomerize at high concentrations above 1 mM (Figure 3.1.6A). Therefore we created the third construct of subunit G, which is G_{61-101}, excluding the last 12 residues, which were shown to be unstructured in the secondary structure prediction. G_{61-101} showed monomer homogeneity until 1mM concentration (Figure 3.1.6B) and this result enabled us to precede with solution NMR studies to solve the structure of the same (see section 3.1.5). G_{1-77} and G_{1-101} were cloned, expressed and purified to study the continuity of the N-terminal helix and also to understand the unstructured region in between the N- and C-terminal helix. Both constructs showed a very good expression and since most of the protein was found in the soluble fractions, they were also purified to homogeneity at significant concentration (1mM respectively). Accordingly, both constructs were checked for resolution and dispersion on the NMR spectroscopy. But since both spectra had numerous overlapping residues on the ^{15}N ^{1}H plane, they were not taken for NMR studies.

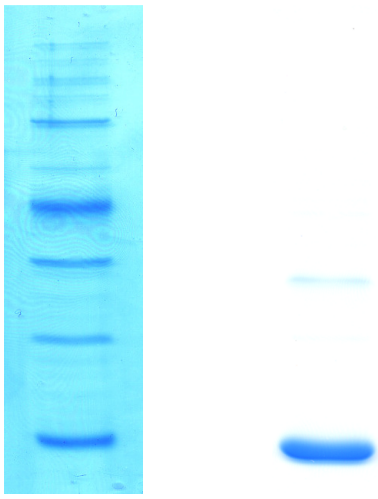

Figure 3.1.6: Concentrated protein of truncated G subunit. (A) G_{61-114} showing oligomerization and **(B)** G_{61-101}. 6 mg/ml of the respective protein was loaded on to a 17% SDS gel.

3.1.4 Structural characterization of G_{1-59} through nuclear magnetic resonance spectroscopy

The structural characterization of G_{1-59} protein through solution state NMR started with 2D ^{1}H ^{15}N HSQC, where the amide group of individual amino acid, except proline, gives an individual peak on the spectrum. Thus the number of peaks on a 2D ^{1}H ^{15}N HSQC spectrum corresponds to the number of amino acids in a properly folded protein. The 2D ^{1}H ^{15}N HSQC spectrum of the G_{1-59} showed that the protein was folded (Figure 3.1.8). There were in total 50

isolated peaks and 9 overlapped peaks observed on the spectrum. The chemical shift dispersion of around 1 ppm for the amide proton resonance may indicate the predominant presence of helical structure on the construct.

3.1.4.1 Backbone assignments of $G_{1\text{-}59}$

The sequential assignments of the $G_{1\text{-}59}$ were performed using ^{15}N and/or ^{13}C signals of double and triple resonance backbone experiments. The initial backbone assignment started with HNCO and HNCACO experiments, which was a classical assignment approach, where the peaks of carbonyl group from previous residues obtained on HNCO experiment were matched with the peaks of carbonyl group from previous residues obtained from HNCACO experiment and in turn the same residue's carbonyl peaks on the same plane on HNCACO were correlated. The carbonyl peaks are dispersed through a ppm range of 174 and 178. A typical example of HNCO and HNCACO sequential assignment is shown in the figure 3.1.7A for the first five residues (M_{01}, V_{02}, S_{03}, Q_{04} and K_{05}) in $G_{1\text{-}59}$ sequence. Here the low and high intense peaks are carbonyl peaks from previous and same residues respectively. Assignments for all the residues in $G_{1\text{-}59}$ sequence were done similarly.

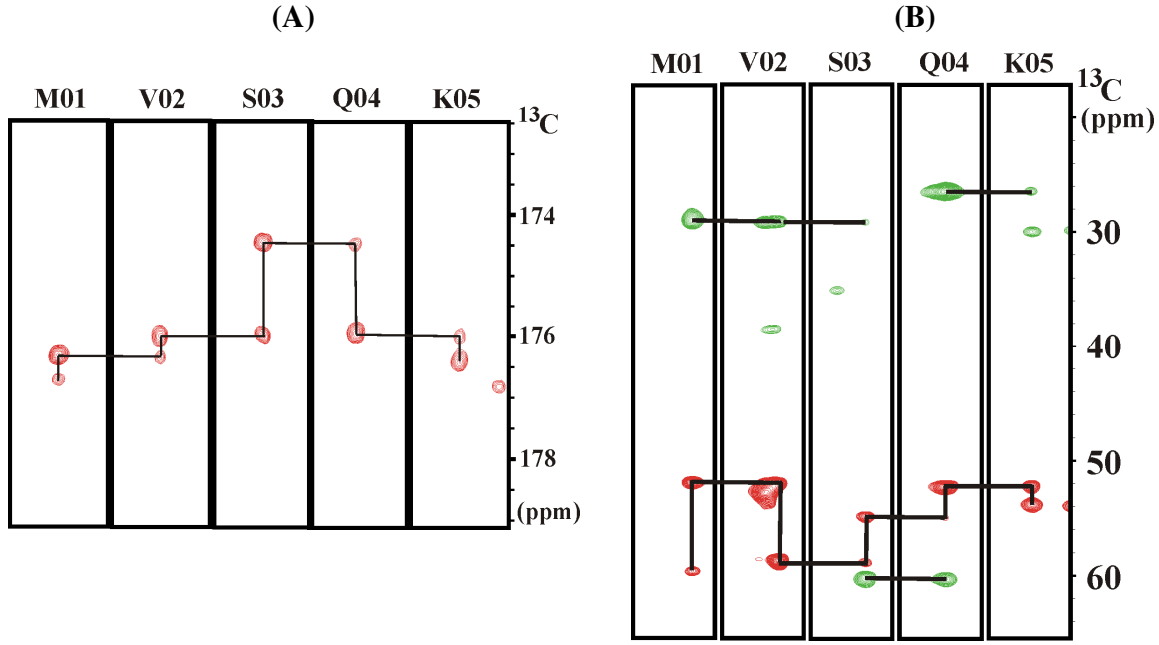

Figure 3.1.7: Strip plots of HNCACO and HNCACB. **(A)** The HNCACO spectrum shows previous and same residues carbonyl peaks obtained at a range of 174 and 178 ppm where previous residue and same residue peaks occurs less and high intense respectively and the sequential connectivity of the first five residues in $G_{1\text{-}59}$ sequence are connected with lines. **(B)** Strip plots from the HNCACB experiments showing the previous and same residue carbon alpha (pCα and Cα, red) in the range between 45 and 70 ppm and carbon beta peaks (pCβ and Cβ, green) obtained between 15 and 40 ppm except serine and threonine. The sequential connectivity of the first five residues in $G_{1\text{-}59}$ sequence are connected with lines.

In the similar way of classical assignment of amino acids, the previous residues carbon alpha (pCα) peaks and previous residues carbon beta (pCβ) peaks are obtained in the CBCA(CO)NH experiments. These peaks from the CBCA(CO)NH experiments are matched to the corresponding previous residues pCα and pCβ peaks, obtained from the HNCACB experiment. From this experiment, the sequential assignments of Cα and Cβ peaks are obtained. A typical example of the sequential assignments of CBCA(CO)NH and HNCACB is shown in figure 3.1.7B for the first five residues (M_{01}, V_{02}, S_{03}, Q_{04} and K_{05}) in the $G_{1\text{-}59}$ sequence. Similarly the sequential assignments of all residues were obtained using the pCα, pCβ, Cα and Cβ peaks.

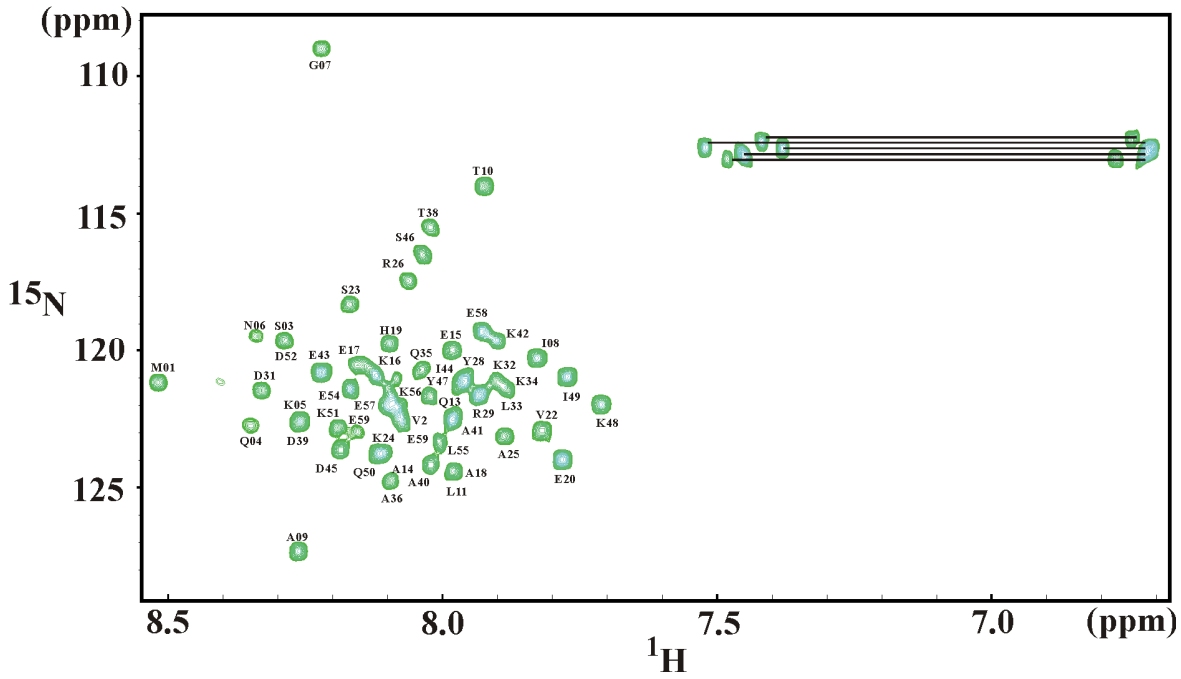

Figure 3.1.8. ^{1}H ^{15}N-HSQC spectrum of $G_{1\text{-}59}$. The spectrum was acquired in 25 mM sodium phosphate buffer (pH 6.8) at 288 K, wherein the backbone and side-chain amide assignments are shown for each residue. Signals from side-chain NH_2 groups are connected by horizontal lines (RISHIKESAN *et al.,* 2009).

With the help of the HNCO, HNCACO, CBCA(CO)NH and HNCACB experiments the backbone atoms of the $G_{1\text{-}59}$ are assigned for all residues except L_{11}, I_{21}, K_{27} and K_{53}. The sequential assignments of the resolved backbone residues of $G_{1\text{-}59}$ are presented in the 2D ^{1}H ^{15}N HSQC spectrum shown in figure 3.1.8. The numberings in the spectrum are according to the residues in the sequence (RISHIKESAN *et al.,* 2009).

3.1.4.2 Side chain and ^{1}H ^{15}N NOESY-HSQC assignment

The side chain peaks of the assigned residues were obtained from triple resonance (H)CCCONH (proton) and HCCCONH (carbon) side chain experiments. From the side chain peaks the 3D ^{1}H ^{15}N NOESY-HSQC peaks were assigned. 3D ^{1}H ^{15}N NOESY-HSQC gives the alpha (α), beta (β), gamma (γ), delta (δ), and epsilon (ε) proton peaks of the same residues and also the previous residues. The typical Hα peaks for the sequentially assigned residues of $G_{1\text{-}59}$ are shown in figure 3.1.9.

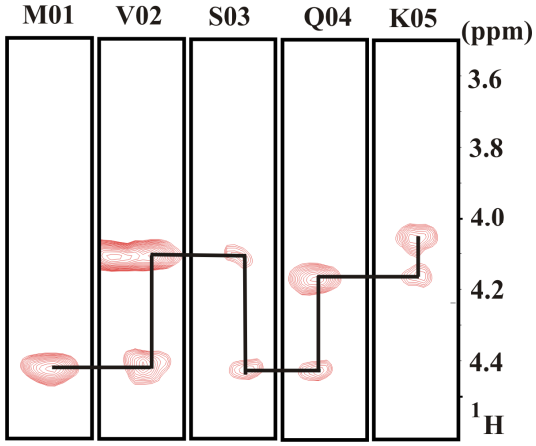

Figure 3.1.9: **Strip plots of the ^{1}H ^{15}N NOESY-HSQC.** The Hα peaks form the same residue are obtained in the range between 3.5 and 5 ppm. The previous residue's Hα peaks are less intense than the same residue Hα peaks and the sequential connectivity for first five residues in $G_{1\text{-}59}$ sequence are shown with connectivity line.

3.1.4.3 Structure calculation of $G_{1\text{-}59}$

From the Cα and Cβ chemical shifts values obtained in the HNCACB experiments, the dihedral angle restraints were calculated by using TALOS (CORNILESCU *et al.,* 1999). The distance constraints for the structure calculation were collected from 3D ^{1}H ^{15}N NOESY-HSQC and 3D ^{1}H ^{13}C NOESY-HSQC by manually and automatically assigned NOE using CYANA 2.1 (GÜNTERT *et al.,* 1997). Seven cycles of automated NOESY assignment using the CYANA 2.1 were performed. In the final CYANA cycle, NOESY cross peaks were assigned, leading to 565 meaningful NOE distance restraints. 10 conformers of the monomeric $G_{1\text{-}59}$ were calculated based on the obtained dihedral angles and NOE restraints. The program MOLMOL 2K. 2.0 (Koradi *et al.,*1996) was used to visualize the result of ensemble of minimized conformers. The connectivity diagram of the calculated structure for $G_{1\text{-}59}$ is shown in figure 3.1.10 (RISHIKESAN *et al.,* 2009).

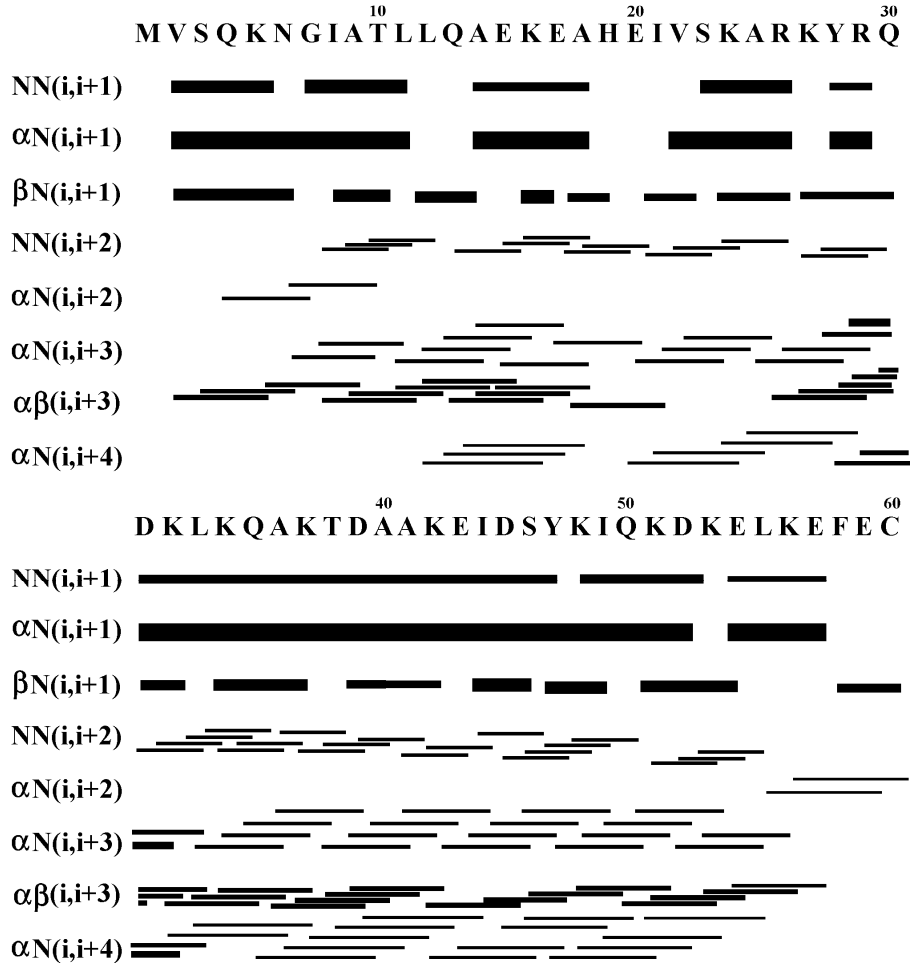

Figure 3.1.10: The connectivity diagram of the calculated structure for $G_{1\text{-}59}$. The line thickness reflects the intensities of the NOE connectivity (RISHIKESAN *et al.,* 2009).

3.1.4.4 Solution structure of $G_{1\text{-}59}$

The structure of $G_{1\text{-}59}$ was calculated on the basis of a total 565 nontrivial NMR-derived distance restraints. Ribbon and cartoon representation of the ten lowest energy structures of $G_{1\text{-}59}$ and the structural statistics are given in figure 3.1.11 and table 3.1.1, respectively. These structures have an overall RMSD of 0.87 Å for the backbone atoms and 1.42 Å for all heavy atoms in the helical region (residue 10-56). All these structures have energies lower than 4 kcal mol^{-1}, no NOE violations greater than 0.3 Å, and no dihedral violations greater than 5 Å (RISHIKESAN *et al.,* 2009). The protein has an extended helical structure from residues T10 to A56 measuring a length of 67.9 Å excluding the unstructured region in the N- (1-9) and C-termini (57-59).

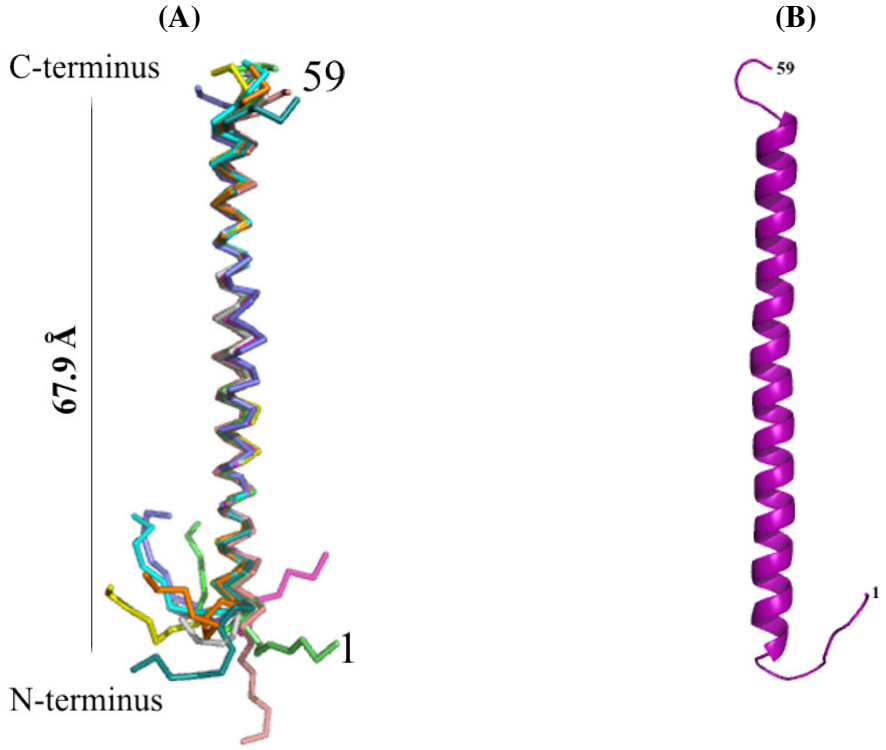

Figure 3.1.11: Structure of $G_{1\text{-}59}$ from yeast V-ATPAse. Ten superimposed ribbon **(A)** and one cartoon **(B)** representation of solution structure of $G_{1\text{-}59}$ from NMR studies (RISHIKESAN *et al.,* 2009), created on PyMOL (DELANO 2001).

Figure 3.1.12 shows the surface charge distribution of $G_{1\text{-}59}$, where the structure exhibits a strip of negatively charged amino acids at the C-terminus. By comparison, the N-terminus shows more amphiphilic character due to both positive and negative charge distribution, attributed by residues K5, K16, K24, R26 and K27 and E15, E17, E20, respectively. The opposite side of the

Total number of NMR restraints	**565**
Number of unambiguous NOE peaks	
Intraresidual (|i-j|=0)	173
Sequential (|i-j|=1)	165
Medium range (2≤|i-j|≤5)	84
Long range (|i-j|>5)	0
Number of Dihedral angle constraints	104
Number of Hydrogen-bond restraints	39
Number of restraints violation	
Total number of restraints violation > 0.3 Å	0
Total number of dihedral angle violations > 5 Å	0
Ramachandran Plot Statistics (%)	
Fractions of residues of most favoured regions (%)	94.7
Fractions of residues in additionally allowed regions (%)	5.3
Fractions of residues in generously allowed regions (%)	0
Fractions of residues in disallowed regions (%)	0
Structural precision of well ordered regions	
RMSD backbone (residues 10-56)	0.87 Å
RMSD heavy atoms (residues 10-56)	1.42 Å

Table 3.1.1: Structural statistics of 10 lowest energy structures of $G_{1\text{-}59}$ (RISHIKESAN *et al.,* 2009).

structure reveals a highly hydrophobic surface at the N-terminus made-up by residues V2, I8, A9, L11, A14, A18, A25 and V22 (RISHIKESAN *et al.,* 2009).

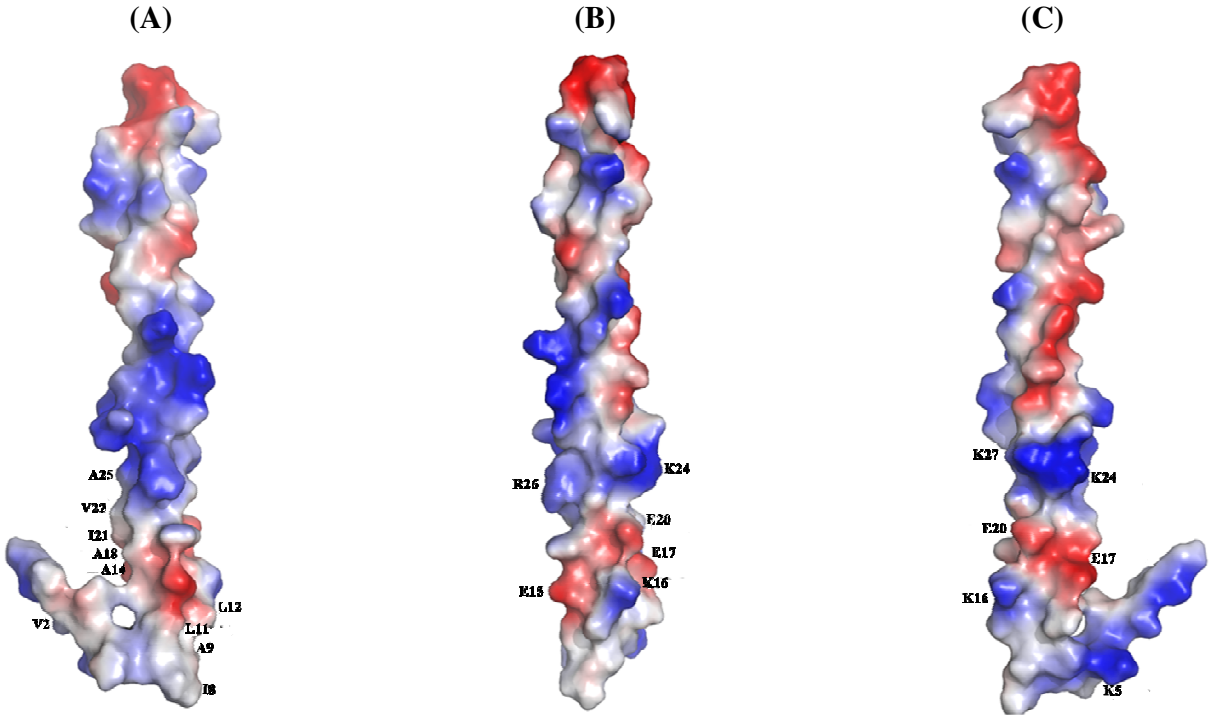

Figure 3.1.12: Surface charge distribution of $G_{1\text{-}59}$. The figure shows the molecular surface with electrostatic potential of the peptide on a 90º rotation, drawn in PyMol (DELANO *et al.,* 2001) that uses Poisson-Boltzmann equation, where the positive potentials are drawn in blue and negative in red (RISHIKESAN *et al.,* 2008).

3.1.5 Structural characterization of G_{61-101} through NMR spectroscopy

Recombinant G_{61-101} was cloned, expressed and the protein was purified to homogeneity (see section 3.1.3) (Figure 3.1.6B). The structural characterization of the protein started initially with 2D ^{1}H ^{15}N HSQC experiment with an expectation to obtain the 42 amino acids dispersed over the ^{1}H ^{15}N plane. Since the peaks were overlapped for a few residues and were less dispersed on the ppm scale, several optimization tools were applied to get clarity over the 42 residues. Upon the effect of TFE (tri-fluoro-ethanol) at various concentration and optimization over a range of temperature, G_{61-101} protein became well isolated for their 42 residues on a 3 ppm dispersion spectrum.

3.1.5.1 Effect of temperature and TFE on G_{61-101}

Initial studies on G_{61-101} protein started with 2D ^{1}H ^{15}N HSQC data at 5 ºC (278 K). The protein was observed for its dispersion over a series of temperatures between 5 ºC-35 ºC and the

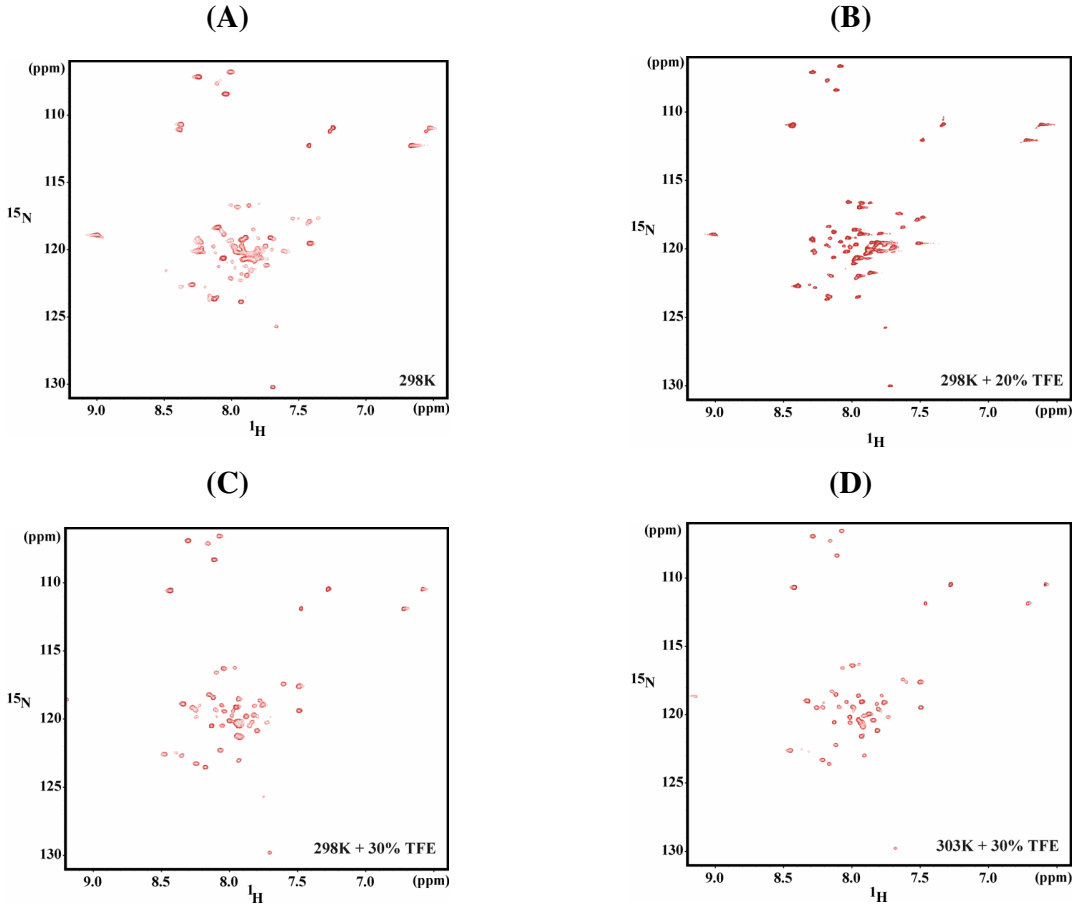

Figure 3.1.13: Effect of temperature and TFE of recombinant G_{61-101}. 2D HSQC acquired at 25 ºC **(A)**, 25 ºC + 20 % TFE **(B)**, 25 ºC + 30 % TFE **(C)** and 30 ºC + 30 % TFE **(D)**.

protein showed a unique characteristics of good dispersion at high temperatures, namely above 20 ºC (293 K). All the spectra acquired above 20 ºC possessed nearly all the 42 residues with few overlaps on the $^{1}H^{15}N$ plane. Since the protein showed better resolution at high temperature, efforts were also taken to see the effects of various concentrations of TFE on the protein. The protein was incubated with 10 %, 20 % and 30 % of TFE for 30 minutes at room temperature (≥ 22 ºC) and was checked for its resolution against different temperatures including 25 ºC, 30 ºC and 35 ºC (Figure 3.1.13).

2D ^{1}H ^{15}N HSQC of $G_{61\text{-}101}$ at 30 ºC with 30 % TFE showed a good resolution of the 42 amino acids with a little overlap on 3 residues. Furthermore the protein was checked for its resolution by increasing the concentration from 30 % TFE to 40 % and 50 % TFE, respectively. But there were negligible effect on the spectrum over the amino acids. Therefore the optimum concentration on the TFE for structure was chosen to be as 30 %. While on the other hand, an increase in the temperature from 30 ºC to 35 ºC resolved the spectrum with the entire amino acids well separated from each other. Figure 3.1.14 shows the 2D ^{1}H ^{15}N HSQC of $G_{61\text{-}101}$ protein acquired at 35 ºC with 30 % TFE. Each peak on the spectrum corresponds to each individual amino acid. The side chains of N61 and Q77 are connected with horizontal lines.

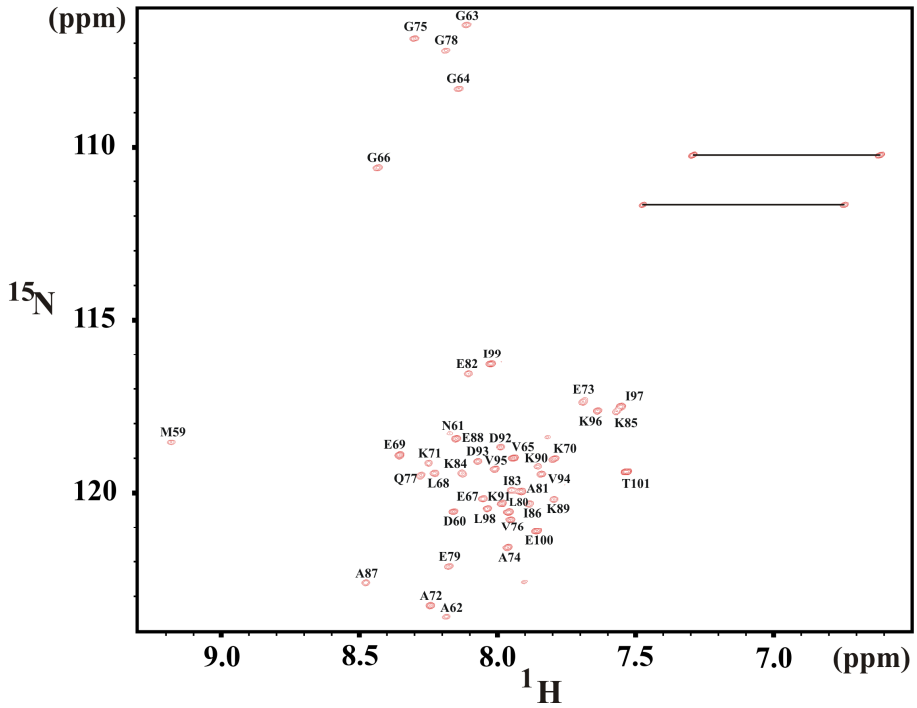

Figure 3.1.14. ^{1}H ^{15}N-HSQC spectrum of $G_{61\text{-}101}$. The spectrum was acquired in 25 mM sodium phosphate buffer (pH 6.8) at 308 K with 30 % TFE. Sequential backbone and side-chain amide assignments are shown for each residue. Signals from side-chain NH_2 groups are connected by horizontal lines (RISHIKESAN *et al.*, 2010).

3.1.5.2 Solution structure of $G_{61\text{-}101}$

The 2D ^{1}H ^{15}N HSQC of $G_{61\text{-}101}$ acquired at 35 ºC with 30 % TFE showed a well dispersed spectrum, enabeled us to assign the respective amino acids. Assignment for the backbone HN, N, Cα, Cβ, and C' resonance of the $G_{61\text{-}101}$ was achieved by a combined analysis of the triple resonance HNCACB, CBCA(CO)NH and HNCO spectra. The chemical shift values for the side chains of the respective amino acids were obtained from the 3D ^{1}H ^{15}N NOESY-HSQC spectrum. Dihedral angle restraints were calculated from C^{α} and C^{β} chemical shifts by using PREDITOR. The distance constraints for structure calculation were collected from 3D ^{1}H-^{15}N NOESY-HSQC by manually and automatically assigned NOE using CYANA 2.1.

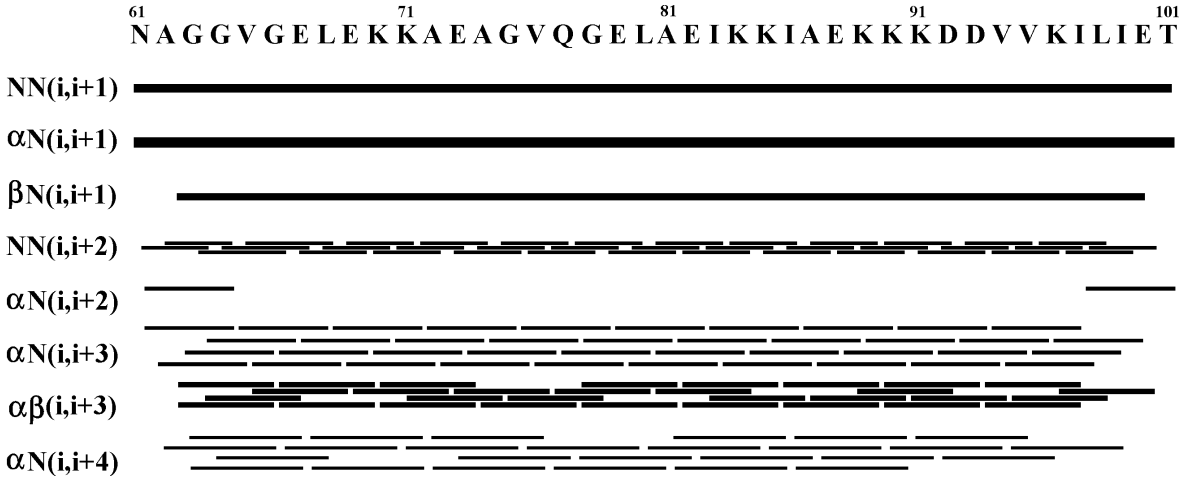

Figure 3.1.15: The connectivity diagram of the calculated structure for $G_{61\text{-}101}$. The line thickness reflects the intensities of the NOE connectivity (RISHIKESAN *et al.,* 2010).

The structure of $G_{61\text{-}101}$ was calculated on the basis of a total 613 nontrivial NMR-derived distance restraints. Hydrogen bonds were identified from the characteristic patterns of homonuclear ^{1}H nuclear Overhauser enhancements (NOEs) and were introduced at the end of structure calculations. Typical α-helical NOE pattern $d_{\alpha N}$ (i, i+3), $d_{\alpha N}$ (i, i+4) and $d_{\alpha\beta}$ (i, i+3) were observed from the amino acid residues 64 to 100 (Figure 3.1.15) (RISHIKESAN *et al.,* 2010). The secondary structure prediction was done from the HA chemical shifts in comparison with the standard random coil values (Figure

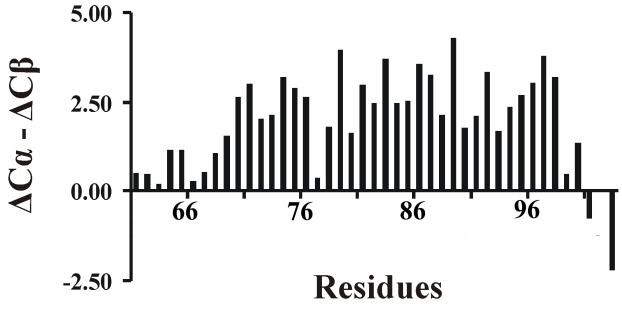

Figure 3.1.16: The secondary structure prediction for $G_{61\text{-}101}$. Calculated through the change in the chemical shifts ($\Delta^{13}C\alpha$ - $\Delta^{13}C\beta$) of $G_{61\text{-}101}$ (RISHIKESAN *et al.,* 2010).

3.1.16). These values show that G_{61-101} is mainly folded as an α-helical structure. Figure 3.1.17A reveals an overlay of the 10 lowest energy structures of G_{61-101} and respective average structure (Figure 3.1.17B). The corresponding statistics on the calculated structure of G_{61-101} are given in table 3.1.2. These structures have an overall RMSD of 0.32 Å for the backbone atoms and 1.72 Å for all the heavy atoms in the helical region of the three dimensional structures (residue 64-100) of the protein. All these structures have energies lower than 4 kcal/mol, no NOE violations greater than 0.3 Å, and no dihedral violations greater than 5 Å. The protein has an extended helical structure from residues E64 to E100 measuring a length of 47.93 Å, excluding the unstructured region in the N- (residues 59-63) and C-terminus (amino acid 101), as predicted from the amino acid sequence.

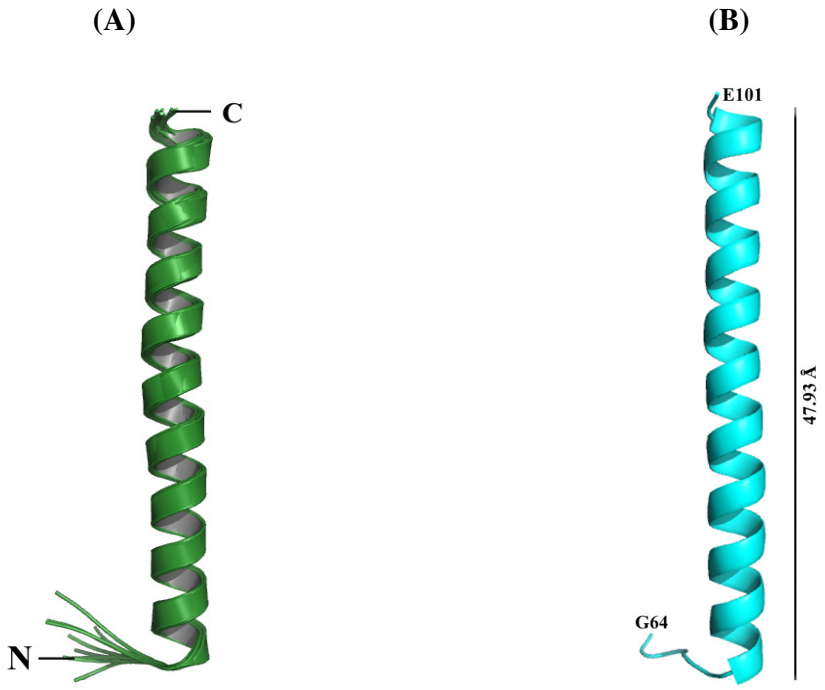

Figure 3.1.17: Ribbon diagram of the NMR solution structure of G_{61-101}. (A) Best fit superimposition of the 10 lowest-energy NMR structures. **(B)** Side view of the average structure of G_{61-101} (RISHIKESAN *et al.,* 2010).

Total number of NMR restraints	613
Intraresidual (|i–j|=0)	192
Sequential (|i–j|=1)	201
Medium-range (2 ≤|i–j|≤ 4)	108
Long-range (|*i*–*j*| > 5)	0
Dihedral angle constraints	77
Hydrogen bond distance restraints	35
Ramachandran plot statistics (%)	
Residues in most favoured regions	94.7
Residues in additionally allowed regions	5.3
Residues in generously allowed regions	0
Residues in disallowed regions	0
Structural precision for well ordered region	
RMSD. backbone (residues 39–72):	0.32 Å
RMSD. heavy (residues 39–72):	1.72 Å

Table 3.1.2: Structural statistics of $G_{61\text{-}101}$ (RISHIKESAN *et al.,* 2010).

The surface charge distribution of $G_{61\text{-}101}$ shows a high degree of negative amino acids at one side and hydrophobic amino acids on the other. The stretch of charged residue distributed on one side of the structure, attributed by K70, K71, E79, E82, K84, K89, K90, K91 and E100 may be involved in its binding with the subunit A and B. This allows the hydrophobic residues like A62, V65, L68, A74, V76, L80, A81, I83, I86 and I97 to take part in the helix-helix interaction of subunit G and thereby a continuation of the hydrophobic stretch (Figure 3.1.18, RISHIKESAN *et al.,* 2010).

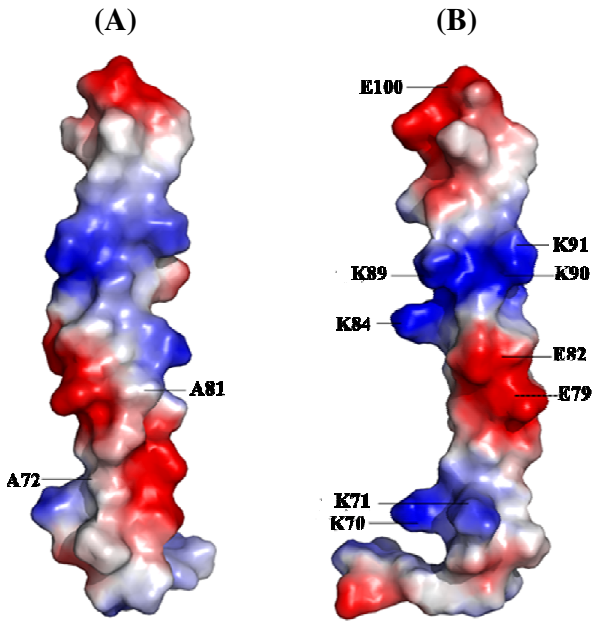

Figure 3.1.18: Surface charge distribution of $G_{61\text{-}101}$. (A) and **(B)** Different orientations of $G_{61\text{-}101}$, showing the molecular surface with the electrostatic potential of the peptide, drawn in PyMol (DELANO 2001), that uses Poisson-Boltzmann equation, where the positive potentials are drawn in blue and negative in red color (RISHIKESAN *et al.,* 2010).

3.1.5.3 Translational diffusion rates of $G_{61\text{-}101}$

Subunit G of the *S. cerevisiae* V-ATPase is dimeric in solution as shown from solution X-ray scattering data (ARMBRÜSTER *et al.,* 2003). Here we analyzed the dimeric feature of $G_{61\text{-}101}$ by measuring the diffusion coefficients of the protein as a function of protein concentration. The DOSY experiment provides accurate, non-invasive, molecular diffusion measurements on biofluids, complex chemical mixtures and multicomponent solutions. In DOSY spectra, chemical shift is along the detected F2 axis and diffusion coefficient is along the other F1 axis. The measurement of diffusion is carried out by observing the attenuation of the NMR signals during a pulsed field gradient experiment. The degree of attenuation is a function of the magnetic gradient pulse amplitude and occurs at a rate proportional to the diffusion coefficient of the molecule. To estimate the dimerization equilibrium constant, we have performed NMR pulsed field gradient (PFG) diffusion experiments in a dilution series, revealing the equilibrium between monomeric and dimeric states of $G_{61\text{-}101}$. Decrease in the experimentally determined diffusion rates with increasing concentration of $G_{61\text{-}101}$ suggested a dimer formation (Figure 3.1.19), assuming that the exchange rate between monomer and dimer is fast on diffusion timescale. The corresponding dimer dissociation constant for $G_{61\text{-}101}$ was estimated by direct fit of translation diffusion rates, as a function of concentration, to be 1.5 mM (RISHIKESAN *et al.,* 2010).

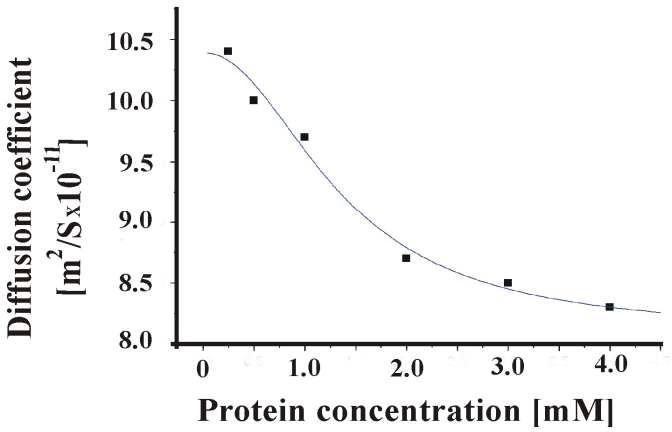

Figure 3.1.19: Graph showing change of diffusion coefficient for $G_{61\text{-}101}$. The diffusion rates decreased upon increasing the protein concentration (RISHIKESAN *et al.,* 2010).

3.1.5.4 Examination of disulfide bond formation by cross linking and mutagenesis of subunit G from *S. cerevisiae*

The solution structure of $G_{61\text{-}101}$ showed a strip of hydrophobic alanine residues like A72, A74 and A81 with a twist to each other (Figure 3.1.20). To analyze the close proximity of the alanine residue of the first and second α-helix of the dimeric $G_{61\text{-}101}$, A72, A74 and A81, respectively, have been replaced by a cysteine residue, generating soluble and monodisperse

mutant proteins of entire subunit G. All three mutant proteins were isolated in high amounts and in high purity. Copper chloride was used as crosslinking reagent to study its effect on the disulfide bond formation in the dimeric subunit G. The cysteine thiol group is nucleophilic and oxidized. $CuCl_2$ reversibly oxidizes thiol groups, which in turn can form intermolecular disulfide bridges, if the thiol groups are in close vicinity to each other without an additional spacer arm. In order to analyse the close proximity of the two chains of subunit G, the mutated cysteine residues on the protein were oxidised by treating with copper chloride, a known zero-length cross-linker that form disulphide bonds (OGILVIE *et al.,* 1997; SCHULENBERG and CAPALDI, 1999; COSKUN *et al.,* 2004).

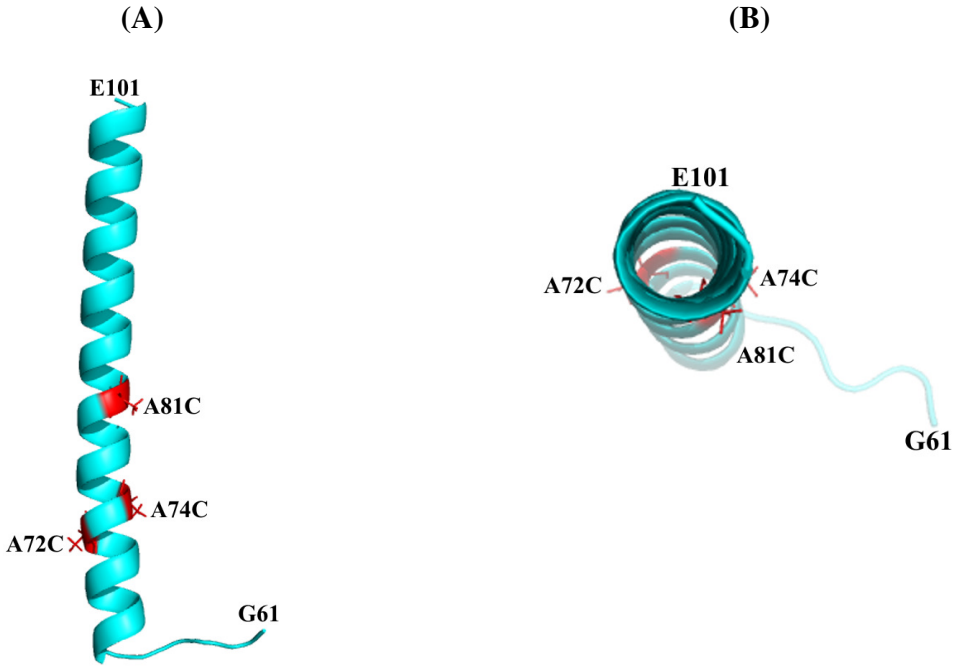

Figure 3.1.20: The solution structure of $G_{61\text{-}101}$. Side **(A)** and top **(B)** views of the average $G_{61\text{-}101}$ structure, illustrating the relative positions of alanine 72, 74 and 81 (*blue*) inside the α-helix (RISHIKESAN *et al.,* 2010).

3.1.5.5 Expression and purification of subunit G mutants

Vma10 gene (ARMBRÜSTER *et al.*, 2003) WAS USED AS THE TEMPLATE FOR PCR AMPLIFICATION OF THE THREE MUTANTS (A72C, A74C AND A81C) AND WAS successfully cloned in modified pET9-d1 expression vector (GRÜBER *et al.,* 2003) as described in section 2.27. The mutations were verified by DNA sequencing. Expression was carried in host BL21 (DE3) *E. coli* strains. Screening tests pointed out that the protein is produced in high quantity and quality, when expressed in BL21 (DE3) *E. coli* strains at 37 °C for 4 h with 1 mM IPTG. Ni^{2+}-NTA

affinity chromatography was used in the first step of purification (Figure 3.1.21A). Imidazole was removed by gel filtration column, Superdex S75, using the buffer containing 50 mM HEPES (pH 7.0), 150 mM NaCl, 0.8 mM DTT and 1mM PMSF. Fractions of constant volumes (200 µl) were collected, pooled, concentrated and subsequently applied onto an SDS gel (Figure 3.1.21B).

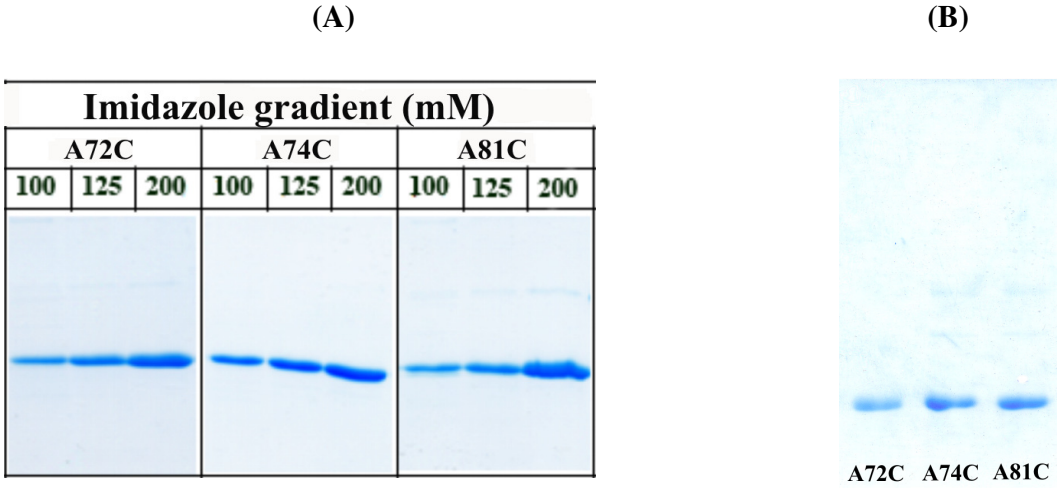

Figure 3.1.21: Purification of subunit G mutants. **(A)** Ni^{2+}-NTA purification of subunit G mutants in 50 mM HEPES (pH 7.0), 150 mM NaCl, 0.8 mM DTT and 1mM PMSF. 15 µl of sample was applied on 17% SDS gel from each elution fraction. **(B)** Subunit G mutants A72C, A74C and A81C in the presence of 1 mM DTT applied on 17% SDS gel (RISHIKESAN *et al.,* 2010).

3.1.5.6 Crosslink formation in cysteine mutants of subunit G

To analyze the proximity of the alanine residue of the first and second α helix of the dimeric $G_{61\text{-}101}$, A72, A74 and A81, respectively, have been replaced by a cysteine residue, generating soluble and mono-disperse mutant proteins of entire subunit G. All three mutant proteins were isolated in high amounts and in high purity. Cross-linking formation in the presence of $CuCl_2$ (5 µM) is shown in figure 3.1.22 *(lanes 1 and 3*) for $G_{61\text{-}101}$, revealing that a significant amount of dimer formation could be generated for the two mutants A72 and A81. In contrast, when the alanine residue 74, located opposite to A72 on $G_{61\text{-}101}$ in the helix, was exchanged by a cysteine, no significant disulfide bond formation could be detected under the conditions used (Figure 3.1.22, *lane 2*).

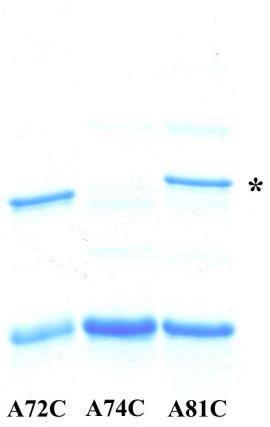

Figure 3.1.22: Cross-linking of subunit G mutants. A72C (*lane 1*), A74C (*lane 2*) and A81C (*lane 3*). Mutant proteins were incubated with 5 µM $CuCl_2$ for 30 min at 4 °C and the reaction was stopped with 1 mM EDTA (RISHIKESAN *et al.,* 2010).

3.2.1 Interaction studies of subunit G and E

3.2.1.1 $G_{1\text{-}59}$ and $E_{18\text{-}38}$ binding characterized through NMR spectroscopy

Precipitation assays of truncated forms of subunit E of the yeast V-ATPase, (JONES *et al.*, 2005) showed that deletions of the N-terminal 38 ($E_{39\text{-}233}$) and 110 amino acids ($E_{110\text{-}233}$) resulted in a complete loss of E-G association, whereby the truncations of the first 19 residues or the C-terminal amino acids 112-233 ($E_{1\text{-}112}$) did not alter the binding traits of both subunits, suggesting that the N-terminal region 19-38 of subunit E might interact with subunit G. In the present NMR titration studies of subunit G and E, when equimolar amount of the peptide $E_{18\text{-}38}$ (section 2.2.10) was added to $G_{1\text{-}59}$, significant chemical shift perturbations were observed. Figure 3.2.1 shows the super-position of HSQC spectra of the ^{15}N-labeled $G_{1\text{-}59}$ (shown in red) and the $G_{1\text{-}59}$-$E_{18\text{-}38}$ complex (shown in green), recorded in the presence or absence of $E_{18\text{-}38}$.

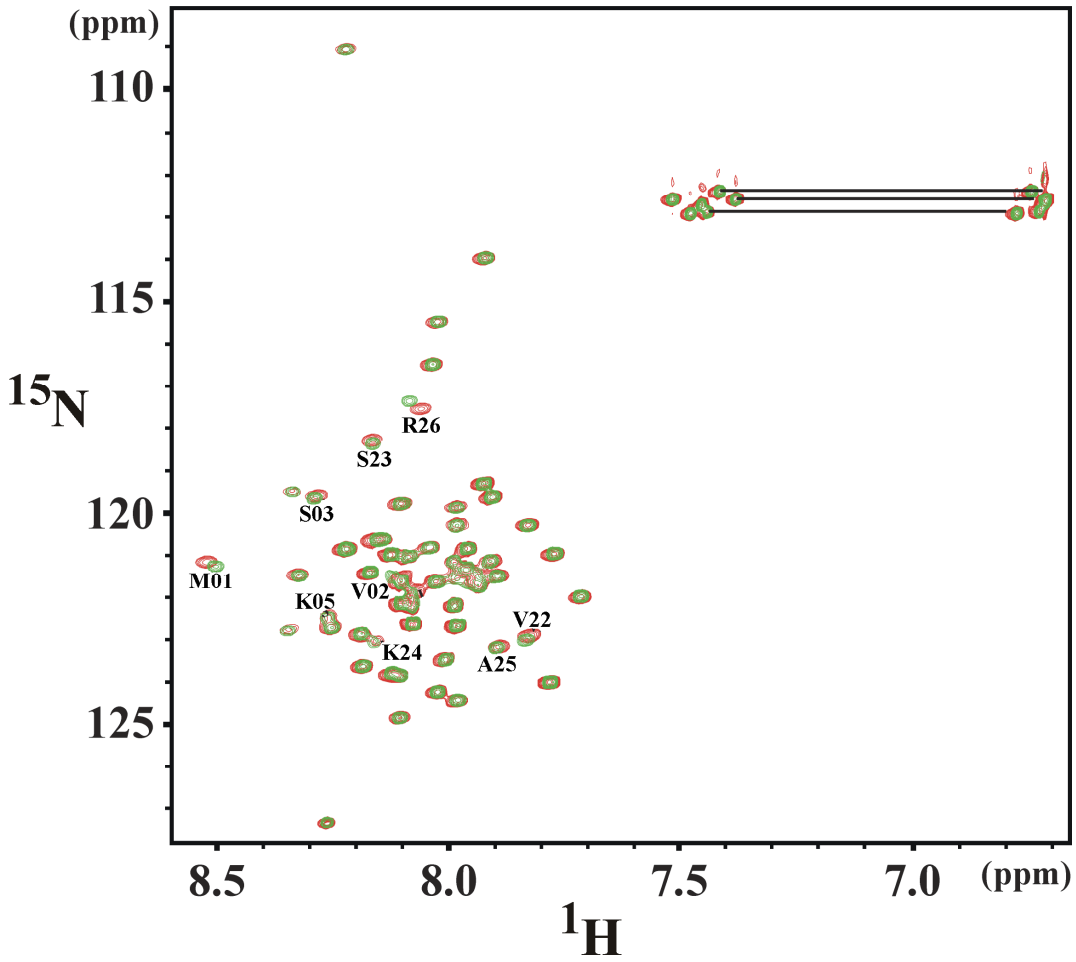

Figure 3.2.1: Superimposition of the ^{1}H ^{15}N HSQC spectra of $G_{1\text{-}59}$. Red color spectrum shows the control and green color spectrum shows the HSQC measured with $G_{1\text{-}59}$ and $E_{18\text{-}38}$.

Cross sections of individual region on the HSQC spectrum of $G_{1\text{-}59}$ depicting the changes in chemical shift due to binding is shown in figure 3.2.2 (A-D). The HSQC spectra of ^{15}N-

labeled $G_{1\text{-}59}$ in the absence and presence of $E_{18\text{-}38}$ yield noticeable differences in terms of changes in chemical shift (Figure 3.2.2, E) specifically for residues M_1, V_2, S_3, and K_5 as well for V_{22}, S_{23}, K_{24}, A_{25} and R_{26} (RISHIKESAN *et al.,* 2008).

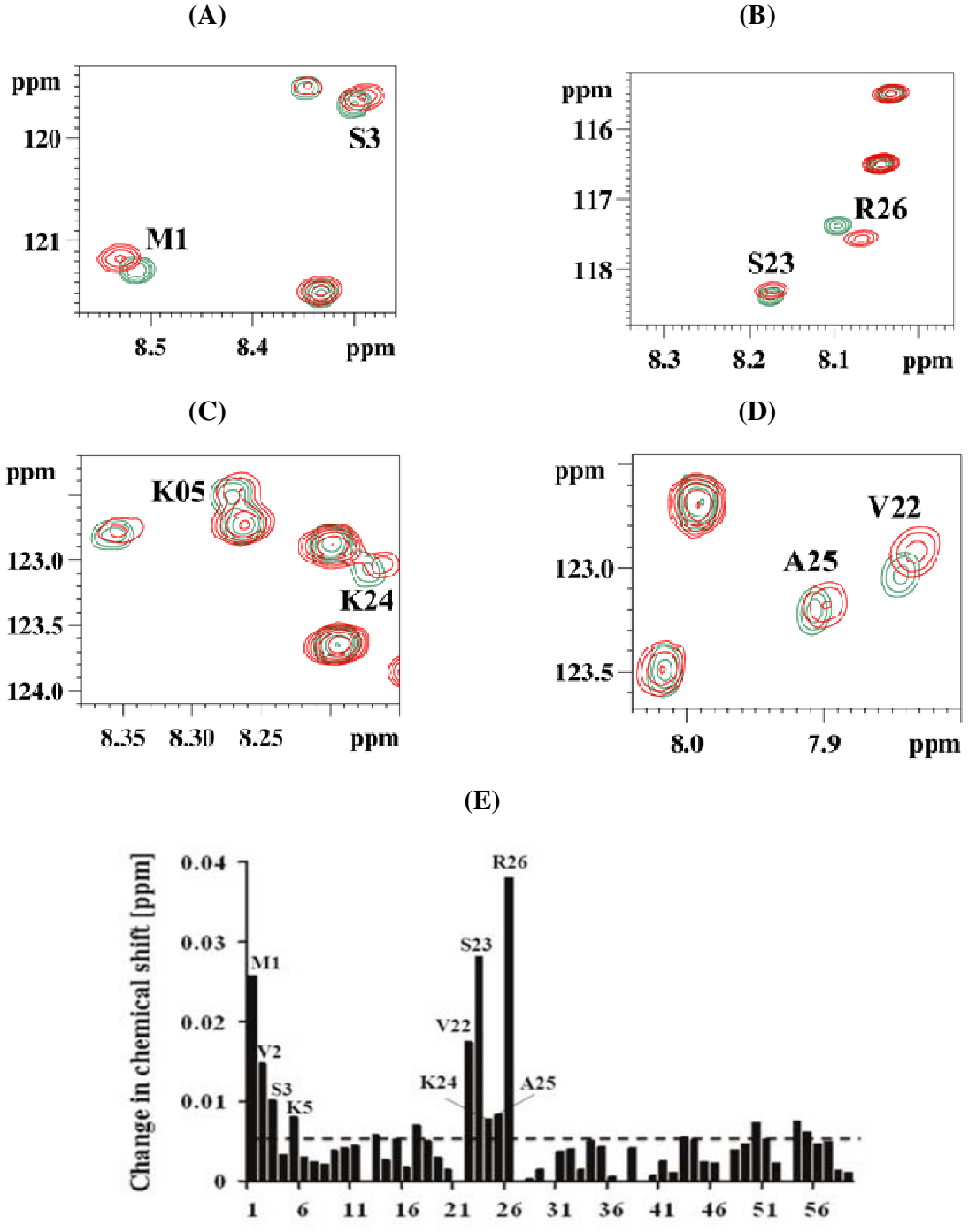

Figure 3.2.2: Sections from the overlaid 2D ^{1}H-^{15}N-HSQC spectra of the $G_{1\text{-}59}$. Spectrum in the absence (red colour) and presence (green colour) of 1.5 equivalent of the unlabeled $E_{18\text{-}38}$ **(A-D).** **(E)** Combined amide (^{1}H) and nitrogen (^{15}N) chemical shift changes $\{[(^{1}H_N)^2 + {}_{15}N_{ppm}/6.51)^2]^{0.5}$ for $G_{1\text{-}59}$ and $E_{18\text{-}38}$ binding as a function of the amino acid sequence. (RISHIKESAN *et al.,* 2008).

Apparently, no binding was observed, when the truncated protein E_{39-233} (protein prepared by Dr. Raj Thaker from our laboratory) or the synthetic peptide E_{1-18}, were titrated against G_{1-59} (Figure 3.2.3 A-B). Furthermore, when ^{15}N labeled G_{61-114} was titrated with E_{39-233} no change in the chemical shift could be observed (Figure 3.2.3 C), indicating that the E-G association occurs only via the N-terminal segment of both subunits (RISHIKESAN *et al.,* 2008).

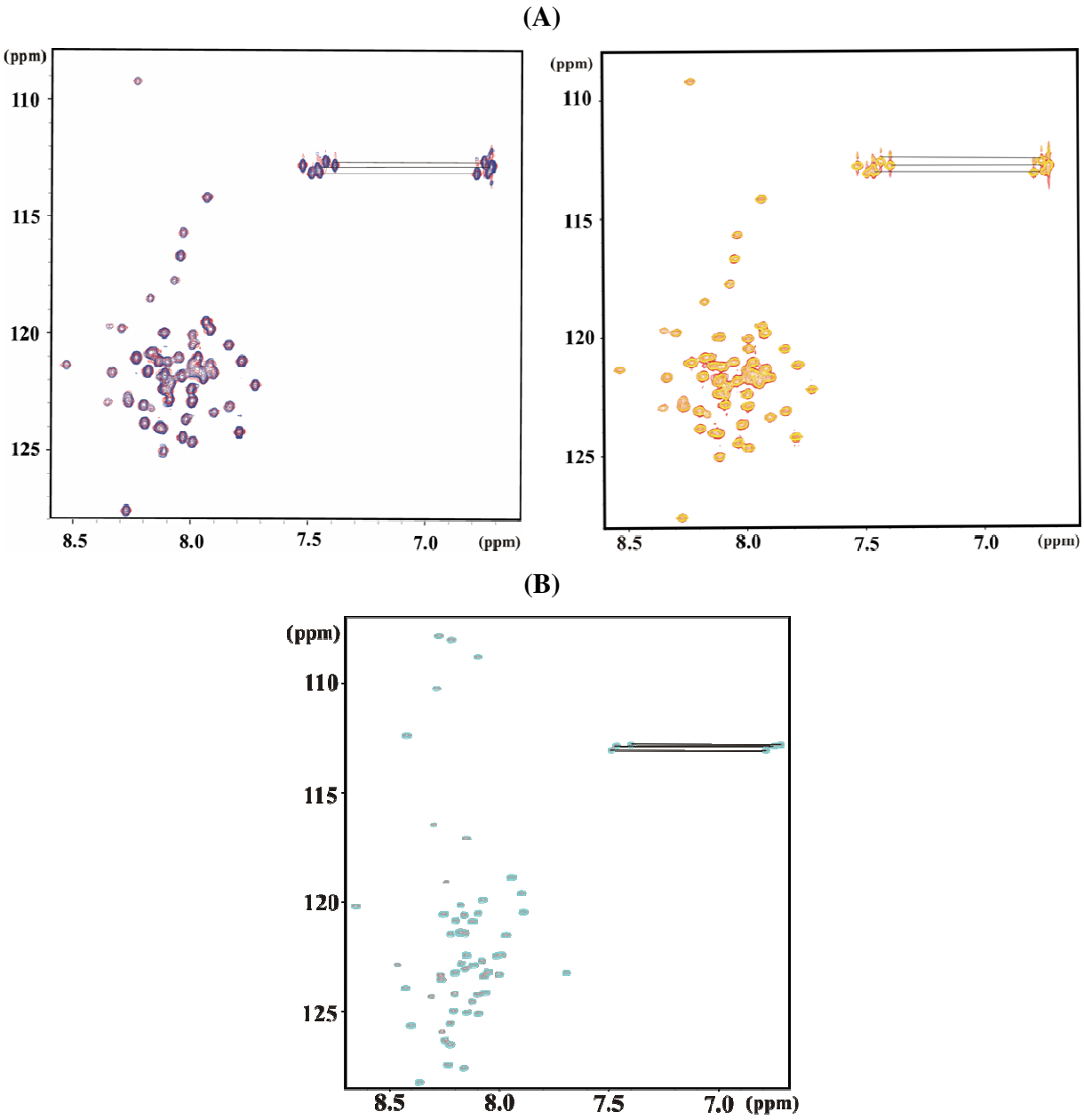

Figure 3.2.3: Solution NMR spectrum of G_{61-114}. (A) Superimposition of the ^{1}H ^{15}N HSQC spectra of G_{1-59} as a control (red) and spectrum with E_{39-233} (green). **(B)** Super position of the G_{1-59} HSQC spectrum with E_{1-18} (yellow). **(C)** ^{1}H ^{15}N HSQC spectra of G_{61-114} as a control (red) and spectrum acquired with E_{39-233} (blue).

3.2.1.2 G_{1-59} and E_{18-38} binding characterized by FCS

Binding of G_{1-59} and E_{18-38} were confirmed and quantified through fluorescence correlation spectroscopy (FCS) by Dr. Hunke, C from our laboratory using LSM-FCS system (ConfoCor 3, Zeiss, Jena/Germany).

(A) **(B)**

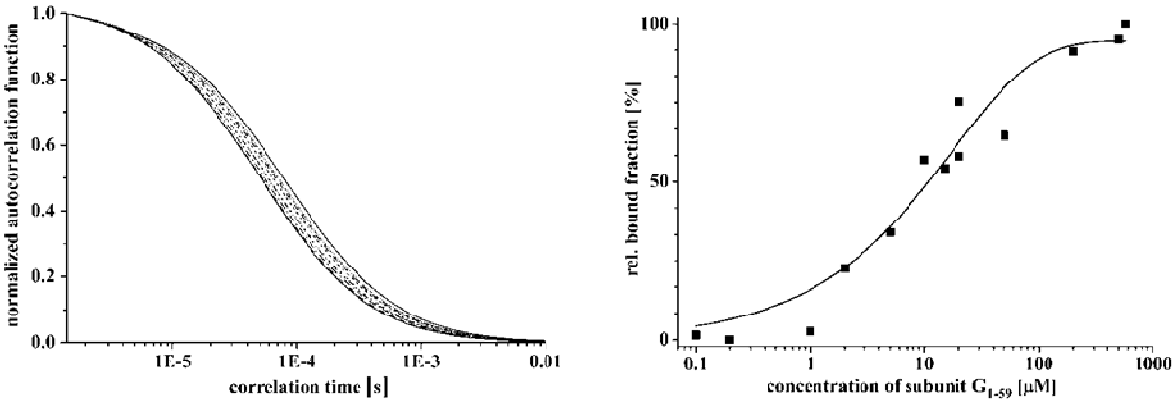

Figure 3.2.4: Binding of G_{1-59} with E_{18-38} studied by FCS. (A) Normalized autocorrelation functions of Atto655 labeled peptide E_{18-38} (5 nM) by increasing the quantity of subunit G_{1-59} (0.1-571 µM). **(B)** Concentration-dependent binding of E_{18-38} to subunit G_{1-59}. The binding constant was calculated by determining the relative bound fraction using a standard autocorrelation function by using two diffusion coefficients normalized triplet model (FCS-LSM software, ConfoCor 3, Zeiss). Best fits yielding the binding constants are represented as fitted line by a non-linear, asymptotic curve fit (Rishikesan *et al.,* 2008).

The fit of the autocorrelation function of Atto655 labeled peptide E_{18-38} resulted in a characteristic diffusion time of 53.5 ms with a mean count rate of 61.1 kHz. Figure 3.16A displays the plotted autocorrelation curves of the fluorescent labeled E_{18-38} in the absence and presence of non-fluorescent-labeled subunit G_{1-59}. The increase of the diffusion time was due to the increase in the mass of the diffusing particle, when Atto655-E_{18-38} was interacting with subunit G_{1-59}. A binding constant of about 10 µM bound E_{18-38} was calculated (Figure 3.2.4B) (RISHIKESAN *et al.,* 2008).

3.2.1.3 Model for the Interface of G_{1-59} and E_{18-38} complex

The solution structure of G_{1-59} and E_{18-38} (RISHIKESAN *et al.,* 2008) were docked by Dr. Manimekalai, MSS from our laboratory to build a model for the interface. NMR-titration experiments demonstrated that subunit G and E are interacting through the residues M1, V2, S3, K5, V22, S23, K24, A25 and R26 of G_{1-59}. With the three dimensional NMR solution structure

of the segment E_{18-38} of yeast V-ATPase, the solution structure of G_{1-59} was docked, iteratively maximizing the favorable interactions between the exposed side chains of both the peptides. The best docking model was chosen and the detailed interaction between the best docked complex configurations is shown in figure 3.2.5.

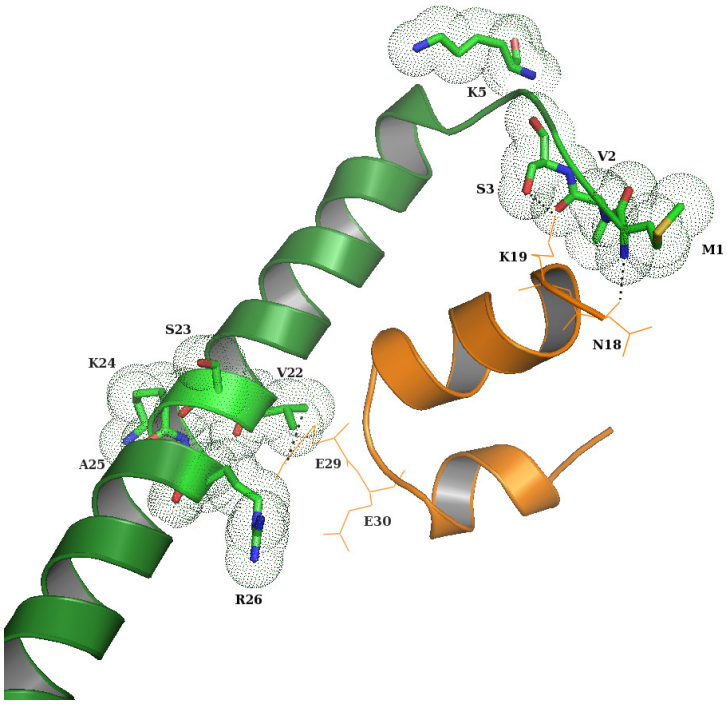

Figure 3.2.5: The docked complex of the solution NMR structure of G_{1-59} (*green*) and E_{18-38} (*orange*). The residues shown in stick representation with dotted surface in G_{1-59} are the residues that are shown by NMR titration experiments to have interaction (M_1, V_2, S_3, K_5, V_{22}, S_{23}, K_{24}, A_{25} and R_{26}). The residues in peptide E_{18-38} that reveal polar contacts (*black dotted lines*) with G_{1-59} are shown in stick representation (RISHIKESAN *et al.,* 2009).

Docking energy of the best docking model was calculated to be -164.58 kJ/mol using the formula Docking energy = Energy of the G_{1-59}-E_{18-38} Complex – (Energy of G_{1-59} + Energy of E_{18-38}); where the final minimized energies of the G_{1-59}-E_{18-38} complex, G_{1-59} and E_{18-38} are -4619.48 ± 0.06, -3336.46 ± 0.02 and -1118.44 ± 0.03 kJ/mol, respectively. From the docked structure, it could be observed that the complex is stabilized by two binding regions, one near the N-termini of the two subunits and the other in the middle (V22-R26) of the G-subunit helix, which is interacting with the hinge region of E_{18-38} peptide. The N-terminal binding is mostly stabilized by polar strong interactions, whereas the second binding region is mostly stabilized through weak hydrogen bonding and van der Waals forces. It could be inferred that in the N-terminal binding region, the main chain carbonyl of M1 of G_{1-59} forms a hydrogen bond with main chain nitrogen atom of N18 of E_{18-38} peptide. In addition, the side chain oxygen atom of S3

of G_{1-59} has hydrogen bond interaction with the side chain nitrogen of K19 of E_{18-38}. In the second binding region, specific interaction is noted for V22 of G_{1-59}, wherein its side chain carbon atom has weak hydrogen bonding interaction with the side chain oxygen atom of E29 of E_{18-38} peptide in the model. The other few residues such as S23, K24, A25 and R26 confer stability to the complex through weak van der Waals forces (RISHIKESAN *et al.,* 2008).

3.2.2 Interactions studies of Subunit G and *d*

3.2.2.1 Residues involved in G_{1-58} and *d* assembly

Precipitation assays of GST-tagged subunit G of yeast V-ATPase with recombinant subunit *d* revealed that both subunits do interact with each other (JONES *et al.,* 2005). Hitherto, the amino acids inside the stalk subunit G, responsible for the G-*d* complex formation, remained undefined. To identify the residues of subunit G involved in the subunit G-*d* assembly, a series of ^{1}H ^{15}N HSQC spectra of ^{15}N-labelled G_{1-59} and G_{61-114} in the presence and absence of recombinant subunit *d* have been performed (figure 3.2.6).

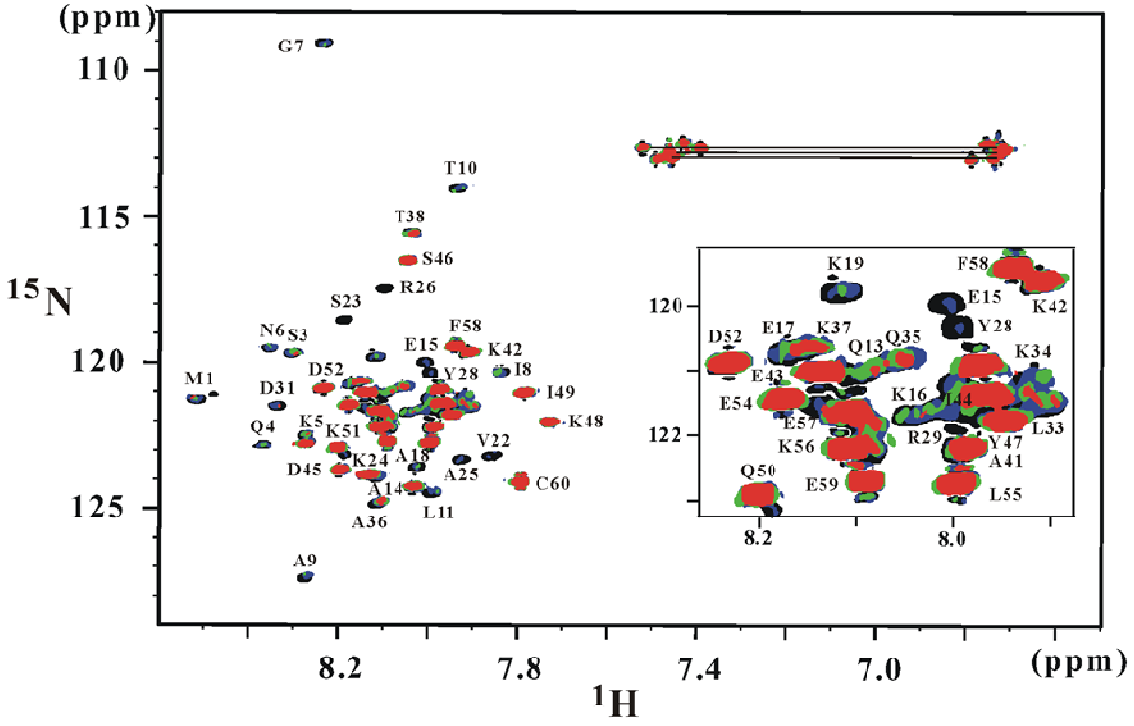

Figure 3.2.6: The ^{1}H ^{15}N HSQC spectra of G_{1-59}. The specta acquired in 25 mM sodium phosphate buffer (pH 6.8) at 288 K. Concentration of unlabelled *d* subunit 0 mM (black), 0.125 mM (blue), 0.159 mM (green) and 0.187 mM (red). The concentration of G_{1-59} was adjusted to 0.15 mM in all samples.

As shown in figure 3.2.6, only the N-terminal region of amide resonances of free G_{1-59} was weakened progressively upon the addition of increasing amount of subunit *d*. Binding of subunit

d induces a structural change in the G_{1-59}, which is in chemical exchange of intermediate rate with respect to the NMR timescale. This causes loss of NMR signals in the resonances affected by the binding. The signal losses observed are indicative of complex formation and result from the formation of either a stable, large molecular weight complex or a complex with an exchange rate between the free and bound forms that is similar to the chemical shift difference (RISHIKESAN *et al.,* 2008). For a quantitative evaluation of the binding of G_{1-59} to *d* subunit, the ratio of G_{1-59} resonance peak intensities [$I(G_{1-59}$ free$)/I(G_{1-59}$ bound$)$] was calculated at a molar ratio of 0.5 (Figure 3.2.7). Intensity changes were observed for residues G7-K34, whereby largest intensity changes were detected for the backbone amides of residues A9, L11, E15, K16, A18, H19, V22 and A25. All these residues are located on the N-terminal segment of G_{1-59}, suggesting that the N-terminus of G_{1-59} forms the recognition site for its interaction with subunit *d* (RISHIKESAN *et al.,* 2008).

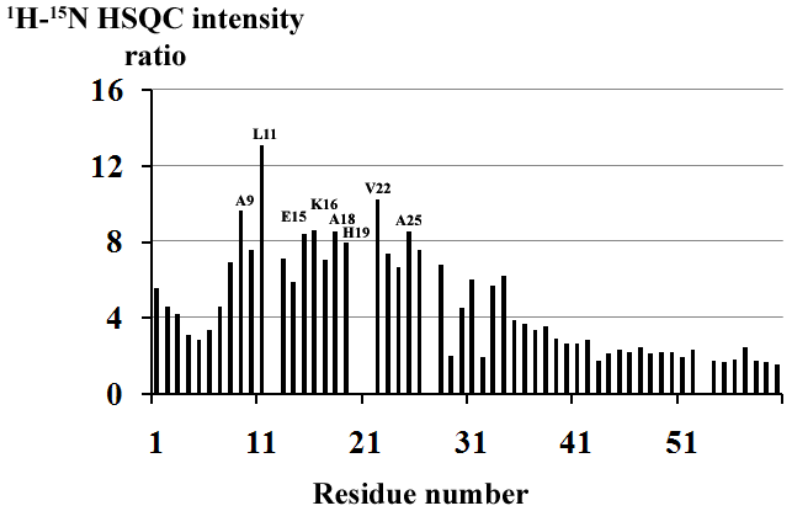

Figure 3.2.7: Loss of ^{1}H ^{15}N HSQC peak intensity upon titration of unlabeled *d* subunit to ^{15}N labeled G_{1-59} at a molar ratio of 0.5. The stronger the decrease of the peak intensity compared with the spectrum without the *d* subunit, the higher the plotted intensity ratio (RISHIKESAN *et al.,* 2008).

3.2.2.2 Interaction of G_{61-114} with the *d* subunit

The titration studies of G_{1-59} with subunit *d*, which gave an insight about the residues involved in the interaction of subunit G-*d* assembly, extended the interest to see the continuity of binding between subunits *d* and G. The ^{15}N labeled recombinant G_{61-114} was titrated with increasing concentrations of *d* subunit until a ratio of 1:2. Figure 3.2.8 shows the ^{1}H ^{15}N-HSQC spectrum of G_{61-114} (red) and G_{61-114} with *d* subunit (green). The spectrum of G_{61-114} showed all 53 peaks well dispersed at an average of 2 ppm. In addition, the side chain peaks were well dispersed. No changes in the chemical shift were observed in G_{61-114} spectrum upon addition of

increasing concentrations of subunit *d*. This implies that the C-terminus of subunit G do not bind with subunit *d* and thus confirms the fact that subunit G-*d* assembly occurs only via the N-terminus of the G subunit.

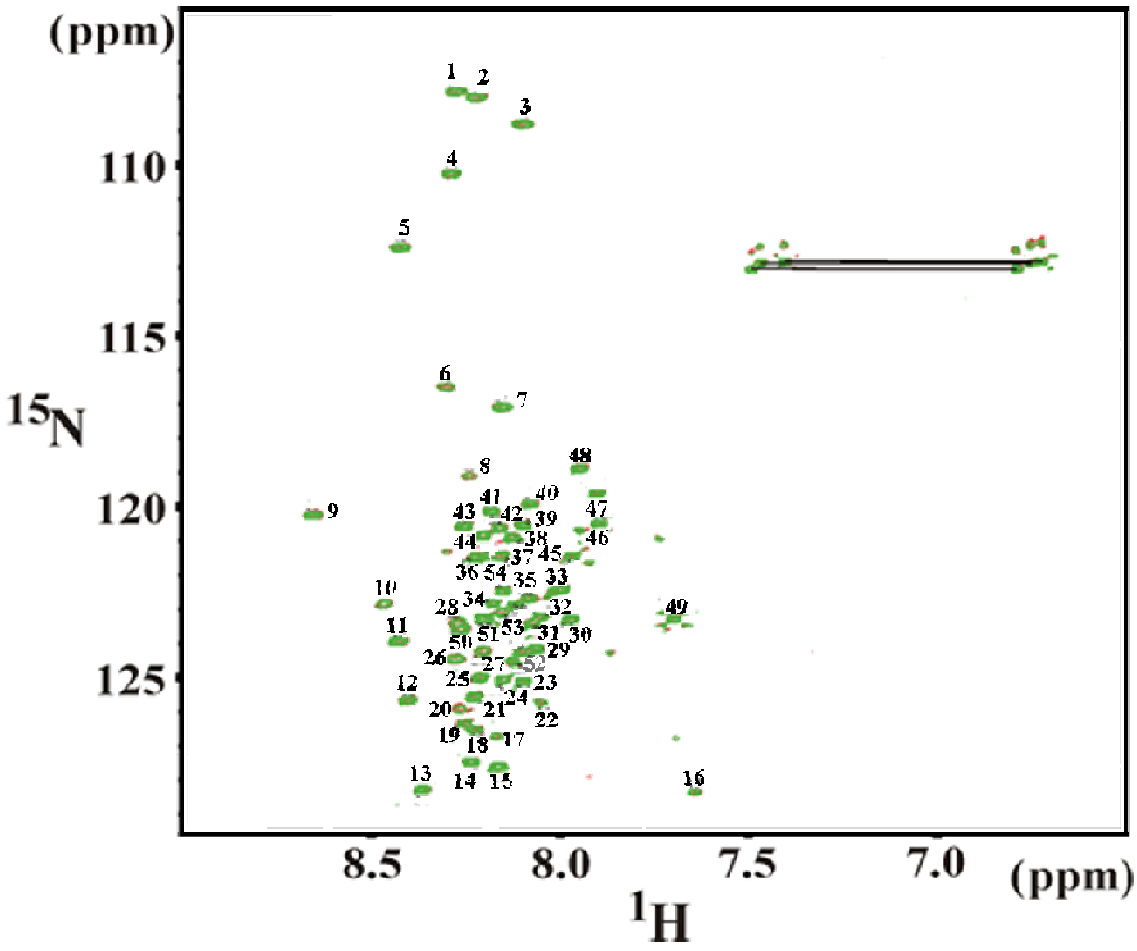

Figure 3.2.8: Superimposition of the ^{1}H ^{15}N HSQC spectra of $G_{61\text{-}114}$. Spectrum shown in red is control spectrum of $G_{61\text{-}114}$ and $G_{61\text{-}114}$-*d* (shown in green). Both spectra were acquired with 0.5 mM (ratio 1:1) of respective protein in 50 mM Tris/HCl (pH 7.5) at 288 K on a 600 MHz spectrometer (RISHIKESAN *et al.*, 2008).

3.3.1 Introduction

Subunit E is described to interact with the three stalk subunits C, G and H (JONES *et al.,* 2005). Disruption of the E-H subunit interaction resulted in a decrease in both ATP hydrolysis and proton transport activities of *S. cerevisiae* V-ATPase (JEFFERIES and FORGAC, 2008). Subunit E is predicted to contain an N-terminal extended α helix and a C-terminal part, consisting of a mixture of α-helices and β-sheet structures. Because of the central role of subunit E and the critical role of its N-terminus in subunit-subunit interaction, knowledge about its structural details is essential. Initail studies in our laboratory revealed that subunit E shows a mixture of α-helix and β-sheeted structure (GRÜBER *et al.,* 2002) and the protein was not stable over a longer period of time to perform any structural studies. Thus, two truncated forms of subunit E were created, including $E_{1\text{-}69}$ and $E_{133\text{-}222}$. Here I describe the production, purification and structural studies of the N- (1-69) and C-terminal region (133-222) of subunit E of yeast V-ATPase.

3.3.2 Purification of $E_{1\text{-}69}$ and production and purification of $E_{133\text{-}222}$

Subunit E constructs, $E_{1\text{-}69}$ (cloned by Dr. Thaker from our laboratory) and $E_{133\text{-}222}$, were amplified through PCR method using *Vma4* gene as template (GRÜBER *et al.,* 2002). The amplified gene products of both the constructs were specific and accurate with respect to the DNA marker. Figure 3.3.1 shows the amplified gene product of $E_{133\text{-}222}$. Following the amplification of gene coding for $E_{133\text{-}222}$, the PCR product was purified and incorporated with *Nco1* and *Sac1* restriction sites. This product was then ligated with the pET9d1-His_3 vector (GRÜBER *et al.,* 2002) and the correct plasmid was transformed into expression cells *E. coli* BL21 (DE3) which were grown on 30 µg/ml kanamycin containing LB agar-plates. Random isolated colonies were picked up and grown to analyse for the expression of the respective proteins. At an OD_{600nm} of 0.6, the cultures were supplemented with IPTG to a final concentration of 1 mM and were further grown for the production of respective proteins. Figure

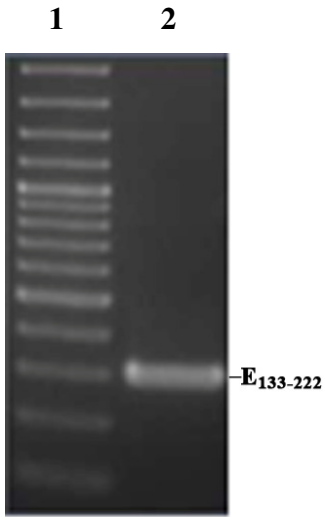

Figure 3.3.1: PCR amplification of $E_{133\text{-}222}$. The amplified genome product (lane 2) was checked for its accuracy against the DNA marker (lane 1) in a 1.7 % agarose gel.

3.3.2 reveals the over-expression patterns of the two constructs, His_3-E_{1-69} and His_3-$E_{133-222}$. All the selected colonies from respective clones showed a good induction pattern after 4 h.

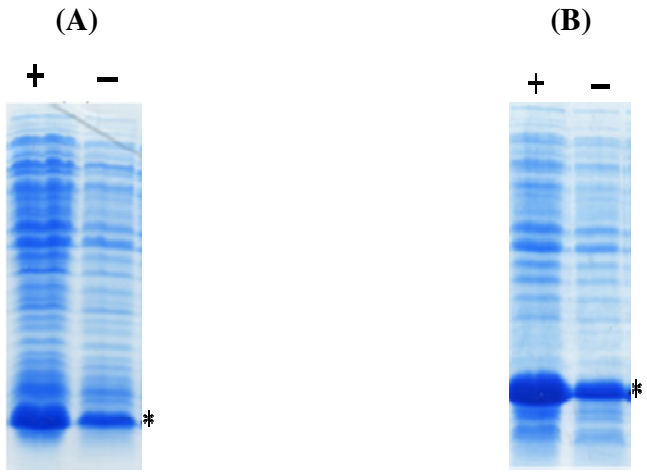

Figure 3.3.2: **SDS-PAGE showing the expression of recombinant subunit E proteins.** Induction of the proteins was done by addition of IPTG to a final concentration of 1mM. (*A*) E_{1-69} and (*B*) $E_{133-222}$. (+) and (-) indicates the presence and absence of IPTG, respectively.

The over-expressed proteins His_3-E_{1-69} and His_3-$E_{133-222}$ were purified through affinity column chromatography, Ni^{2+}-NTA resin against 50 mM HEPES (pH 7.0) and 150 mM NaCl buffer containing freshly prepared protease inhibitor, PMSF (2 mM) and Pefabloc^{Sc} (2 mM) with reducing agent DTT to a final concentration of 1 mM. Figure 3.3.3 shows the elution profile of the Ni^{2+}-NTA purified His_3-E_{1-69} (A) and His_3-$E_{133-222}$ (B). The His_3-tagged subunit E proteins were mostly found as the soluble fractions and were eluted between imidazole concentrations of 75 mM to 250 mM.

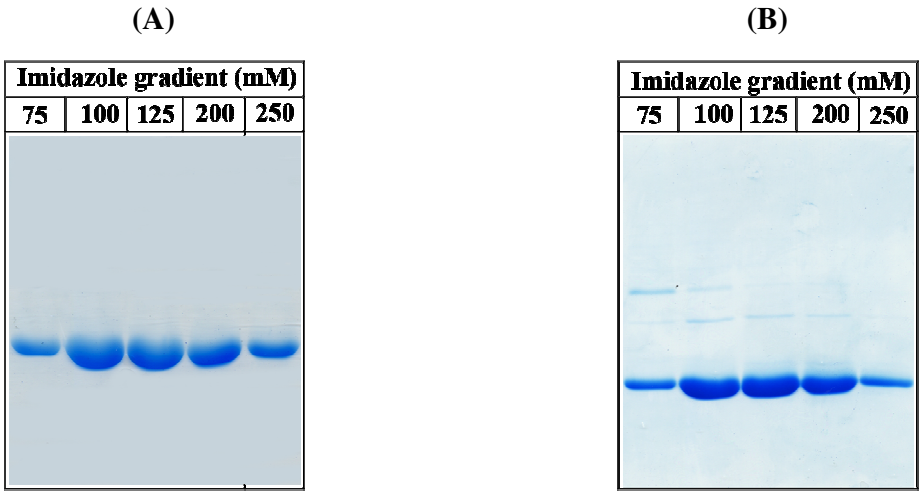

Figure 3.3.3: Ni^{2+}-NTA purification of truncated E subunit proteins. 17% SDS gel showing the Ni^{2+}-NTA elution profile of E_{1-69} **(A)** and $E_{133-222}$ **(B)**. Both recombinant proteins were eluted nearly pure at 75 to 250 mM Imidazole concentrations.

All fractions containing the respective His_3-tagged protein were pooled together and passed through the size exclusion column, Superdex HR75, against the respective buffer conditions. Figure 3.3.4 demonstrate the elution profile of His_3-E_{1-69} (A) and His_3-$E_{133-222}$ (B). The fractions including the respective proteins were concentrated using Centriprep YM-3 (3 kDa molecular mass cut-off) spin concentrator and 1 µl of the respective concentrated protein sample (E_{1-69} and $E_{133-222}$) was loaded on to the gel and showed a high purity.

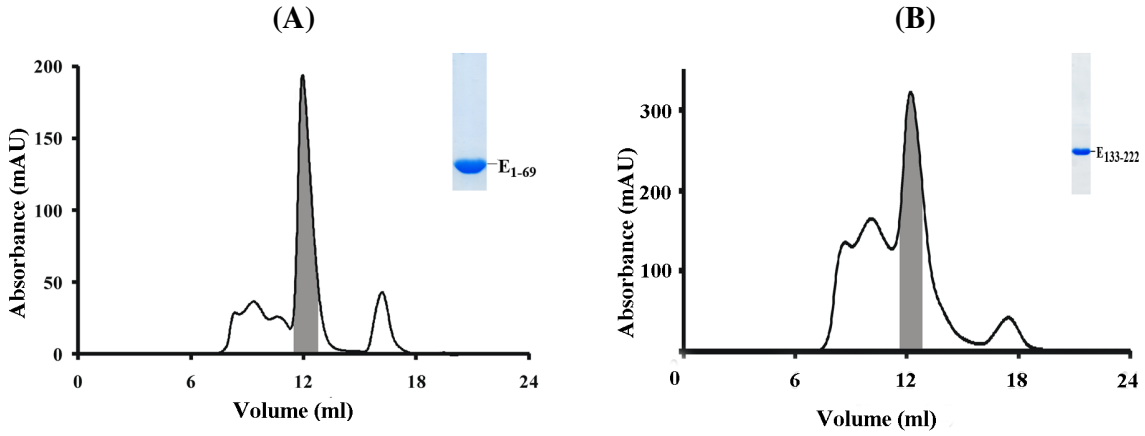

Figure 3.3.4: Purification of E subunit proteins by gel filteration. Elution chromatogram of E_{1-69} **(A)** and $E_{133-222}$ **(B)** from Superdex HR75. The respective shaded peaks were concentrated with YM-3 and 1 µl was loaded on a 17% SDS gel to show the purity of the protein (top right corner of the chromatogram).

3.3.3 Circular dichroism spectra of E_{1-69}

Secondary structure of the proteins can be determined by CD spectroscopy in the "far-UV" spectral region (190-260 nm). At these wavelengths, the chromophore is the peptide bond, and the signal arises when it is located in a regular, folded environment. α-helix, β-sheet, and random coil structures, give rise to a characteristic shape and magnitude of the CD spectrum. Like most spectroscopic techniques, the CD signal reflects an average of the entire molecular population. The secondary structure of E_{1-69} was determined from circular dichroism spectra, measured between 185-260 nm (Figure 3.3.5). The minima at 222 and 208 nm and the maximum at 192 nm indicate

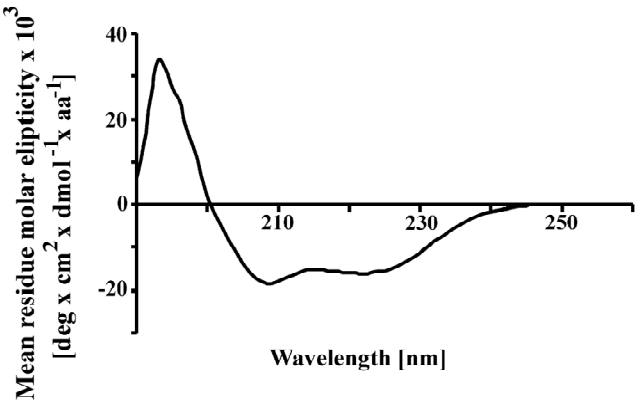

Figure 3.3.5: Circular dichroism of E_{1-69}. Spectrum measured at the concentration of 2 mg/ml (RISHIKESAN *et al.*, 2010).

the presence of α-helical structure in the proteins. The average secondary structure content was calculated to be 81% α-helix and 19% random coil (RISHIKESAN *et al.,* 2011).

3.3.4 Structural characterization of E_{1-69} by NMR spectroscopy

The $^{15}N/^{1}H$ HSQC experiment of E_{1-69} was performed by using the isotopically labeled protein. The structural characterization of the E_{1-69} protein through solution state NMR started with 2D ^{1}H ^{15}N HSQC, where the amide group of the individual amino acids, except proline, gives an individual peak on the spectrum. Thus the number of peaks on a 2D ^{1}H ^{15}N HSQC spectrum corresponds to the number of amino acids in a properly folded protein. Figure 3.3.6 shows the ^{1}H ^{15}N HSQC spectrum of E_{1-69} recorded in 25 mM sodium phosphate (pH 7.0), 200 mM NaCl and 5 mM EDTA at 288 K on a Bruker Avance 600 MHz spectrometer (RISHIKESAN *et al.,* 2011).

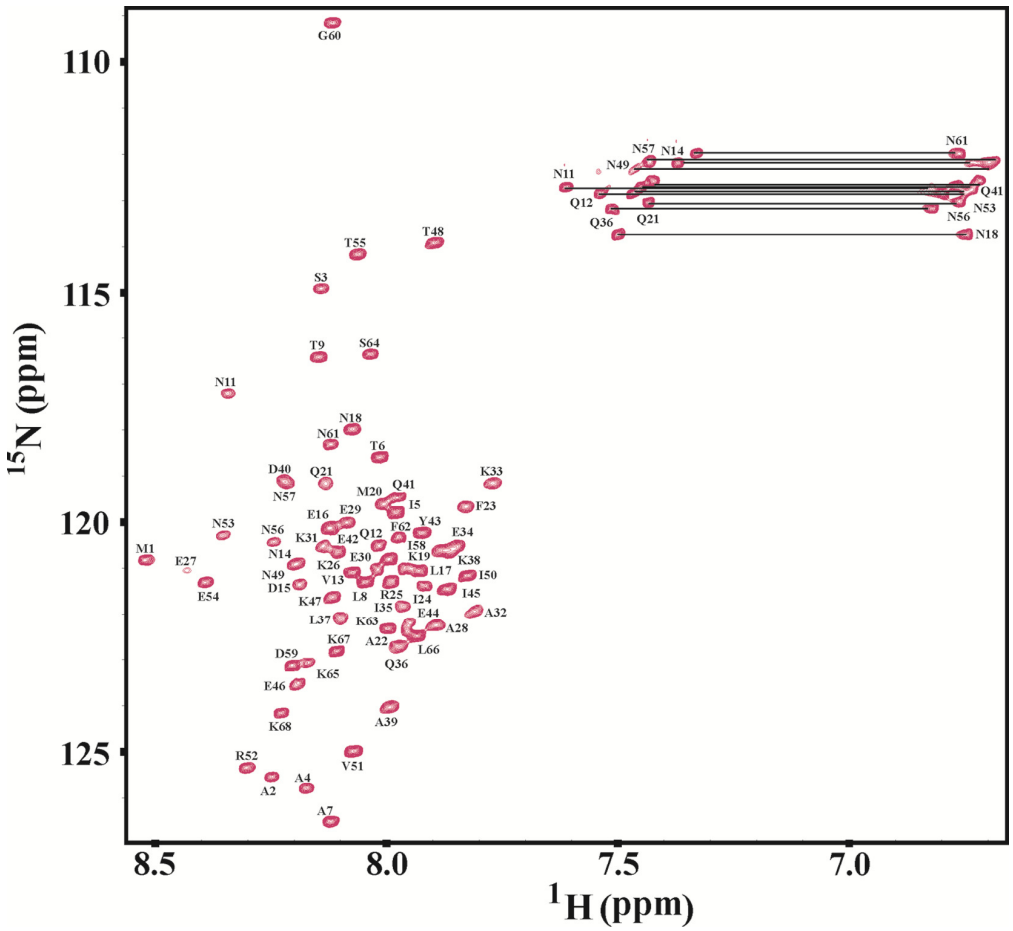

Figure 3.3.6: **^{1}H ^{15}N-HSQC spectrum of E_{1-69}.** Spectrum acquired in 25 mM sodium phosphate buffer (pH 7.0), 200 mM NaCl and 5 mM EDTA at 288 K. Signals from side-chain NH_2 groups are connected by horizontal lines (RISHIKESAN *et al.,* 2011).

The HSQC spectrum of E_{1-69} appeared to be properly folded and the peaks are well dispersed, and most of the individual peaks are distinguished. All 69 amino acid residues were observed in the $^{15}N/^{1}H$ HSQC spectrum (RISHIKESAN *et al.,* 2011). The chemical shift dispersion of around ~ 2.0 for the amide proton resonance indicates the predominant presence of helical structure on the construct. Assignment for the backbone HN, N, Cα, Cβ, and C' resonance of E_{1-69} was achieved by a combined analysis of the triple resonance HNCACB, CBCA(CO)NH and HNCO spectra. Overall, the limited chemical shift dispersion of ~ 2.0 ppm for the amide proton resonance indicates a predominantly helical protein.

3.3.4.1 NMR Solution structure of E_{1-69}

Two- and three dimensional NMR experiments were performed to observe the solution structure of E_{1-69}. The structure of E_{1-69} was calculated on the basis of a total 921 nontrivial NMR-derived distance restraints (284 were intraresidual, 304 were sequential and 160 were medium range) through molecular dynamics and simulated annealing (Table 3.3.1).

Total number of NMR restraints	921
Intraresidual (|i−j|=0)	284
Sequential (|i−j|=1)	304
Medium-range (2 ≤|i−j|≤ 4)	160
Long-range (|*i*−*j*| > 5)	0
Dihedral angle constraints	118
Hydrogen bond distance restraints	55
Ramachandran plot statistics (%)	
Residues in most favoured regions	87.9
Residues in additionally allowed regions	12.1
Residues in generously allowed regions	0
Residues in disallowed regions	0
Structural precision for well ordered region	
RMSD. backbone (residues 12−68):	0.59 Å
RMSD. heavy (residues 12−68):	1.70 Å

Table 3.3.1: Structural statistics of E_{1-69} (RISHIKESAN *et al.,* 2011).

Hydrogen bonds were identified from the characteristic patterns of homonuclear ^{1}H nuclear Overhauser enhancements (NOEs) and were introduced at the end of structure calculations. Typical α-helical NOE pattern $d_{\alpha N}$ (i, i+3), $d_{\alpha N}$ (i, i+4) and $d_{\alpha\beta}$ (i, i+3) were observed from

amino acid residues 12 to 68 (RISHIKESAN *et al.,* 2011). A bar diagram summarizing the backbone and the backbone/sidechain NOE connectivities of $E_{1\text{-}69}$ is illustrated in figure 3.3.7 Statistics of the 10 lowest energy structures of $E_{1\text{-}69}$ are described in the table 3.3.1. These 10 structures have an overall RMSD of 0.59 Å for backbone atoms and 1.72 Å for all the heavy atoms in the helical region of the three dimensional structures (Q12-K68) of the peptide. All these structures have energies lower than 4 kcal/mol, no NOE violations greater than 0.3 Å, and no dihedral angle violations greater than 5° (RISHIKESAN *et al.,* 2011).

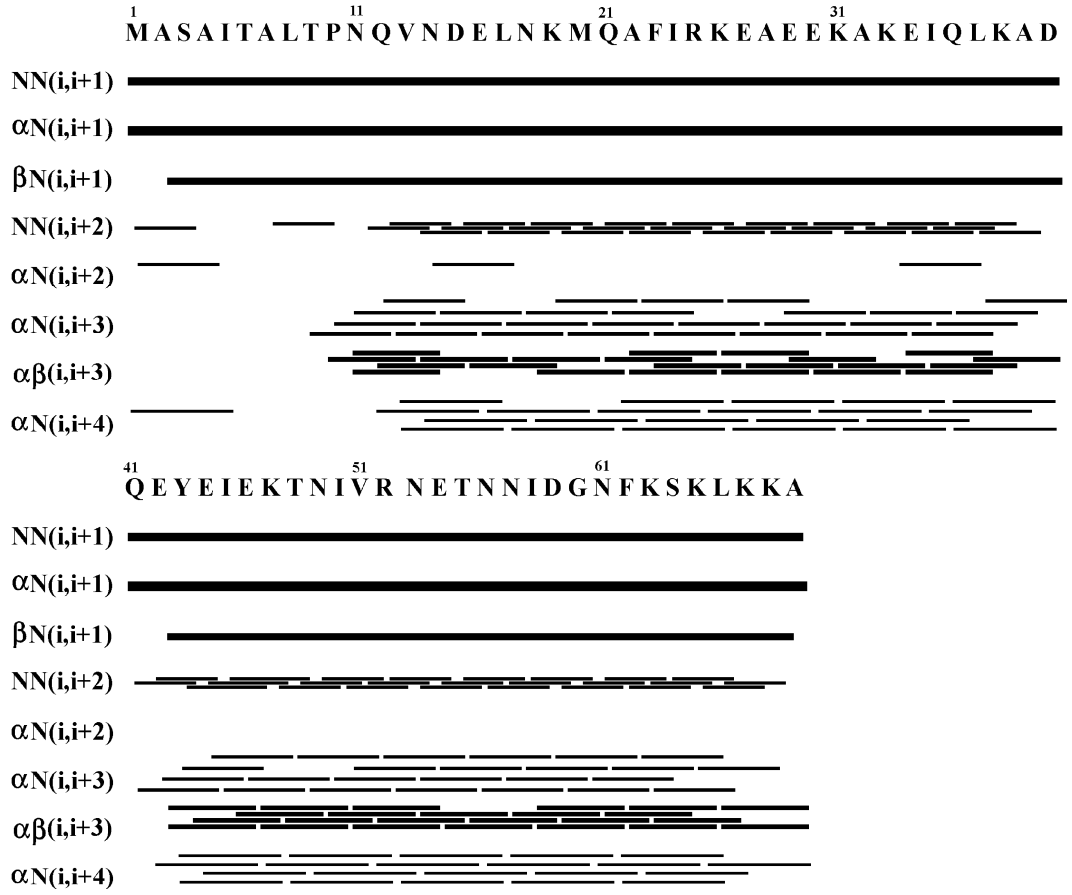

Figure 3.3.7: The connectivity diagram of the calculated structure for $E_{1\text{-}69}$. The line thickness reflects the intensities of the NOE connectivity (RISHIKESAN *et al.,* 2011).

Analysis of the Ramachandran plot for the calculated structure shows 87.9% residues in the most favored regions and 12.1% of the residues in the additionally allowed regions. As shown in figure 3.3.8A, $E_{1\text{-}69}$ has an extended helical structure from residues Q12 to K68 measuring a length of 83.19 Å, as predicted from the amino acid sequence and the secondary structure prediction of $E_{1\text{-}69}$. The peptide consists of 34.8% charged residues, 27.5% other polar residues and 37.7% non-polar residues in the sequence. The solution structure illustrates a clear

amphipathic helix with a hydrophobic N-terminus on one side of the helix and a highly charged C-terminus, exposing the charged residues towards the outer surface of the structure (Figure 3.3.8B and C).

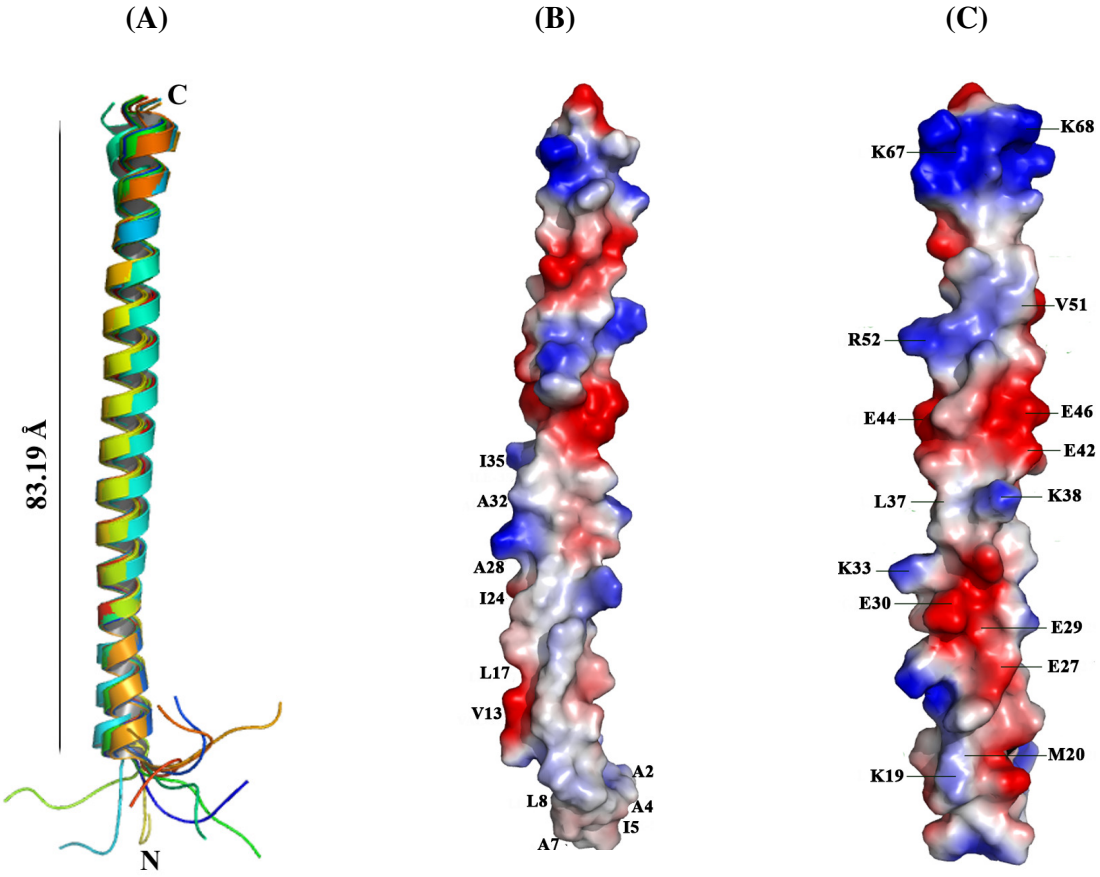

Figure 3.3.8. NMR solution structure of *S. cerevisiae* $E_{1\text{-}69}$. (A) Side view of the average structure of $E_{1\text{-}69}$. **(B-C)** Orientation of $E_{1\text{-}69}$ showing the molecular surface with electrostatic potential of the peptide, drawn in PyMol (DELANO 2001), where the positive potentials are drawn in blue, negative in red and hydrophobic surface in white color (RISHIKESAN *et al.,* 2011).

3.3.5 Structural characterization of $E_{133-222}$

3.3.5.1 Circular dichroism analysis of $E_{133-222}$

The secondary structure content of the peptide $E_{133-222}$ was determined from the CD spectra, measured between 190 and 260 nm (Figure 3.3.9). The overall spectrum is a typical characteristic of the presence of α-helical and β-sheeted structures in the protein. Secondary structure was calculated to be 44 % α-helix, 21 % β-sheet and 38 % random coil.

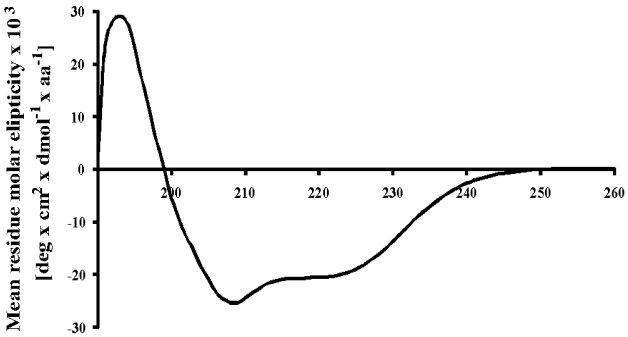

Figure 3.3.9: Circular dichroism of $E_{133-222}$: Spectrum measured with 2 mg/ml of protein (RISHIKESAN and GRÜBER, 2011, *manuscript in preparation*)

3.3.5.2 One dimensional NMR analysis of $E_{133-222}$

One dimensional NMR spectrum of $E_{133-222}$ was recorded in 50 mM HEPES, pH 7.0, 200 mM NaCl. The spectrum showed that the protein was well folded, as concluded from the pattern of peaks where there is a very good dispersion of resonance lines of amide protons (6-10 ppm). The resonance lines of uphill shifted methyl proton (-0.5 to 1.0 ppm), are characteristic peaks of folded protein (Figure 3.3.10). Therefore, NMR spectroscopy was chosen as a tool for structural studies of $E_{133-222}$ due to its structural features. The usual backbone finger printing assignment procedures were followed to determine the solution structure of the same.

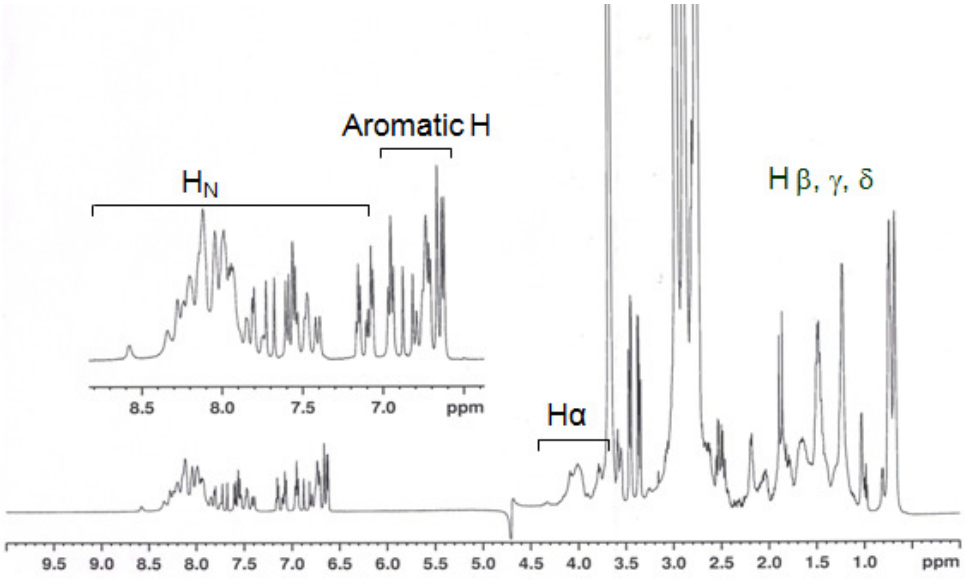

Figure 3.3.10: One dimensional NMR spectrum of $E_{133-222}$. The spectrum was recorded at 293 K in 50 mM HEPES, pH 7.0, 200 mM NaCl on a Bruker Avance 600 MHz machine.

3.3.5.3 NMR solution structure analysis of $E_{133-222}$

The structural characterization of $E_{133-222}$ protein through solution state NMR started with the 2D ^{1}H ^{15}N HSQC of isotopically labeled protein. Here the amide group of the respective amino acid (except proline), gives an individual peak on the spectrum. Thus the number of peaks on a 2D ^{1}H ^{15}N HSQC spectrum corresponds to the number of amino acids in a properly folded protein.

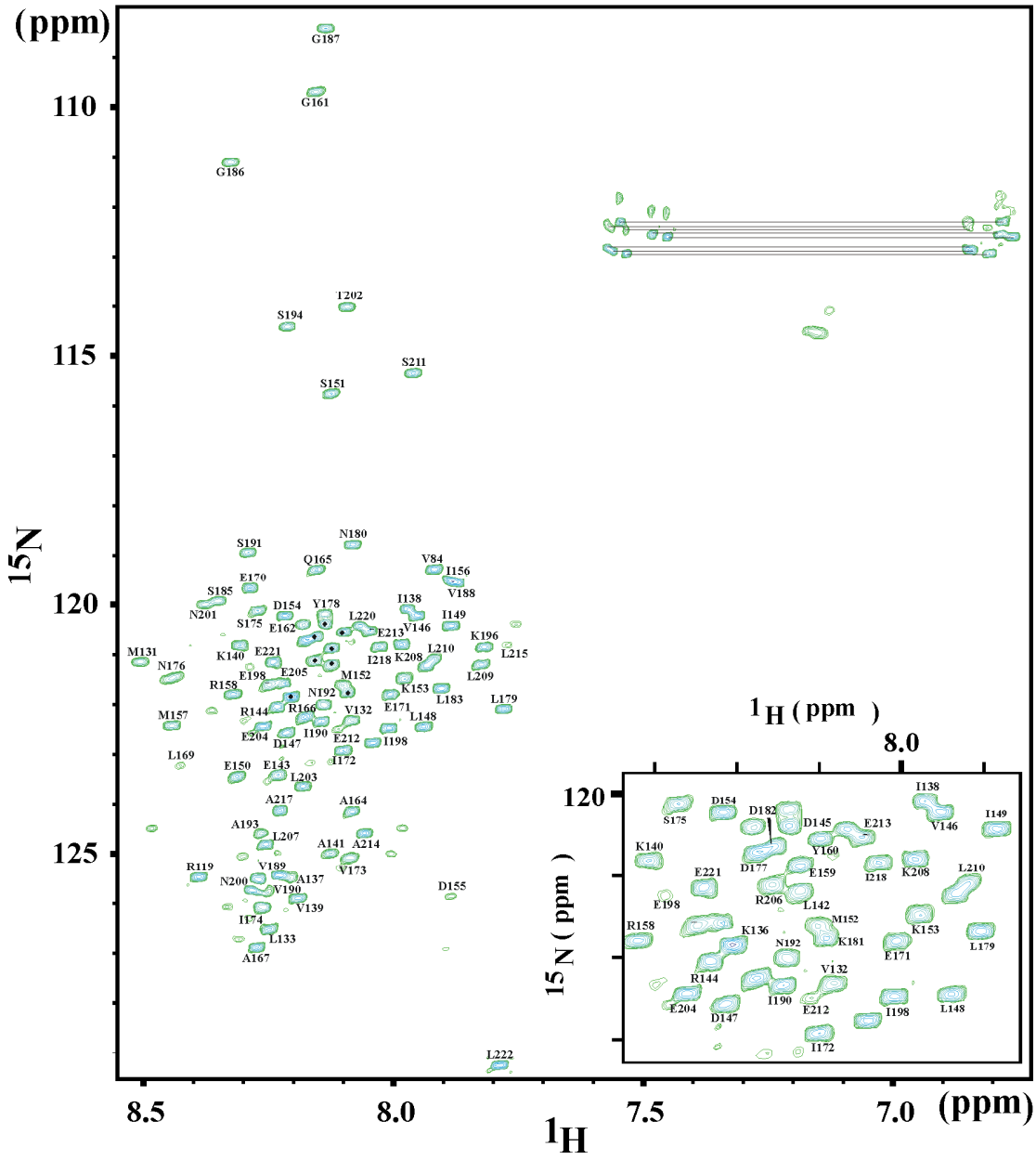

Figure 3.3.11: ^{1}H ^{15}N-HSQC spectrum of $E_{133-222}$. The spectrum was acquired in 25 mM sodium phosphate buffer (pH 6.0), 200 mM NaCl and 5 mM EDTA at 293 K. Signals from side-chain NH_2 groups are connected by horizontal lines.

The HSQC spectrum of $E_{133-222}$ appeared to be properly folded and the peaks are well dispersed, and most of the individual peaks are distinguished. 92 amino acid residues were observed in the $^{15}N/^{1}H$ HSQC spectrum except E134, R158 and D195 excluding three proline at residues 135, 168 and 216. The chemical shifts on the NH plane were dispersed to ~ 2.5 ppm for the amide proton resonance and this predominantly indicates the presence of a mixed population of helix and sheeted conformation. Figure 3.3.11 presents the ^{1}H ^{15}N HSQC spectrum of $E_{133-222}$ recorded in 25 mM sodium phosphate (pH 6.0), 200 mM NaCl and 5 mM EDTA at 293 K on a Bruker Avance 600 MHz spectrometer.

The sequential assignments of $E_{133-222}$ were performed using the ^{15}N and/or ^{13}C signals of the double and triple resonance backbone experiments on a combined analysis of the triple resonance spectrum HNCACB versus CBCA(CO)NH and HNCAO versus HNCO spectra. Overall, the limited chemical shift dispersion of ~ 2.5 ppm for the amide proton resonance indicates a predominantly mixed population of α-helix and β-sheets on the protein. 85 amino acids possessed the respective α-, β- and carbonyl peaks except the above mentioned seven residues, which include three proline residues as well. Most of the cross peaks in the ^{1}H-^{15}N HSQC spectrum of $E_{133-222}$ could be unambiguously assigned. To identify the region corresponding to the α-helix and β-strands on the secondary structure of the $E_{133-222}$, the deviation of the $^{13}C^{\alpha}$ and $^{13}C^{\beta}$ chemical shifs from random coil values were calculated (Figure 3.3.12).

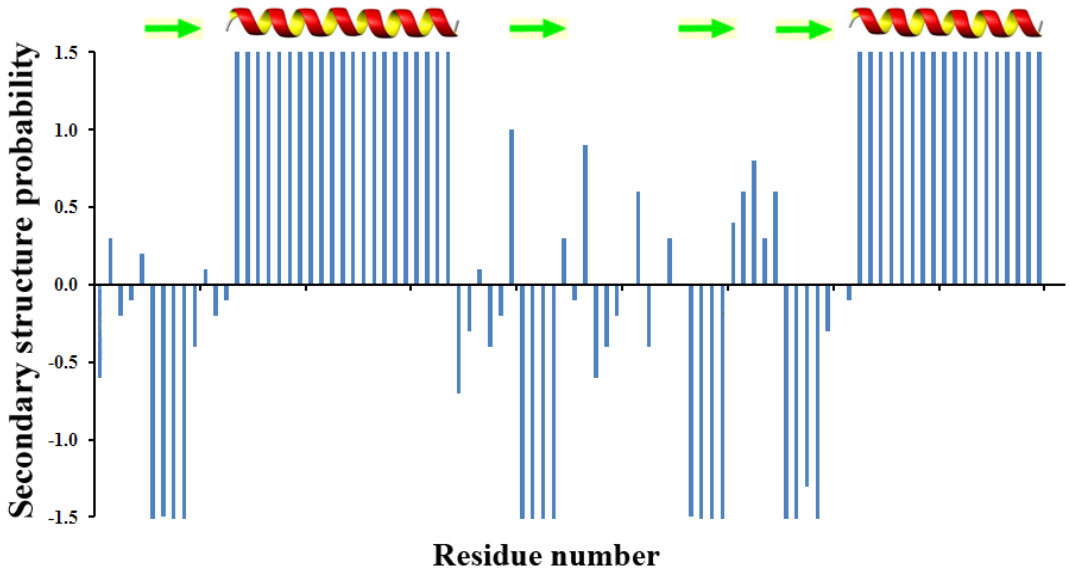

Figure 3.3.12: Chemical shift index (CSI, (WISHART *et al.,* 1992)) **plot of $E_{133-222}$.** In the vaules of CSI (ΔCα-ΔCβ), '+1' represents α-helical tendency, while '-1' represents the β-strand tendency.

These plotted values illustrate that the protein contains four β-strands and two α-helices (β1:α1:β2:β3:β4:α2). The β-strands consists of 4 residues including, K136-V139, E170-V173, G186-V189, D195-E198 on each strand, respectively. The helix between the first and the second β-strand comprises of 20 residues from R144-A164 and the helix on the C-terminus of the peptide includes T202-I218. A predicted topological model for the arrangements of the α- and β-sheeted region on the domain is given in figure 3.3.13. The four β-strands on the C-terminal structure of $E_{133\text{-}222}$, are connected by linker regions with 4-5 amino acids. Together the four β-strands with the α-helical region depict a compact globular domain. The 11 residues at the very C-terminus of subunit E sequence are predicted to be unstructured (MCGUFFIN *et al.,* 2000).

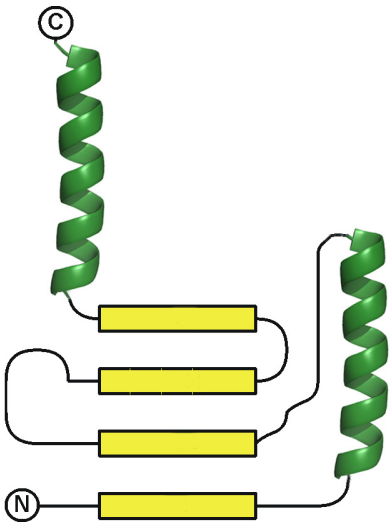

Figure 3.3.13: Topological model based on the determined secondary structure of $E_{133\text{-}222}$, as per CSI. The yellow color represents the four β-strands and green color represents the two α-helices. The strands and/or helix are connected by unstructured loop regions.

4.1 Stalks of the yeast V-type ATPases

The 3D structures of V_1 ATPase without subunit C from *C. fervidus* (BOEKEMA *et al.,* 1998) and *M. sexta* (RADERMACHER *et al.,* 2001, Figure 4.1) reveal a single compact stalk with no peripheral stalk(s). V_1V_O ATPase from *C. fervidus* showed a peripheral stalk on a side projection of the negatively stained V_1V_O ATPases (BOEKEMA *et al.,* 1998). Existence of a second (WILKENS *et al.,* 1999) and a third (DIEPHOLZ *et al.,* 2008) peripheral stalk in the V_1V_O ATPase has been described in negatively stained images. The composition of V_1 ATPase in the dissociated form constitutes subunits A and B in three copies, which is revealed by the intensities on the SDS gel (insert on the top left corner of the figure 4.1). The gel picture also validate the fact of one copy of each D, H and F subunits and at least 2 copies of subunit G and E on the V_1 ATPase (GRÜBER, 2003). These structural concepts debate the arrangements of various subunits on the respective stalks and/or the V_1 complex to become a more compact stator following the dissociation of V_1V_O complex, where the peripheral stalk(s) crumple to form a single central stalk in the free V_1 ATPase, leaving the V_O domain attached to the membrane.

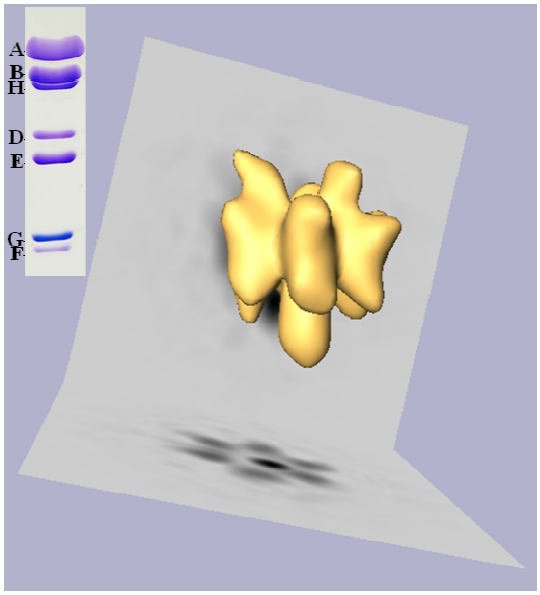

Figure 4.1: The 18 Å structure of V_1 ATPase without subunit C from *M. sexta* (RADERMACHER *et al.,* 2001)**.** The gel picture inserted on to the top left corner of the figure corresponds to individual subunits on the dissociated V_1 complex Courtesy: GRÜBER et al., 2003.

4.2 Stoichiometry and importance of subunit G in V_1V_O ATPase

The arrangement of subunits in the stalk regions of V-type ATPases and the distribution of subunits between the central and peripheral stalks have been investigated using a number of research approaches in recent years. Subunit G of *S. cerevisiae* has been shown to be present in more than one copy per enzyme (KITAGAWA *et al.,* 2008), and multiple functions of this subunit on the enzyme explain such an occurrence on the V_1V_O ATPases. Subunit G is required for proton pumping in the V_1V_O complex (TOMASHEK *et al.,* 1997; CHARSKY *et al.,* 2000), hydrolytic activity of V_1-ATPase (TOMASHEK *et al.,* 1997) and V_1V_O assembly (CHARSKY *et al.,* 2000). Precipitation assays demonstrate that subunit G interacts strongly with subunit *d*

(JONES *et al.,* 2005). The NMR titration data and the surface charge distribution of $G_{1\text{-}59}$ structure (Figure 3.2.6 and 3.1.11) illustrates that subunit G-*d* assembly occurs via the hydrophobic epitope at the very N-terminus of subunit G. No binding could be observed for $G_{61\text{-}114}$ with subunit *d* (Figure 3.2.8) and this confirms that subunit G binds to subunit *d* only via the N-terminus (RISHIKESAN *et al.,* 2009, Figure 4.2). Mutation studies of N-terminal region of subunit G demonstrated that substitutions affect the enzyme in assembly and/or its function (CHARSKY *et al.,* 2000). However, deletion in the C-terminal end of subunit G did not alter the enzyme assembly or its function. Subunit G is described to be strongly associated with the nucleotide binding subunit B and also weakly with subunit A of the catalytic V_1 sector (ARATA *et al.,* 2002, JONES *et al.,* 2005). The interaction of subunit G with residues A15 and A45 of subunit B (ARATA *et al.,* 2002), which are predicted to be on the external surface of subunit B, confirms that subunit G exists as a straight helix and also extends until the head domain and possibly represents a part of the peripheral stalk on V_1V_O ATPases (CHARSKY *et al.,* 2000). These data can also suggest that subunit *d* and G may together form a peripheral stalk to reach the head domain of V_1V_O complex. Mutation studies of subunit G on the N-terminus resulted in a complete destabilization of V_1V_O complexes (CHARSKY *et al.,* 2000). Thus, rearrangement of subunit G from the peripheral stalk to the component of central stalk in the dissociated V_1 ATPases also signifies the importance of subunit G to maintain the assembly of the V_1 ATPases and V_1V_O ATPases.

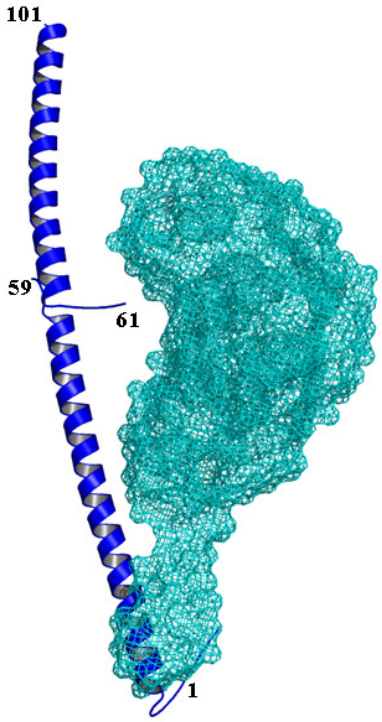

Figure 4.2: The proposed model of arrangement of subunit G and *d*. Solution NMR structure of $G_{1\text{-}59}$ (PDB-2K88), $G_{61\text{-}101}$ (PDB-2KWY) and mesh representation of solution X-ray structure of subunit *d* (cyan).

The copy numbers of stalk subunits of V-ATPase is still a matter of debate. The stoichiometry of one for subunits C, D and F of the V_1 domain and subunits *a* and *d* of V_O domain is defined (GRAHAM *et al.,* 2003). The presence of two copies of subunit G has been described by SAXS (ARMBRÜSTER *et al.,* 2003) and existence of two or three copies of subunit E is described by the staining intensities in coomassie-stained gels (NELSON and HARVEY, 1999). Isolation of Myc-tagged G subunit with V_1 isolated by affinity chromatography via a FLAG-

tagged subunit G provides strong support for the presence of multiple G subunits in each V_1 complex (OHIRA *et al.,* 2006). Subunit *d*, with a copy number of one, does bind to segment G7 to K34 of subunit G (RISHIKESAN *et al.,* 2009). The N-terminal fragment M1 to K5 as well as V22 to R26 of subunit G binds to amino acids on the N-terminal region of subunit E, specifically to E_{18-38} (JONES *et al.,* 2005; RISHIKESAN *et al.,* 2008). These phenomena indicate that the two or more copies of subunit G interact with different binding partners in its N-terminus implying different roles inside the V_1V_O complex. Subunits E and G are both present in more than one copies per complex (OHIRA *et al.,* 2006) and form a tight heterodimer (OHIRA *et al.,* 2006; FETHIERE *et al.,* 2005), thereby forming an essential structural element of two separate peripheral stalks that may probably contain either subunit H or C (WILKENS *et al.,* 2004; VENZKE *et al.,* 2005; ZHANG *et al.,* 2006). Consistent with this, domain analysis of subunit E has demonstrated that the N-terminal domain of this subunit can interact with both subunits H (LU *et al.,* 2002) and C (JONES *et al.,* 2005). The peripheral stalks can therefore be non-identical, and the reason for this complexity can be related to the fact that these stalks must not only stabilize the complex during rotary catalysis but must also participate in the regulation of ATPases activity *in vivo* through the reversible dissociation of V_1 and V_O complex (FORGAC, 2007).

4.3 Putative Role of subunit G in V_1 ATPase

Disassembled V_1 complex or V_1 ATPase contains three copies of subunit A and B (ARAI *et al.,* 1988). Copy numbers of subunit E and G are debated to great extent in recent times. However, existence of more than one copy of subunit E and G per V_1 complex is authenticated (OHIRA *et al.,* 2006). The remaining V_1 subunits except subunit C are confirmed to be one copy per complex (ARAI *et al.,* 1988). The V_1 sector showed decreased Mg^{2+} dependent ATPase activity and proton pumping at the membrane in both *M. sexta* (SUMNER *et al.,* 1995) and in yeast cells (KANE, 1995). Deletion mutant of subunit H on V_1 ATPase showed an increased Ca-ATPase activity (KANE and SMARDON, 2003). This indicates that subunit H, which appears to be a co-participant on the ATPase activity in the membrane-bound V-ATPase (V_1V_O ATPase), could be an inhibitor of the enzyme activity in free V_1 sector (KANE and SMARDON, 2003). These results suggest that subunit H must be involved in and/or accompanied with altering the subunit arrangements in V_1 domain, causing the release of V_O domain in a functional manner. This also provides an evidence on the central stalk formation below the head piece as seen in *M. sexta* of

V-ATPase (RADERMACHER *et al.,* 1996; SVERGUN *et al.,* 1998) after the dissociation of the V_1 sector from the V_O domain.

The appearance of a compact central stalk on the dissociated V_1 ATPase answers numerous questions on the subunit-subunit interaction. Deletion of subunit H showed normal V-ATPase assembly, but complete removal of ATPase activity and proton transport (HO *et al.,* 1993). Hybrid assay experiments confirmed the interaction of subunits E and H and also demonstrated the physiological significance of the interaction (LU *et al.,* 2002). Cross linking product were obtained for subunit E and D by to zero-length crosslink reagents EDC and $CuCl_2$ (COSKUN *et al.,* 2004). This result would position subunit E in-contact with subunit D in the V_1 complex. Induction of the E-F and E-G crosslinks on V_1-ATPase by Ca-ATP (GRÜBER *et al.,* 2000) is confirmed by precipitation assay (JONES *et al.,* 2005). The presented titration result obtained from NMR spectroscopy and FCS of subunits G and E would corroborate these facts (section 3.2) (RISHIKESAN *et al.,* 2008). The amino acid characterization of GE assembly would motivate any further mutation studies on subunit G to understand the subunits arrantement on the enzyme. Genetic deletion of subunit G destabilizes the E subunit significantly (TOMASHEK *et al.,* 1997). Point mutations in the N-terminal half of subunit G (E14A) resulted in a complete destabilization of subunit E and C (CHARSKY *et al.,* 2000). This could be caused by an alteration of the flexible part between K5 and K16 of subunit G and thereby weakening the interaction between subunit E and G. Together, these results suggest the functional importance of this interaction. Thus, these results confirm the position of subunit G on the compact central stalk of the V_1-ATPase as a crucial subunit for the assembly and proper function of the V_1-ATPase.

4.4 Arrangement of subunit G in the V_1 -ATPase

Most of the models on V-ATPases assign both subunits E and G to the peripheral stalks of the enzyme. Variations on how they are envisaged among themselves and/or with the neighboring subunits C, H, *a*, and A_3B_3 make the complexity of the proposed models. The NMR and FCS titration data presented in the figure 3.2.1, support the view that the association of subunit E and G occurs only via the N-terminal region of both subunits, and allows for the first time, the identification of amino acids M1, V2, S3, K5, V22, S23, K24, A25 and R26 of subunit G that are involved in the assembly of subunits E and G (RISHIKESAN *et al.,* 2008). This interaction was also described earlier (FETHIERE *et al.,* 2004) based on the isolation of a tight E-G complex from *E. coli* expressing yeast subunit E and G genes from a bicistronic plasmid.

Precipitation experiments exploiting the affinity of the GST component with truncated forms of subunit E (JONES *et al.,* 2005) revealed that removal of the first 38 amino acids of subunit E prevented interaction with subunit G, whereas removal of amino acids 1–19 did not alter the binding trait of the subunits. The N-terminus of subunit E is predicted to have a high propensity for coiled-coil formation and studies also suggested that it might form the same with subunit G (FETHIERE *et al.,* 2004). Point mutations in the N-terminal half of subunit G (E14A) resulted in destabilization of subunit E and C (CHARSKY *et al.,* 2000). In addition, subunit E forms a zero-length crosslink with subunit F and G in the V_1 complex, when Ca^{2+}ATP is bound to the enzyme (GRÜBER *et al.,* 2000). Taken together, all of these data suggest that the subunits E and G interact via their N-terminal regions, both of which are predicted to be highly helical and possibly capable of coiled-coil formation at the N-terminus.

4.5 Dimeric model of subunit G

A number of current models for V-ATPase structures incorporate a dimer of the G subunit, but the evidence for a G subunit dimer is primarily from *in vitro* analysis of pair wise subunit interactions (JONES *et al.,* 2005; ARMBRÜSTER *et al.,* 2003). The yeast G subunit expressed and purified from *E. coli* formed an elongated dimer, and dimer formation was eliminated by deletion of amino acids 1-38 (ARMBRÜSTER *et al.,* 2003). Yeast G subunit expressed *in vitro* was also able to bind to a glutathione *S*-transferase-G subunit fusion protein bound to a column (JONES *et al.,* 2005). Significantly, there was no E subunit present in either of these experiments, and the region (N-terminus) required for G subunit dimerization appears to be very similar to that required for formation of an E-G subunit complex. Subunit G expressed in *E. coli* was significantly more stable when expressed with the E subunit, conditions where an E-G subunit complex is formed (FETHIERE *et al.,* 2004). One possibility is that in the absence of the E subunit, two G subunits can form a coiled-coil structure similar to that formed by the N-terminal section of subunit E and the G subunit. There might even be competition between the E subunit and other G subunits for binding to the N-terminus of subunit G. Although there is no direct evidence for this, G subunit can bind to subunit E more readily than to subunit G. Perhaps more significantly, a competition between G subunit dimerization and E-G complex formation might help to explain the effects of G subunit overexpression *in vivo*. It is possible that in the presence of excess subunit G, dimerization (or multimerization) begins to compete with E subunit binding.

This may result in destabilization of the G-G dimer, because binding to subunit G is critical for E subunit stability *in vivo* (TOMASHEK *et al.,* 1997).

Solution X-ray scattering data revealed that subunit G is elongated and dimeric in solution (ARMBRÜSTER *et al.,* 2003), with an α-helical and highly conserved N-teminal half and a proposed α-helical C-terminal sequence (CHARSKY *et al.,* 2000; HUNT *et al.,* 1997). The decrease in experimentally determined diffusion rates with increasing concentrations of $G_{61\text{-}101}$ suggested a dimer formation (Figure 3.1.23), assuming that the exchange rate between monomer and dimer concentration of subunit G construct ($G_{61\text{-}101}$) is fast on the diffusion timescale in NMR spectroscopy. The corresponding dimer dissociation constant for $G_{61\text{-}101}$ was estimated by direct fit of the translation diffusion rates as a function of concentration (1.5 mM, RISHIKESAN *et al.,* 2010). The cross link formation of subunit G mutants demonstrate that residues in position 72 and 72', 81 and 81' of the first and second helix are in close proximity as represented in the dimeric model of $G_{61\text{-}101}$ (Figure 4.3) (RISHIKESAN *et al.,* 2010). In contrast, no cross link product could be observed for cysteine at position 74, reflecting the location of residue 74 at the opposite side of the two helices (Figure 3.1.24B). Consequently, these results suggests that the C-terminal helix of subunit G would not be arranged in a left-handed coiled-coil manner as proposed (KITAGAWA *et al.,* 2008), since such a fold is dictated by a heptide repeat $(a\text{-}b\text{-}c\text{-}d\text{-}e\text{-}f\text{-}g)_n$, with hydrophobic residues at position *a* and *d* arranged at the interface between the two helices (PARRY *et al.,* 2008).

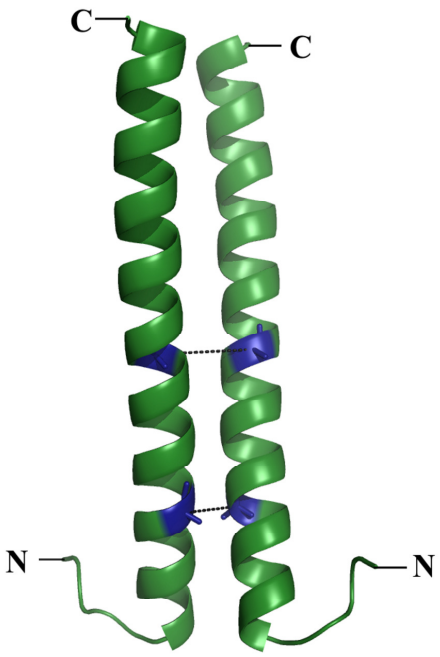

Figure 4.3 Dimeric model of $G_{61\text{-}101}$ based on cross linking data and diffusion coefficient measurements. Residues in blue color exhibiting A74 and A81, respectively, form a zero-length crosslink in the presence of $CuCl_2$ (RISHIKESAN *et al.,* 2010).

4.6 Comparison of the peripheral stalk subunits

V-ATPases share an evolutionary history with F-type ATP synthases and A-type ATP synthases (NELSON AND TAIZ, 1989; MÜLLER and GRÜBER, 2003). Although direct sequence similarities are limited primarily to the ATP binding catalytic and regulatory subunits, V-ATPases utilizes a rotary mechanism like that of F_1-ATPases to couple ATP hydrolysis and

proton transport across the membrane (HIRATA *et al.,* 2003). One structural requirement of rotational catalysis in F_1F_O ATP synthase is the presence of a "stator", a complex of protein that physically ties the *a* subunit to the F_1 head piece containing catalytic and regulatory subunits to allow productive relative rotation of the rotor subunits (DUNN *et al.,* 2000). The subunit-subunit interaction provides the stability essential for rotational catalysis through a combination of relatively strong interactions (WEBER *et al.,* 2004). Despite limited homology between V-ATPase, F- and A-ATP synthase subunits (BOWMAN *et al.,* 1988; GOGARTEN *et al.,* 1992), some sequence similarities between soluble domain of subunit G, *b* and H of V-ATPase, F- and A-ATP synthase, respectively, have led to the proposal that these proteins are functionally analogous to each other (SUPEK *et al.,* 1994; HUNT and BOWMAN, 1997; BIUKOVIĆ *et al*., 2007).

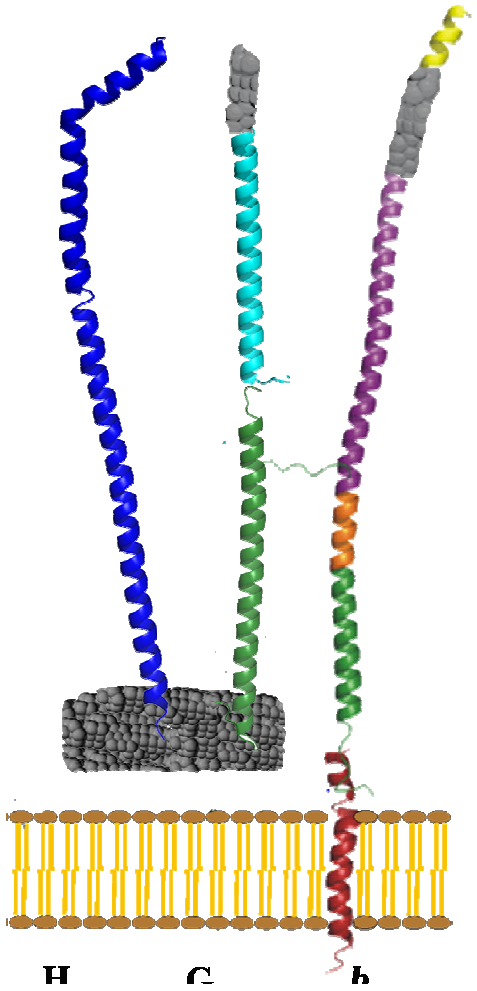

Figure 4.4. Comparision of the structures of subunits H, G and *b* of A_1A_O ATP synthase, V_1V_O-ATPase and F_1F_O ATP synthase respectively. Subunit H shows the crystal structure (LEE *et al.,* 2010), subunit G shows solution structure of $G_{1\text{-}59}$ and $G_{61\text{-}101}$ (RISHIKESAN *et al.,* 2009, 2010) and subunit *b* shows the solution structures of $b_{1\text{-}34}$, (DMITRIEV *et al.,* 1999), $b_{30\text{-}82}$, $b_{140\text{-}156}$ (PRIYA *et al.,* 2009) and crystallographic structure of $b_{62\text{-}122}$ (DEL RIZZO *et al.,* 2002). The grey color mesh connecting the structures of subunits H and G represent the collar like domain from the respective A_1A_O ATP synthase and V-ATPase.

Dimeric subunits *b* of bacterial F-ATP synthase serve to fix F_1 to F_O and forms a stator through its membrane anchor, thereby preventing rotation of the F_1 domain during catalysis (HERMOLIN *et al.,* 1983; PERLIN *et al.,* 1983). When positioned on to the low resolution X-ray model of subunit $b_{22\text{-}156}$, of F_1F_O ATP synthase, the NMR solution structure of $G_{1\text{-}59}$ and $G_{61\text{-}101}$ from yeast V-ATPase, which excludes the 13 residues from the C-terminus, occupies the length until the delta binding site of the subunit *b* from F_1F_O ATP synthase (Figure 4.4). The striking difference between the three classes of peripheral stalks is that both subunit G (V-ATPase) and subunit H (A-ATP synthase) have no membrane-traversing region, when compared with the peripheral stalk subunit *b* of F-ATP synthases (HUNT *et al.,* 1997), and is therefore assumed to interact with another subunit to fulfil this presumed role (HUNT and BOWMAN 1997). This might imply that peripheral stalk subunits like G (V-ATPase) and H (A-ATP synthase) of the closely related V-ATPase and A-ATP synthase, respectively, have a different and additional function inside the enzyme complex (BIUKOVIĆ *et al.,* 2007). The ability of all the three subunits (G, H and *b* from V-ATPase, A- and F-ATP synthase respectively) to interact with the catalytic subunits (ARATA *et al.,* 2002; SCHÄFER *et al.,* 2006; KERSTEN *et al.,* 2000) proposes the potential to influence catalytic events more directly. This would therefore clarify that all the three subunits would function beyond the generally accepted role of providing linkage between the cytosolic and membrane domains (KERSTEN *et al.,* 2000).

4.7 Structure and arrangement(s) of the subunit E in V_1V_O ATPase

The number of peripheral stalks, its composition and the stoichiometry per complex are the imperative issues that are yet to be resolved. When the quantitative amino acid analysis suggests the presence of only one subunit E (ARAI *et al.,* 1995), significant research evidence shows the presence of two or more copies (SUPEKOVA *et al.,* 1996; WIECZOREK *et al.,* 2000). Cross-linking studies position subunit E as extended and running from top of V_1 to V_O and also interacting with the external surface of subunit B at the A_3B_3 hexamer (ARATA *et al.,* 2002). Subunit E is in close proximity to the stalks subunits C, H and G of the V_1 sector (XU *et al.,* 1999) and to the *a* subunit of the V_O sector, which is predicted to anchor V_1 at the membrane (LANDOLT-MARTICORENA *et al.,* 2000; KAWASAKI-NISHI, S. *et al.,* 2001). Biochemical data with truncated forms of subunit E of the *S. cerevisiae* V-ATPase showed that deletion of the N-terminal 38 residues resulted in a complete loss of E-G association (JONES *et al.,* 2005). Characterization of the N-terminal region of subunit E through solution NMR showed that $E_{18\text{-}38}$ peptide strongly

interacts with N-teriminal fragment of subunit G (RISHIKESAN *et al.,* 2008). More precisely amino acids M20, E29 and E30 of the E_{18-38} are described to be involved in subunit E-G assembly (RISHIKESAN *et al.,* 2008). The presented solution NMR structure of E_{1-69} reveals highly charged residues on these sides, which includes K19, M20, E27, E29, E30, K33, K37, K38, E42, E44, E46, V51, R52, K67 and K68 (Figure 4.5A) (RISHIKESAN *et al.,* 2011). Most of these residues are universally conserved among eukaryotic V-ATPases and these charged residues of subunit E together with the high intensity of charged residues on subunit G may form the interacting area of both stalk subunits as predicted from the site directed mutagenesis of yeast G subunit (CHARSKY *et al.,* 2000).

While the evidence of subunits E and G forming part of the stator is getting clearer, the crystal structure of subunit C has also provided the proof of its participation in the stator and also illustrated some insights into the regulatory mechanism of the enzyme (DRORY *et al.,* 2004). Precipitation assay showed no effects on the E-G interaction when the N-terminal 19 amino acids were deleted. But it significantly reduced the association of C and E subunits upon removal of E_{1-19} from subunit E of yeast V-ATPase (JONES *et al.,* 2005). Lack of this N-terminal segment (E_{1-19}) in the related A_1A_O ATP synthases from archea explains the fact that it does not have any counterpart of the eukaryotic subunit C (GRÜBER and MARSHANSKY 2008) and thus making this as a key determinant in the interaction of subunits C and E. Mutagenesis studies have shown that subunit C-E assembly in the *S. cerevisiae* V-ATPase are mediated primarily by hydrophobic residues, like V13 and L17, pointing to the role for hydrophobic interaction (JONES *et al.,* 2005). The solution NMR structure of E_{1-69} shows that both residues are located on one side of the helix and would also support a hydrophobic interaction of both the subunits (Figure 4.5B). Interestingly, *in vivo* mutagenesis also demonstrated that single substitutions of the hydrophobic residues V13 and L17 and the positively charged K19 on the other side of the helix, respectively, resulted in loss of V-ATPase function (JONES *et al.,* 2005). Subunit C consists of two globular domains, a so-called foot and head domain which are linked via a helical coiled coil region (OMRI *et al.,* 2004). From *in vitro* data it has been proposed, that the head region of subunit C would strongly interact with subunit E (OOT *et al.,* 2010). Because of the globular shape of the head region of subunit C, we propose that the very N-terminus of E may become anchored in the globular domain of subunit C, allowing the hydrophobic and polar residues of subunit E to interact with the corresponding amino acids in subunit C.

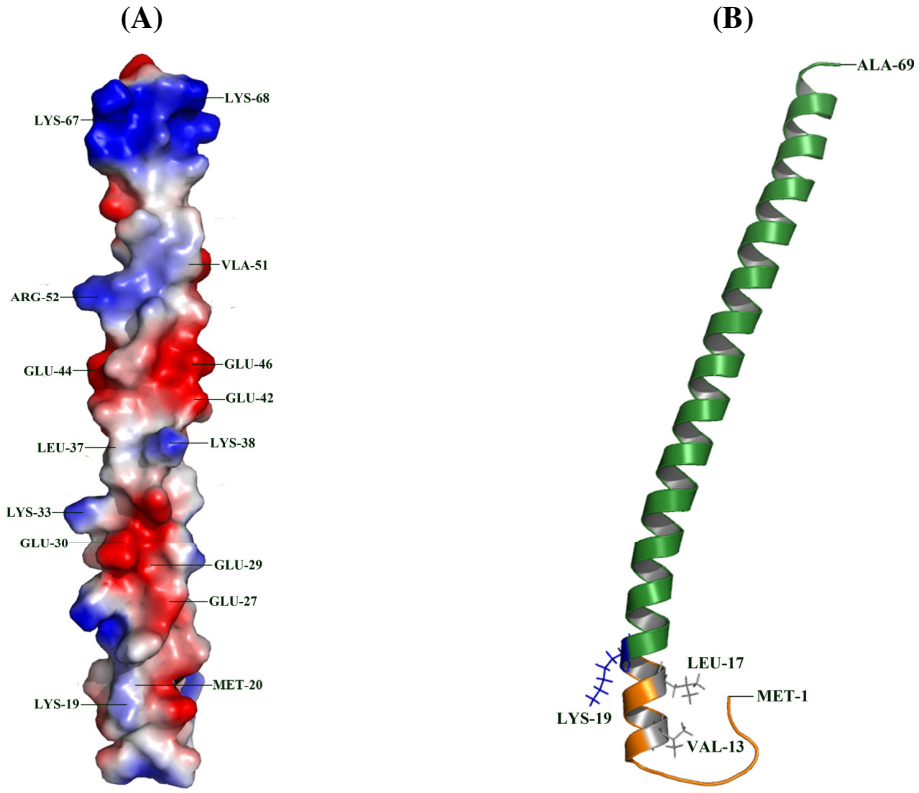

Figure 4.5. NMR solution structure of *S. cerevisiae* E_{1-69}. (A) Orientation of E_{1-69} showing the molecular surface with electrostatic potential, drawn in PyMol, where positive potentials are drawn in blue, negative in red and hydrophobic surface in white color (RISHIKESAN *et al.,* 2011). **(B)** Ribbon diagram of E_{1-69} revealing the first 19 amino acids in orange. The hydrophobic residues V13 and L17 are highlighted in grey and the positively charged residue K19 is shown in blue (RISHIKESAN *et al.,* 2011).

Deletion of subunit E on the V-ATPase disrupts its assembly and results in decreased ATPase and proton transport activites (FOURY, 1990). On the contrary, deletion of subunit H showed normal V-ATPase assembly, but no ATPase activity and proton transport (HO *et al.,* 1993). Hybrid assay experiments confirmed the interaction of subunits E and H and also demonstrated the physiological significance of the interaction (LU *et al.,* 2002). Removal of 78 residues from the N-terminus of subunit E resulted in a complete loss of both subunits E-H assembly and also proper function of V-ATPase. The determined solution NMR structure (Figure 4.5A) reveals the exposure of charged residues on both sides of E_{1-69} structure and allows to propose, that residues K19, R25, K26, E27, E29, E30, K31, Lys33, E34, K38, E42, E44, E45, K46, R52, E54, K63, K65, K67 and/or K68 may be important for its assembly with subunit H (LU *et al.,* 2002). The role of subunits E-H assembly in controlling V-ATPase activity in response to proteins interating with V-ATPase is still unclear. Elucidation of the physiological significance of these protein-protein interactions will likely advance the understanding of this fundamental proton pump.

Subunit E forms cross linking contacts between C, H, D and F of the V_1 domain and subunit *a* of V_O domain (XU *et al.,* 1999) of the V_1V_O ATPase complex. Because subunit *a* is observed to be part of the stationary V_O complex, it is less likely that E subunit forms part of the central stalk on the V_1V_O ATPase. Furthermore, the contact between subunit C and H with E would suggest that they could occupy a more exposed position in the complex, and this would be consistant to play a part of the peripheral stalk along with subunit G and/or subunit C and H. On the contrary, from the electron micrograph of A_3B_3DEFG from the V_1 ATPase of *M. sexta*, the subunit arrangements of stalk subunits is also justified on the central stator region under A_3B_3 head piece (GRÜBER, 2003). Importance of subunit E can be described by its interaction with various stalk subunits on the V_1 ATPase complex and also signifying that subunit E would rearrange itself from the peripheral stalk of V_1V_O ATPase to become a part of the central stalk on the disassembled V_1 ATPase.

4.8 Structural position of subunit E with respect to subunit B

Subunit E is predicted to contain an extended N-terminal α-helix and a globular C-terminal domain with a mixture of α-helix and β-sheet structures (JONES *et al.,* 2005). The described solution NMR structure of $E_{1\text{-}69}$ shows an extended length of 83.19 Å and confirms the prediction. When positioned inside the crystal structure of subunit E in A_1A_O ATP synthase from *Thermus thermophilus*, $E_{1\text{-}69}$ accommodated well with an R.M.S.D of 1.481 Å for residues F23-A69 ($E_{1\text{-}69}$) and residues S29-A75 ($E_{19\text{-}206}$), confirming the presence of a highly α-helical N-terminal region (Figure 4.6A) (LEE *et al.,* 2010). Considering the knowledge of a homologous existence, both subunits would share a similar structure on the complex. Thus prediction of a globular C-terminal domain on subunit E of V_1V_O ATPase similar to the one on subunit E of A_1A_O ATP synthase would be consistent. Structural analysis of the solution NMR studies of subunit E ($E_{133\text{-}222}$, Figure 4.6B), which is a homologous region of the recently solved crystal structure of $E_{101\text{-}206}$ of subunit E from A_1A_O ATP synthase of *M. jannaschii* (BALAKRISHNA *et al.,* 2010), showed a similar secondary structure pattern with four folds of β-sheets and a helical region on both the N- and C-termini of the construct (Figure 4.6C). The four folds of β-sheets are connected by linker regions between each strand. The additional β-sheeted folding on C-terminus of subunit E can also be justified with the fact that E subunit can extend nearly two fold the distance between the membrane and V_1 head piece, if it forms a continueous helix (WILKENS *et*

al., 1999) and thus this β-sheeted folding at the carboxyl terminal of subunit E makes it to form a globular domain.

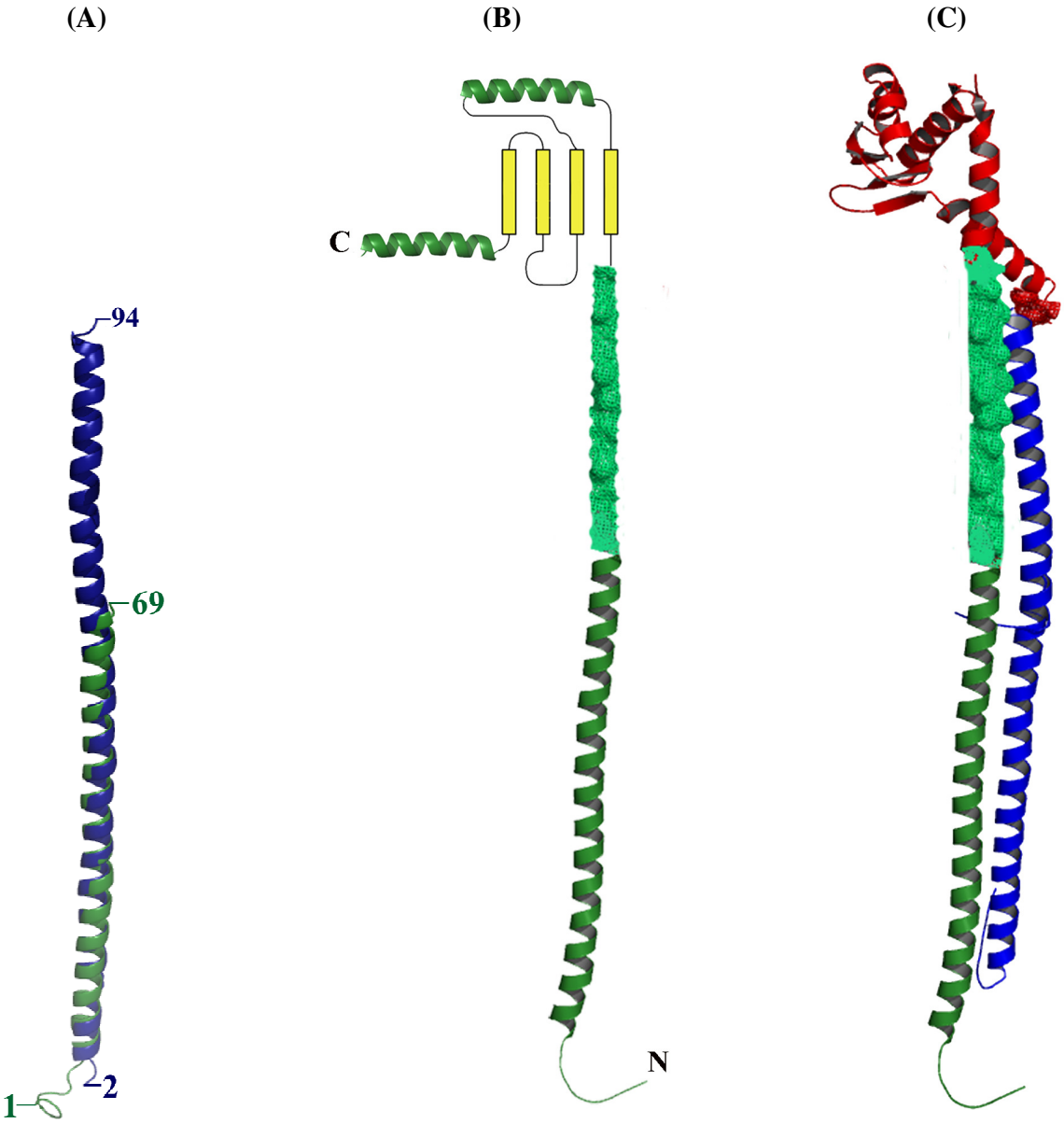

Figure 4.6: Structural model of subunit E of yeast V-ATPase. (A) NMR solution structure of $E_{1\text{-}69}$ (green) from yeast V-ATPase superimposed on to the crystallographic structure of $E_{2\text{-}94}$, of the *T. thermophilus* (blue (LEE *et al.,* 2010)). **(B)** The arrangements of subunitE ($E_{1\text{-}69}$ (green), $E_{133\text{-}222}$ (2D Cartoon, with green α-helix and yellow β-sheet) and uncharacterized region (lime green mesh) from yeast V-ATPase. **(C)** The arrangements of subunit G, $G_{1\text{-}59}$ (blue) and $G_{61\text{-}101}$ (blue) with subunit E, ($E_{1\text{-}69}$ (green) from yeast V-ATPase, $E_{101\text{-}206}$ from A_1A_O ATP synthase. The lime green color mesh region is the un-characterized region of subunit E from yeast V-ATPase.

Cysteine based cross linking studies showed that subunit E of V-ATPases is in close proximity to subunit B (ARATA *et al.,* 2002). Mutational studies on subunit B of V_1-ATPase showed that subunit E would communicate with subunit B at the outer surface of the A_3B_3 hexamer. In line with the above mentioned facts and also considering the contacts of subunit E

with subunit B, it is more likely that the C-terminus of subunit E ($E_{133-222}$) from V_1V_O ATPase, which forms a globular domain with 4 folds of β-sheets and some helix, would be the region of contact between B and E subunit. Considering all these contacts of subunit E with the components of V_1 sector, it can also be suggested that subunit E may represent the foundation of the stalk region (KANE and SMARDON 2003; ARATA *et al.,* 2002), together with subunit G, as a peripheral stalk on the V_1V_O ATPase and with all the other stalk subunits (subunit C and H forming the rotor; subunit D and F forming the central stalk) in the V_1 ATPase.

4.9 Subunit E and G with RAVE and aldolase on V-ATPase assembly

V-ATPases function in numerous physiological processes and regulation of its activity is of prime importance. This is attributed by a number of mechanisms which include reversible dissociation of the V_1V_O complex, control of its cellular localization, and changes in the efficiency on coupling of ATP hydrolysis and proton transport. Literature gives evidence for several interacting partners of V-ATPase that are identified to be important for its regulation. V-ATPase complex can reversibly dissociate *in vivo* into their respective components V_1 and V_O domains and also shuts down the ATP-dependent proton transport across the membrane. This phenomenon was observed in insects during molting (SUMNER *et al.,* 1995), due to glucose depletion in yeast cells (KANE, 1995), in kidney epithelial cells (SAUTIN *et al.,* 2005) and in the salivary glands of blowfly through cAMP (DAMES *et al.,* 2006). Conversely, V-ATPase was also found to assemble normally in a panel of yeast mutants which were deficient in the glucose-sensing pathways, including the Ras-cAMP, Snf1p, protein kinase C and Rts1p pathways (PARRA and KANE 1998). This suggests, that glucose-induced assembly of V-ATPase is independent of these pathways. On the other hand, evidence of glycolytic enzyme aldolase binding to the V-ATPase complexes is verified by *in vitro* and *in vivo* binding assays (LU *et al.,* 2001). Precipitation assays show evidence that aldolase binds to *a*, B and E subunits of V-ATPase from *S. cereviseae* (LU *et al.,* 2004). V-ATPases are in a dynamic equilibrium with free V_1 and V_O (KANE 2000). Considering the importance of subunit E to bind with aldolase (LU *et al.,* 2001; MIURA *et al.,* 2001) and many other regulatory proteins like Db1 homology domain of guanine nucleotide exchange factors mSOS (LU *et al.,* 2001), it can also be suggested that association of aldolase and subunit E may mediate V-ATPase assembly by binding simultaneously to free V_1 and V_O sectors.

RAVE is a new complex that was recently isolated and implicated in glucose-dependent reassembly of V-ATPase complexes which had been disassembled in response to glucose deprivation (SEOL *et al.,* 2001). RAVE complex binds to the free V_1 domain on the cytosol but not to the V_O and/or fully assembled V-ATPase (SMARDON *et al.,* 2002). RAVE-V_1 interactions were specifically disrupted in cells lacking V_1 subunits E or G, suggesting a direct interaction of these subunits with RAVE (SMARDON *et al.,* 2002). When the interaction between RAVE and V_1 complex increased in the absence of glucose (SMARDON *et al.,* 2002), enhanced interaction of aldolase and V-ATPase was observed in the presence of glucose (LU *et al.,* 2003). Deletion mutation of subunit E and/or G altered the conformation of V_1 such that it prevented the binding of RAVE to V_1 subunit. It is also evident that the deletion of three other stalk subunits, H, D and F, had meager effect on Rav1 binding, indicating that RAVE does not require an intact V_1 complex for binding (SMARDON *et al.,* 2002). The E and G subunits show genetic and biochemical interactions with each other (TOMASHEK *et al.,* 1997; CHARSKY *et al.,* 2000), and thus can place them in the peripheral, or stator, stalk of the entire V-ATPase (ARATA *et al.,* 2002). The cytoplasmic domain of the V_O, subunit *a*, is believed to be part of this stalk (LANDOLT-MARTICORENA *et al.,* 2000), and is also believed to interact with aldolase (KAWASAKI-NISHI *et al.,* 2001). This would suggest that RAVE binds at a site on V_1 that becomes available only when the V_1 portion is released from V_O and thus RAVE plays a role in proper assembly of the peripheral stalk (KAWASAKI-NISHI *et al.,* 2001). Interaction of subunits B and E is also crucial for the assembly of V_1V_O-ATPase and thus the position of subunits B, E, G and *a* with respect to aldolase and RAVE is at most important when considering the fact of its assembly and the function.

5.1 Conclusion

Vacuolar ATPases (V_1V_O ATPases) are ATP dependent proton pumps that actively transport ions across the bio-membranes. Acidification of the intracellular compartments and generation of an ion gradient to drive the secondary transport reaction serves as an important function of V_1V_O ATPases in the eukaryotic cells. In addition, V_1V_O ATPases are also described as an important component of endosomal sensing machinery. The V-ATPase is composed of 13 subunits in a proposed stoichiometry of A_3:B_3:C_1:D_1:E_x:F_1:G_y:H_z: a_1:d_1:$c_{4\text{-}5}$:c'_1:c''_1. The enzyme comprises a peripheral V_1 sector and a proton-conducting V_O part. Hitherto, the high resolution structure of two subunits, C and H, of the 13 subunits could only be solved. Despite common macromolecular architecture and rotational mechanism with F_1F_O-ATP synthases, the organization of the V_1V_O ATPase subunits on the rotary molecular motor remains uncertain. Electron microscopy and image analysis of V-ATPases have suggested the presence of at least one, or possibly more peripheral stalks, which could provide the stator function, but definitive assignment of specific subunits to these stalks has been rather difficult (WILKENS *et al.,* 1999; VENZKE *et al.,* 2005). However, recent studies have placed subunit C, B, D and F in close proximity with subunit G and E of V-ATPase (JONES *et al.,* 2005; LIU *et al.,* 2005; SHAO and FORGAC, 2004).

Sequence similarities between the soluble domain of subunit *b* of the *E. coli* F_1F_O ATP synthases and subunit G of V-ATPase have led to the proposal that these proteins are functionally analogous to each other (SUPEKOVA *et al.,* 1995). Dimer subunit b_2 of F-ATP synthase serves to fix F_1 to F_O and forms a stator through its membrane anchor, thereby preventing rotation of the F_1 domain during catalysis (HERMOLIN *et al.,* 1983). In V-ATPases, subunit G lacks the length required to reach the top of the catalytic head and to bridge V_1 to V_O in a similar fashion (ARMBRÜSTER *et al.,* 2003). Thus it is important to understand the putative role of subunit G on its interaction with the stalk subunits and the A_3B_3 head domain together with clarification of the position of subunit G on the assembly in V_1 ATPases as component of central stalk and/or in V_1V_O ATPass as a part of peripheral stalk. As part of the preliminary study, subunit G has been cloned and purified to homogeneity (ARMBRÜSTER *et al.,* 2003). The secondary structure of the protein was predicted by sequence and biochemical studies of the protein, and was shown to be an extended helix on the V_1V_O complex. This extended helical conformation of subunit G was not stable at high concentrations, which was important for investigating on spectroscopic studies. Thus the 114 residues subunit was split into two halves as

individual constructs with G_{1-58} as the N-terminal segment and G_{61-101} as the C-terminal segment. Both the constructs were cloned and purified to homogeneity and showed a well folded and helical conformation on a CD-spectrum. Both proteins were analyzed individually for its solution structure in NMR studies and showed an extended helix from 10-56 and 64-100 respectively (RISHIKESAN *et al.,* 2009, 2010).

Precipitation assay showed that subunit G interacts with subunit E on the N-terminus. This inspiring work allowed me to study the interaction of subunit G with E using various spectroscopic approaches like FCS and NMR. The intensive study revealed that subunit G interacts with subunit E only on their respective N-termini. The residues on subunit G that are involved in an interaction with subunit E were characterized. Apart from its interaction with subunit E, subunit G is also predicted to interact with subunit *d* to meet the length required to reach the head domain of the V_1 ATPases to interact with subunit A and/or B. To confirm this binding trait of subunit G, purified subunit *d* was titrated against increasing concentrations of subunit G (G_{1-58} and G_{61-114}, respectively) in the NMR spectroscopic experiments and we showed that subunit *d* interacts with the N-terminus of subunit G, with the first 40 residues in the subunit G sequence showing an extensive decrease on the NMR signal. This interaction was also confirmed by surface plasmon resonance spectroscopy (SPR), and multiple interacting partners on the complex confirm the existence of more than one copy of subunit G per enzyme (RISHIKESAN *et al.,* 2009); and varied location of its interaction including the peripheral stalk subunits and/or central stalk subunit also suggests the presence of dual and/or different role on the respective V_1 ATPases and V_1V_O ATPases.

The knowledge of subunits E and G forming part of the stator was well established in recent years and the solution structure of subunit G analyzed in this study allows us to understand the structure and its different function on the respective two enzymes. Despite this, subunit E also forms cross linking contacts between C, H, D and F of V_1 domain and subunit *a* of V_O domain (XU *et al.,* 1999). Because of the critical role of subunit E playing as a part of central and/or peripheral stalk, understanding the structure of subunit E was necessary. Preliminary study on subunit E showed an extended N-terminus with helical conformation and a globular C-terminal domain (ARMBRÜSTER *et al.,* 2002) with a mix of helical and sheeted structures. Purified subunit E was not stable enough at high concentration to execute any structural studies. Thus, to study the structure of N-terminal domain, the first 69 residues were cloned and purified to homogeneity. The E_{1-69} protein showed a helical conformation on the CD-spectrum, which

motivated us to study the solution structure of the protein by NMR spectroscopy. The protein acquired an extended helical conformation from 12-68 and the charge distribution of the protein allowed us to speculate the possible residues participating on the interaction with subunit C, H, D and F (RISHIKESAN *et al.,* 2011).

Deletion of subunit E on the V-ATPase disrupts its assembly and results in decreased ATPase and proton transport activites (FOURY, 1990). The described solution NMR structure of $E_{1\text{-}69}$ shows an extended length of 83.19 Å. When positioned inside the crystal structure of related subunit E of A_1A_O ATP synthase from *Thermus thermophilus*, $E_{1\text{-}69}$ accommodated well, with an R.M.S.D value of 1.481 Å for residues F23-A69 ($E_{1\text{-}69}$) and residues S29-A75 ($E_{19\text{-}206}$), confirming the presence of a highly α helical N-terminal region (LEE *et al.,* 2010). Considering the knowledge of a homologous existence, both subunits would share a similar structure on the complex. On such a context, prediction of a globular C-terminal domain on the subunit E of V_1V_O ATP synthase similar to the one on subunit E of A_1A_O ATP synthase would be consistent. Secondary structure prediction of $E_{133\text{-}222}$, which is a homologous region of the recently solved crystal structure of $E_{101\text{-}206}$ of subunit E from A_1A_O ATP synthase of *M. jannaschii* (BALAKRISHNA *et al.,* 2010), showed a similar secondary structure pattern. Therfore, this segment of subunit E was cloned and purified to homogeneity. The solution structure of this protein fragment ($E_{133\text{-}222}$) was analysed through NMR studies and was observed to have four fold of β-sheets and two helical regions (RISHIKESAN and GRÜBER, 2011). As described by the secondary structure of subunit E, if it forms a continuous helix that extends from V_1 to V_O, it would extend about 2-fold the distance between the top of V_1 and the membrane (WILKENS *et al.,* 1999). Subunit E thus shows a better fit with additional sheeted folding at the C-terminus as described above from peptide $E_{133\text{-}222}$ of yeast V-ATPase.

Cysteine-based cross-linking studies showed that subunit E of V-ATPase is in close proximity to subunit B (ARATA *et al.,* 2002). Mutation studies on subunit B of V_1-ATPase showed that subunit E would communicate with subunit B at the outer surface of the A_3B_3 hexamer. In line with the above mentioned facts and also considering the contacts of subunit E with subunit B, it is more likely that the C-terminus of subunit E ($E_{133\text{-}222}$) from V_1V_O ATPase, which forms a globular domain with 4 folds of β-sheets and some helix, would be the region of contact between subunit B and E. Considering all these contacts of subunit E with most components of V_1 sector and with subunit *a*, which is part of the stationary complex, it is less likely that E subunit forms part of the central stalk in V_1V_O ATPase and thus subunit E may

represent the foundation of the stalk region. Furthermore, the contact between subunit C and H with E would suggest that they occupy a more exposed position in the complex, and this would be consistent to play a part of the peripheral stalk along with subunit G and/or subunit C and H on the intact V_1V_O complex. The interaction of subunit E with the stalk subunit F, which is proposed to take the central position on the V_1 ATPase to perform the role of the γ subunit of F_1F_O ATP synthase, is considered important. In conjunction to this the interaction of subunits G and E along with the other stalk subunits D and H would position all these five stalk subunits (E, F, G, H and D) as a single compact central stalk in the dissociated V_1 ATPase.

5.2 Future prospectives

Vacuolar ATPases (V_1V_O ATPases) are ATP dependent proton pumps that are important for an active transport of ions across the bio-membranes. Electron microscopy and image analysis of V-ATPases have suggested the presence of at least one, or possibly more peripheral stalks, which could provide the stator function, but definitive assignment of specific subunits to these stalks has been rather difficult (WILKENS *et al.,* 1999; VENZKE *et al.,* 2005). Recent studies have placed subunit C, B, D and F in close proximity with subunit G and E of V-ATPase (JONES *et al.,* 2005; LIU *et al.,* 2005; SHAO and FORGAC, 2004). The present research has described the solution structure of subunits G and E through NMR spectroscopic studies. These solutions structures have characterized the amino acids and its folding pattern on the individual subunits. Various literatures have described the close proximity of subunits F, D, C, A and B to subunits G and E. Thus having known the structures of subunit G and E at solution level, titration studies can be performed to characterize the interaction of subunits F, D, C, A and B with subunit G and/or E. Accordingly, specific mutations can also be incorporated on to subunits G and/or E to understand the arrangements of subunits G and E on the V_1V_O ATPase complex.

ARATA, Y., BALEJA, J. D. and FORGAC, M. (2002). *Localization of subunits d, E and G in the yeast V-ATPase complex using cysteine-mediated crosslinking to subunit B*. Biochemistry **41**: 11301-11307.

ARMBRÜSTER, A., BAILER, S. M., KOCH, M. H. J., GODOVAC-ZIMMERMANN, J. and GRÜBER, G. (2003). *Dimer formation of subunit G of the yeast V-ATPase*. FEBS Lett. **546**: 395-400.

ARMBRÜSTER, A., CHRISTINA, H., ANNE, H., KARIN, S., MICHAEL, B. R. and GERHARD, G. (2005). *Evidence for major structural changes in subunit C of the vacuolar ATPase due to nucleotide binding*. FEBS Lett. **579**: 1961-1967.

AZUMA, M., HARVEY, W. R. and WIECZOREK, H. (1995). *Stoichiometry of K^+/H^+ antiport helps to explain extracellular pH 11 in a model epithelium*. FEBS Lett. **361**: 153-156.

BALAKRISHNA, A., MANIMEKALAI, M. S. S, HUNKE, C., GAYEN, S., RÖSSLE, M., JEYAKANTHAN, J. and GRÜBER. G (2010). *Crystal and solution structure of the C-terminal part of the Methanocaldococcus jannaschii A_1A_O ATP synthase subunit E revealed by X-ray diffraction and small-angle X-ray scattering*. J. Bioenerg. Biomembr. **42**: 311-320.

BASAK, S., GAYEN, S., THAKER, Y. R., MANIMEKALAI, M. S. S., ROESSLE, M., HUNKE, C. and GRÜBER, G. (2011) *Solution structure of subunit F (vma7p) of the eukaryotic V_1V_o ATPase from Saccharomyces cerevisiae derived from SAXS and NMR spectroscopy*. Biochim. Biophys. Acta - Biomembranes **1808**: 360-368.

BAUERLE, C., HO, M. N., LINDORFER, M. A. and STEVENS, T. H. (1993). *The Saccharomyces cerevisiae Vma6 gene encodes the 36-kDa subunit of the vacuolar H (+)-ATPase membrane sector*. J. Biol. Chem. **268**: 12749-12757.

BERENBAUM, M. (1980). *Adaptive significance of midgut pH in larval lepidoptera*. The American Naturalist **115**: 138-146.

BEYENBACH, K. (2001). *Energizing epithelial transport with the vacuolar H^+-ATPase*. News Physiol. Sci. **16**: 145-151.

BEYENBACH, K. W. and WIECZOREK, H. (2006). *The V-type H^+ ATPase: Molecular structure and function, physiological roles and regulation*. J. Experi. Biol. **209**: 577-589.

BIUKOVIĆ, G., ROSSLE, M., GAYEN, S., MU Y. and GRÜBER, G. (2007). *Small-angle X-ray scattering reveals the solution structure of the peripheral stalk subunit H of the A_1A_O ATP synthase from Methanocaldococcus jannaschii and its binding to the catalytic A subunit.* Biochemistry **46**: 2070-2078.

BOEKEMA, E. J., UBBINK-KOK, T., LOLKEMA, J. S., BRISSON, A. and KONINGS, W. N. (1998). *Visualization of a peripheral stalk in V-type ATPase: evidence for the stator structure essential to rotational catalysis.* Proc. Natl. Acad. Sci. USA. **26**: 14291-14293.

BRAUNSCHWEILER, L. and ERNST, R. R. (1983). *Coherence transfer by isotropic mixing: Application to proton correlation spectroscopy*. J. Mag. Reson. (1969) **53**: 521-528.

CAVANAGH, J., FAIRBROTHER, W. J., PALMER. A. G. III and SKELTON, N. J. (1995). *Protein NMR spectroscopy: Principles and practice*

CHABAN, Y. L., JULIANO, S., BOEKEMA E. J. and GRÜBER, G. (2005). *Interaction between subunit C(vma5p) of the yeast vacuolar ATPase and the stalk of the C-depleted V_1 ATPase from Manduca sexta midgut*. Biochim. Biophys. Acta - Bioenergetics **1708**: 196-200.

CHARSKY, C. M. H., SCHUMANN N. J. and KANE, P. M. (2000). *Mutational analysis of subunit G (Vma10p) of the yeast vacuolar H^+-ATPase*. J. Biol. Chem. **275**: 37232-37239.

CHEN, S. H., BUBB, M. R., YARMOLA, E. G., ZUO, J., JIANG, J., LEE, B. S., LU, M., GLUCK, S. L., HURST, I. R. and HOLLIDAY, L. S. (2004). *Vacuolar H+-ATPase binding to microfilaments: Regulation in response to phosphatidylinositol 3-kinase activity and detailed characterization of the actin-binding site in subunit B*. J. Biol. Chem. **279**: 7988-7998.

CORNILESCU, G., DELAGLIO, F. and BAX, A. (1999). *Protein backbone angle restraints from searching a database for chemical shift and sequence homology*. J. Biomol. NMR **13**: 289-302.

COSKUN, Ü., RIZZO, V. F., KOCH, M. H. J. and GRÜBER. G. (2004). *Ligand-dependent structural changes in the V_1 ATPase from Manduca sexta*. J. Bioenerg. Biomembr. **36**: 249-256.

CRUCIAT, C. M., OHKAWARA, B., ACEBRON, S. P., KARAULANOV, E., REINHARD, C., INGELFINGER, D., BOUTROS, M. and NIEHRS, C. (2010). *Requirement of prorenin receptor and Vacuolar H^+-ATPase-mediated acidification for WNT signaling*. Science **327**: 459-463.

CURTIS, K. K., FRANCIS, S. A., OLUWATOSIN, Y. and KANE, P. M. (2002). *Mutational analysis of the subunit C (Vma5p) of the yeast vacuolar H^+-ATPase*. J. Biol. Chem. **277**: 8979-8988.

DADD, R. H. (1975). *Alkalinity within the midgut of mosquito larvae with alkaline-active digestive enzymes*. J. Ins. Physio. **21**: 1847-1853.

DAMES, P., ZIMMERMANN, B., SCHMIDT, R., REIN, J., VOSS, M., SCHEWE, B., WALZ, B. and BAUMANN. O. (2006). *cAMP regulates plasma membrane Vacuolar-type H^+-ATPase assembly and activity in blowfly salivary glands*. Proc. Natl. Acad. Sci. USA, **103**: 3926-3931.

DELAGLIO, F., GRZESIEK, S., VUISTER, G., ZHU, G., PFEIFER, J. and BAX, A. (1995). *NMRpipe: A multidimensional spectral processing system based on unix pipes*. J. Biomol. NMR **6**: 277-293.

DELANO, W. (2001). *The pymol molecular graphics systemsan carlos,* CA:. DeLano Scientific.

DOW, J. (1984). *Extremely high pH in biological systems: A model for carbonate transport*. Am. J. Physiol. **246**: 633-666.

DOW, J. A. T. and PEACOCK, J. M. (1988). *Microelectrode evidence for the electrical isolation of goblet cell cavities in Manduca sexta middle midgut*. J. Exp. Biol. **143**: 101-114.

DUNN, S. D., REVINGTON, M., CIPRIANO, D. J. and SHILTON. B. H. (2000). *The b subunit of Escherichia coli ATP synthase*. J. Bioenerg. Biomembr. **32**: 347-355.

FORGAC, M. (1999). *Structure and properties of the Vacuolar (H^+)-ATPases*. J. Biol. Chem. **274**: 12951-12954.

FORGAC, M. (2007). *Vacuolar ATPases: Rotary proton pumps in physiology and pathophysiology*. Nat. Rev. Mol. Cell Biol. **8**: 917-929.

FRATTINI, A., ORCHARD, P. J., SOBACCHI, C., GILIANI, S., ABINUN, M., MATTSSON, J. P., KEELING, D. J., ANDERSSON, A. K., WALLBRANDT, P., ZECCA, L., NOTARANGELO, L. D., VEZZONI, P. and VILLA, A. (2000). *Defects in Tcirg1 subunit of the Vacuolar proton pump are responsible for a subset of human autosomal recessive osteopetrosis*. Nat. Genet. **25**: 343-346.

GOGARTEN, J. P., STARKE, T., KIBAK, H., FISHMAN, J. and TAIZ, L. (1992). *Evolution and isoforms of V-ATPase subunits*. J. Exp. Biol. **172**: 137-147.

GRAHAM, L. A., FLANNERY, A. R. and STEVENS, T. H. (2003). *Structure and assembly of the yeast V-ATPase*. J. of Bioenerg. Biomembr. **35**: 301-312.

GRAHAM, L. A., HILL, K. J. and STEVENS, T. H. (1995). *Vma8 encodes a 32-kda Vo subunit of the Saccharomyces cerevisiae vacuolar H^+-ATPase required for function and assembly of the enzyme complex*. J. Biol. Chem. **270**: 15037-15044.

GRINSTEIN, S. and FURUYA, W. (1986). *Cytoplasmic pH regulation in activated human neutrophils: Effects of adenosine and pertussis toxin on Na^+/H^+ exchange and metabolic acidification.* Biochim. Biophys. Acta. **889:** 301-309.

GRINSTEIN, S., WOODSIDE, M., WADDELL, T., DOWNEY, G., ORLOWSKI, J., POUYSSEGUR, J., WONG, D. and FOSKETT, J. (1993). *Focal localization of the nhe-1 isoform of the Na^+/H^+ antiport: Assessment of effects on intracellular pH*. EMBO J. **12**: 5209-5218.

GRÜBER, G. (2003). *Introduction: A close look at the vacuolar ATPase*. J. Bioenerg. Biomembr. **35**: 277-280.

GRÜBER, G., GODOVAC-ZIMMERMANN, J., LINK, T. A., COSKUN, U., RIZZO, V. F., BETZ, C. and BAILER, S. M. (2002). *Expression, purification, and characterization of subunit E, an essential subunit of the vacuolar ATPase*. Biochem. Biophys. Res. Commun. **298**: 383-391.

GRÜBER, G. and MARSHANSKY, V. (2008). *New insights into structure-function relationships between archeal ATP synthase (A_1A_O) and vacuolar type ATPase (V_1V_O)*. BioEssays **30**: 1-14

GRUBER, G., RADERMACHER, M., RUIZ, T., GODOVAC-ZIMMERMANN, J., CANAS, B., KLEINE-KOHLBRECHER, D., HUSS, M., HARVEY, W. R. and WIECZOREK, H. (2000). *Three-dimensional structure and subunit topology of the V_1 ATPase from Manduca sexta midgut.* Biochemistry **39**: 8609-8616.

GRUENBERG, J. and VAN DER GOOT, F. G. (2006). *Mechanisms of pathogen entry through the endosomal compartments*. Nat. Rev. Mol. Cell Biol. **7**: 495-504.

GU, F. and GRUENBERG, J. (2000). *Arf1 regulates ph-dependent cop functions in the early endocytic pathway*. J. Biol. Chem. **275**: 8154-8160.

GUEX, N. and PEITSCH, M. (1997). *Swiss-model and the swiss-pdb viewer: An environment for comparative protein modeling*. Electrophoresis **18**.

HARVEY, W. R. and WIECZOREK, H. (1997). *Animal plasma membrane energization by chemiosmotic H^+ V-ATPases*. J. Exp. Biol. **203–216**: 203–216.

HO, S. N., HUNT, H. D., HORTON, R. M., PULLEN, J. K. and PEASE, L. R. (1989). *Site-directed mutagenesis by overlap extension using the polymerase chain reaction*. Gene **77**: 51-59.

HOLLIDAY, L., BUBB, M., JIANG, J., HURST, I. and ZUO, J. (2005). *Interactions between vacuolar H^+-ATPases and microfilaments in osteoclasts*. J. Bioenerg. Biomembr. **37**: 419-423.

HONG-HERMESDORF, A., BRUX, A., GRÜBER, A., GRÜBER, G. and SCHUMACHER, K. (2006). *A WNK kinase binds and phosphorylates V-ATPase subunit C*. FEBS Lett. **580**: 932-939.

HURTADO-LORENZO, A., SKINNER, M., ANNAN, J. E., FUTAI, M., SUN-WADA, G. H., BOURGOIN, S., CASANOVA, J., WILDEMAN, A., BECHOUA, S., AUSIELLO, D. A., BROWN, D. and MARSHANSKY, V. (2006). *V-ATPase interacts with ARNO and ARF6 in early endosomes and regulates the protein degradative pathway*. Nat. Cell Biol. **8**: 124-136.

IMAMURA, H., IKEDA, C., YOSHIDA, M., and YOKOYAMA, K. (2004). *The F subunit of thermus thermophilus V_1-ATPase promotes ATPase activity but is not necessary for rotation*. J. Biol. Chem. **279**: 18085-18090.

INOUE, T., WILKENS, S. and FORGAC, M. (2003). *Subunit structure, function, and arrangement in the yeast and coated vesicle V-ATPases*. J. Bioenerg. Biomembr. **35**: 291-299.

JEFFERIES, K. C. and FORGAC, M. (2008). *Subunit H of the vacuolar (H^+) ATPase inhibits ATP hydrolysis by the free V_1 domain by interaction with the rotary subunit F*. J. Biol. Chem. **283**: 4512-4519.

JONES, R. P. O., DUROSE, L. J., FINDLAY, J. B. C. and HARRISON, M. A. (2005). *Defined sites of interaction between subunits E (vma4p), C (vma5p), and G (vma10p) within the stator structure of the vacuolar H(+)-ATPase*. Biochemistry **44**: 3933-3941.

KANE, P. M. (1995). *Disassembly and reassembly of the yeast vacuolar H[+]-ATPase in vivo*. J. Biol. Chem. **270**: 17025-17032.

KANE, P. M. (2000). *Regulation of v-ATPases by reversible disassembly*. FEBS Lett. **469**: 137-141.

KANE, P. M. and SMARDON, A. M. (2003). *Assembly and regulation of the yeast vacuolar h+-ATPase*. J. Bioenerg. Biomembr. **35**: 313-321-321.

KARET, F. (2005). *Physiological and metabolic implications of V-ATPase isoforms in the kidney*. J. Bioenerg. Biomembr. **37**: 425-429-429.

KAWASAKI-NISHI, S., BOWERS, K., NISHI, T., FORGAC, M. and STEVENS, T. H. (2001). *The amino-terminal domain of the vacuolar proton-translocating ATPase a subunit controls targeting and in vivo dissociation, and the carboxyl-terminal domain affects coupling of proton transport and ATP hydrolysis*. J. Biol. Chem. **276**: 47411-47420.

KAWASAKI-NISHI, S., NISHI, T. and FORGAC, M. (2001). *Yeast V-ATPase complexes containing different isoforms of the 100-kda a-subunit differ in coupling efficiency and in vivo dissociation*. J. Biol. Chem. **276**: 17941-17948.

KITAGAWA, N., MAZON, H., HECK, A. J. R. and WILKENS, S. (2008). *Stoichiometry of the peripheral stalk subunits E and G of yeast V_1-ATPase determined by mass spectrometry*. J. Biol. Chem. **283**: 3329-3337.

KLUGE, C., LAHR, J., HANITZSCH, M., BOLTE, S., GOLLDACK, D. and DIETZ, K. J. (2003). *New insight into the structure and regulation of the plant vacuolar H^+-ATPase*. J. Bioenerg. Biomembr. **35**: 377-388-388.

KNELLER, D. and GODDARD, T. (1997). *SPARKY 3.105 edit.* San Francisco, CA, University of California.

LAEMMLI, U. (1970). *Cleavage of structural proteins during the assembly of the head of bacteriophage t4*. Nature **227**: 680-685.

LANDOLT-MARTICORENA, C., WILLIAMS, K. M., CORREA, J., CHEN, W. and MANOLSON, M. F. (2000). *Evidence that the nh2 terminus of Vph1p, an integral subunit of the V_O sector of the yeast V-ATPase, interacts directly with the vma1p and vma13p subunits of the V_1 sector*. J. Biol. Chem. **275**: 15449-15457.

LENG, X. H., MANOLSON, M. F. and FORGAC, M. (1998). *Function of the CooH-terminal domain of Vph1p in activity and assembly of the yeast V-ATPase*. J. Biol. Chem. **273**: 6717-6723.

LOLKEMA, J. S., CHABAN, Y. and BOEKEMA, E. J. (2003). *Subunit composition, structure, and distribution of bacterial V-type ATPases*. J. Bioenerg. Biomembr. **35**: 323-335.

LU, M., SAUTIN, Y. Y., HOLLIDAY, L. S. and GLUCK, S. L. (2004). *The glycolytic enzyme aldolase mediates assembly, expression and activity of V-ATPase*. J. Biol. Chem. **10** 8732-8739.

MANOLSON, M. F., PROTEAU, D., PRESTON, R. A., STENBIT, A., ROBERTS, B. T., HOYT, M. A., PREUSS, D., MULHOLLAND, J., BOTSTEIN, D. and JONES, E. W. (1992). *The Vph1 gene encodes a 95-kda integral membrane polypeptide required for in vivo assembly and activity of the yeast vacuolar H^+-ATPase*. J. Biol. Chem. **267**: 14294-14303.

MANOLSON, M. F., WU, B., PROTEAU, D., TAILLON, B. E., ROBERTS, B. T., HOYT, M. A. and JONES, E. W. (1994). *Stv1 gene encodes functional homologue of 95-kda yeast vacuolar H^+-ATPase subunit Vph1p*. J. Biol. Chem. **269**: 14064-14074.

MARSHANSKY, V. and FUTAI, M. (2008). *The V-type H^+-ATPase in vesicular trafficking: Targeting, regulation and function*. Curr. Opi. Cell Biol. **20**: 415-426.

MATSUYAMA, S., LLOPIS, J., DEVERAUX, Q. L., TSIEN, R. Y. and REED, J. C. (2000). *Changes in intramitochondrial and cytosolic pH: Early events that modulate caspase activation during apoptosis*. Nat. Cell Biol. **2**: 318-325.

MATSUYAMA, S., XU, Q., VELOURS, J. and REED, J. C. (1998). *Mitochondrial F_OF_1-ATPase proton-pump is required for function of pro-apoptotic protein bax in yeast and mammalian cells*. Mol. Cell **1**: 327-336.

MCGUFFIN, L., BRYSON, K. and JONES, D. (2000). *The psipred protein structure prediction server*. Bioinformatics **16**: 404-405.

MORIYAMA, Y. and NELSON, N. (1989). *Cold inactivation of vacuolar proton-ATPases*. J. Biol. Chem. **264**: 3577-3582.

MÜLLER, V. and GRÜBER, G. (2003). *ATP synthases: Structure, function and evolution of unique energy converters*. Cell. Mol. Life Sci. **60**: 474-494.

MURATA, Y., SUN-WADA, G. H., YOSHIMIZU, T., YAMAMOTO, A., WADA, Y. and FUTAI, M. (2002). *Differential localization of the vacuolar H^+ pump with G subunit isoforms (G_1 and G_2) in mouse neurons*. J. Biol. Chem. **277**: 36296-36303.

NELSON, H. and NELSON, N. (1989). *The progenitor of ATP synthases was closely related to the current vacuolar H^+-ATPase*. FEBS Lett. **247**: 147-153.

NELSON, N. and HARVEY, W. R. (1999). *Vacuolar and plasma membrane proton-ATPase*. Physiol. Rev. **79**: 361-385.

NISHI, T. (2005). *Subunit isoforms controlling the functions of the V-ATPase*. Saikaguku. J. Japanese Biochemical Society **77**: 354-358.

OGILVIE, I., AGGELER, R. and CAPALDI, R. A. (1997). *Cross-linking of the delta subunit to one of the three alpha subunits has no effect on functioning, as expected if delta is a part of the stator that links the F_1 and F_O parts of the Escherichia coli ATP synthase*. J. Biol. Chem. **272**: 16652-16656.

OHIRA, M., SMARDON, A. M., CHARSKY, C. M. H., LIU, J., TARSIO, M. and KANE, P. M. (2006). *The E and G subunits of the yeast V-ATPase interact tightly and are both present at more than one copy per V_1 complex*. J. Biol. Chem. **281**: 22752-22760.

OMRI, D., FELIX, F. and NATHAN, N. (2004). *Crystal structure of yeast V-ATPase subunit C reveals its stator function* EMBO Rep. **5**: 1148-1152.

OWEGI, M. A., CARENBAUER, A. L., WICK, N. M., BROWN, J. F., TERHUNE, K. L., BILBO, S. A., WEAVER, R. S., SHIRCLIFF, R., NEWCOMB, N. and PARRA-BELKY, K. J. (2005). *Mutational analysis of the stator subunit E of the yeast V-ATPase*. J. Biol. Chem. **280**: 18393-18402.

PARRA, K. J. and KANE, P. M. (1998). *Reversible association between the V_1 and V_O domains of yeast vacuolar H^+-ATPase is an unconventional glucose-induced effect*. Mol. Cell. Biol. **18**: 7064-7074.

PIETREMENT, C. (2006). *Distinct expression patterns of different subunit isoforms of the V-ATPase in the rat epididymis*. Biol. Reprod. **74**: 185-194.

POWELL, B., GRAHAM, L. A. and STEVENS, T. H. (2000). *Molecular characterization of the yeast vacuolar H^+-ATPase proton pore*. J. Biol. Chem. **275**: 23654-23660.

PRESTON, R. A., MURPHY, R. F. and JONES, E. W. (1989). *Assay of vacuolar pH in yeast and identification of acidification-defective mutants*. Proc. Natl. Acad. Sci. USA. **86**: 7027-7031.

PRIYA, R., BIUKOVIĆ, G., GAYEN, S., VIVEKANANDAN, S. and GRÜBER, G. (2009). *NMR solution structure of the b_{30-82} domain of subunit b of Escherichia coli F_1F_O ATP synthase*. J. Bacteriol. 24: 7538-7544.

PUOPOLO, K., SCZEKAN, M., MAGNER, R. and FORGAC, M. (1992). *The 40-kda subunit enhances but is not required for activity of the coated vesicle proton pump*. J. Biol. Chem. **267**: 5171-5176.

RADERMACHER, M., RUIZ, T., WIECZOREK, H. and GRÜBER, G. (2001). *The structure of the V_1-ATPase determined by three-dimensional electron microscopy of single particles*. J. Struct. Biol. **135**: 26-37.

RISHIKESAN, S., THAKER, Y. R., PRIYA, R., GAYEN, S., MANIMEKALAI, M. S. S., HUNKE, C. and GRÜBER, G. (2008). *Spectroscopical identification of residues of subunit G of the yeast V-ATPase in its connection with subunit E*. Mol. Memb. Biol. **25**: 400-410.

RISHIKESAN, S., GAYEN, S., THAKER, Y. R., VIVEKANANDAN, S., MANIMEKALAI, M. S. S., YAU, Y. H., SHOCHAT, S. G. and GERHARD. G. (2009). *Assembly of subunit d (Vma6p) and G (Vma10p) and the NMR solution structure of subunit G (G_{1-59}) of the Saccharomyces cerevisiae V_1V_O ATPase*. Biochim. Biophys. Acta - Bioenergetics **4**: 242-251.

RISHIKESAN, S., MANIMEKALAI, M. S. S. and GRÜBER, G. (2010). *The NMR solution structure of subunit G (G_{61-101}) of the eukaryotic V_1V_o ATPase from Saccharomyces cerevisiae*. Biochim. Biophys. Acta - Biomembranes **1798**: 1961-1968.

RISHIKESAN, S., THAKER, Y. R. and GRÜBER, G. (2011). *NMR solution structure of subunit E ($fragment_{1-69}$) of the Saccharomyces cerevisiaeV_1V_O-ATPase*. J. Bioenerg. Biomembr. **43**: 187-193.

RISHIKESAN, S. and GRÜBER, G. (2011). *Structural elements of the C-terminal domain of subunit E ($E_{133-222}$) from the Saccharomyces cerevisiae V_1V_O ATPase determined by solution NMR spectroscopy*. J. Bioenerg. Biomembr. **PMID: 21826517**.

RIZZO, V. F., COSKUN, U., RADERMACHER, M., RUIZ, T., ARMBRÜSTER, A. and GRÜBER, G. (2003). *Resolution of the V_1 ATPase from manduca sexta into subcomplexes and visualization of an ATPase-active A_3B_3EG complex by electron microscopy*. J. Biol. Chem. **278**: 270-275.

SAGERMANN, M., STEVENS, T. H. and MATTHEWS, B. W. (2001). *Crystal structure of the regulatory subunit H of the V-type ATPase of saccharomyces cerevisiae*. Proc. Natl. Acad. Sci. USA. **98**: 7134-7139.

SAUTIN, Y. Y., LU, M., GAUGLER, A., ZHANG, L. and GLUCK, S. L. (2005). *Phosphatidylinositol 3-kinase-mediated effects of glucose on vacuolar H^+-ATPase assembly, translocation, and acidification of intracellular compartments in renal epithelial cells*. Mol. Cell. Biol. **25**: 575-589.

SCHÄFER, I. B., BAILER, S. M., DÜSER, M. G., BÖRSCH, M., BERNAL, R. A., STOCK, D. and GRÜBER, G. (2006). *Crystal structure of the archaeal A_1A_O ATP synthase subunit B from Methanosarcina mazei gö1: Implications of nucleotide-binding differences in the major A_1A_O subunits A and B*. J. Mol. Biol. **358**: 725-740.

SCHNEIDER, D. (2004). *Intracellular acidification by inhibition of the Na^+/H^+-exchanger leads to caspase-independent death of cerebellar granule neurons resembling paraptosis*. Cell Death Differ. **11**: 760-770.

SCHULENBERG, B. and CAPALDI, R. A. (1999). *The epsilon subunit of the F_1F_0 complex of escherichia coli. Cross-linking studies show the same structure in situ as when isolated*. J. Biol. Chem. **274**: 28351-28355.

SCHUMACHER, K. (2006). *Endomembrane proton pumps: Connecting membrane and vesicle transport*. Curr. Opin. Plant Biol. **9**: 595-600.

SCHWEIKL, H., KLEIN, U., SCHINDLBECK, M. and WIECZOREK, H. (1989). *A vacuolar-type ATPase, partially purified from potassium transporting plasma membranes of tobacco hornworm midgut.* J. Biol. Chem. **264**: 11136-11142.

SENNOUNE, S. R., BAKUNTS, K., MARTINEZ, G. M., CHUA-TUAN, J. L., KEBIR, Y., ATTAYA, M. N. and MARTINEZ-ZAGUILAN, R. (2004). *Vacuolar H^+-ATPase in human breast cancer cells with distinct metastatic potential: Distribution and functional activity*. Am. J. Physiol. Cell Physiol. **286**: 1443-1452.

SEOL, J. H., SHEVCHENKO, A. and DESHAIES, R. J. (2001). *Skp1 forms multiple protein complexes, including rave, a regulator of V-ATPase assembly*. Nat. Cell Biol. **3**: 384-391.

SHAO, E. and FORGAC, M. (2004). *Involvement of the nonhomologous region of subunit A of the yeast V-ATPase in coupling and in vivo dissociation*. J. Biol. Chem. **279**: 48663-48670.

SMARDON, A. M., TARSIO, M. and KANE, P. M. (2002). *The rave complex is essential for stable assembly of the yeast V-ATPase*. J. Biol. Chem. **277**: 13831-13839.

STROMPEN, G., DETTMER, J., STIERHOF, Y. D., SCHUMACHER, K., JU?RGENS, G. and MAYER, U. (2005). *Arabidopsis Vacuolar H^+-ATPase subunit E isoform is required for Golgi organization and vacuole function in embryogenesis*. Plant J. **41**: 125-132.

SUMNER, J.P., DOW, J. A. T., EARLEY, F. G. P., KLEIN, U., JÄGER, D. and WIECZOREK, H. (1995). *Regulation of plasma membrane V-ATPase activity by dissociation of peripheral subunits*. J. Biol. Chem. **270**: 5649-5653.

SUN-WADA, G.H., YOSHIMIZU, T., IMAI-SENGA, Y., WADA, Y. and FUTAI, M. (2003). *Diversity of mouse proton-translocating ATPase: Presence of multiple isoforms of the c, d and G subunits*. Gene **302**: 147-153.

SUPEK, F., SUPEKOVA, L., MANDIYAN, S., PAN, Y. C. E., NELSON, H. and NELSON, N. (1994). *A novel accessory subunit for vacuolar H^+-ATPase from chromaffin granules*. J. Biol. Chem. **269**: 24102-24106.

SVERGUN, D. I., KONRAD, S., HUSS, M., KOCH, M. H. J., WIECZOREK, H., ALTENDORF, K., VOLKOV, V. V. and GRÜBER, G. (1998). *Quaternary structure of V_1 and F_1 ATPase: Significance of structural homologies and diversities.* Biochemistry **37**: 17659-17663.

TAKEUCHI, K. and WAGNER, G. (2006). *NMR studies of protein interactions*. Curr. Opin. Struct. Biol. **16**: 109-117.

THAKER, Y. R., HUNKE, C., YAU, Y. H., SHOCHAT, S. G., LI, Y. and GRÜBER, G. (2009). *Association of the eukaryotic V_1V_O ATPase subunits a with d and d with a*. FEBS Lett. **583**: 1090-1095.

THAKER, Y. R., ROESSLE, M. and GRÜBER, G. (2007). *The boxing glove shape of subunit d of the yeast V-ATPase in solution and the importance of disulfide formation for folding of this protein*. J. Bioenerg. Biomembr. **39**: 275-289.

TOMASHEK, J. J. and BRUSILOW, W. S. A. (2000). *Stoichiometry of energy coupling by proton-translocating ATPases: A history of variability*. J. Bioenerg. Biomembr. **32**: 493-500-500.

TOMASHEK, J. J., GRAHAM, L. A., HUTCHINS, M. U., STEVENS, T. H. and KLIONSKY, D. J. (1997). *V1-situated stalk subunits of the yeast vacuolar proton-translocating ATPase.* J. Biol. Chem. **272**: 26787-26793.

TOYOMURA, T., OKA, T., YAMAGUCHI, C., WADA, Y. and FUTAI, M. (2000). *Three subunit a isoforms of mouse vacuolar H^+-ATPase. Preferential expression of the a3 isoform during osteoclast differentiation*. J. Biol. Chem. **275**: 8760-8765.

UMEMOTO, N., YOSHIHISA, T., HIRATA, R. and ANRAKU, Y. (1990). *Roles of the Vma3 gene product, subunit C of the vacuolar membrane H^+-ATPase on vacuolar acidification and protein transport. A study with Vma3-disrupted mutants of Saccharomyces cerevisiae.* J. Biol. Chem. **265**: 18447-18453.

VAYNBERG, J. and QIN, J. (2006). *Weak protein-protein interactions as probed by NMR spectroscopy*. Trends Biotechnol. **24**: 22-27.

VENZKE, D., DOMGALL, I., KOCHER, T., FETHIERE, J., FISCHER, S. and BOTTCHER, B. (2005). *Elucidation of the stator organization in the V-ATPase of Neurospora crassa*. J. Mol. Biol. **349**: 659-669.

VENZKE, D., DOMGALL, I., KÖCHER, T., FÉTHIÈRE, J., FISCHER, S. and BÖTTCHER, B. (2005). *Elucidation of the stator organization in the V-ATPase of Neurospora crassa*. J. Mol. Biol. **349**: 659-669.

VITAVSKA, O., MERZENDORFER, H. and WIECZOREK, H. (2005). *The V-ATPase subunit C binds to polymeric f-actin as well as to monomeric g-actin and induces cross-linking of actin filaments*. J. Biol. Chem. **280**: 1070-1076.

WANG, S. Y., MORIYAMA, Y., MANDEL, M., HULMES, J. D., PAN, Y. C., DANHO, W., NELSON, H. and NELSON, N. (1988). *Cloning of cDNA encoding a 32-kda protein. An accessory polypeptide of the H^+-ATPase from chromaffin granules*. J. Biol. Chem. **263**: 17638-17642.

WASSMER, T., KISSMEHL, R., COHEN, J. and PLATTNER, H. (2006). *Seventeen a-subunit isoforms of paramecium V-ATPase provide high specialization in localization and function*. Mol. Biol. Cell **17**: 917-930.

WEBER, J., MUHAREMAGIC, A., WILKE-MOUNTS, S. and SENIOR, A. E. (2004). *Analysis of sequence determinants of F_1F_O-ATP synthase in the N-terminal region of α subunit for binding of δ subunit*. J. Biol. Chem. **279**: 25673-25679.

WEISZ, O. A. (2003). *Organelle acidification and disease.* Traffic. **4**: 57-64.

WHITTEN, S. T., GARCÍA-MORENO, E. B. and HILSER, V. J. (2005). *Local conformational fluctuations can modulate the coupling between proton binding and global structural transitions in proteins*. Proc. Natl. Acad. Sci. USA. **102**: 4282-4287.

WIECZOREK, H., M. HUSS, H. MERZENDORFER, S. REINEKE, O. VITAVSKA and W. ZEISKE. (2003). *The insect plasma membrane h⁺ v-ATPase: Intra-, inter-, and supramolecular aspects*. J. Bioenerg. Biomembr. **35**: 359-366-366.

WIECZOREK, H., WOLFERSBERGER, M. G., CIOFFI, M. and HARVEY, W. R. (1986). *Cation-stimulated ATPase activity in purified plasma membranes from tobacco hornworm midgut*. Biochim. Biophys. Acta - Biomembranes **857**: 271-281.

WILKENS, S. and FORGAC. M. (2001). *Three-dimensional structure of the vacuolar ATPase proton channel by electron microscopy*. J. Biol. Chem. **276**: 44064-44068.

WILKENS, S., INOUE, T. and FORGAC. M. (2004). *Three-dimensional structure of the Vacuolar ATPase*. J. Biol. Chem. **279**: 41942-41949.

WILKENS, S., VASILYEVA, E. and FORGAC, M. (1999). *Structure of the Vacuolar ATPase by electron microscopy*. J. Biol. Chem. **274**: 31804-31810.

WISHART, D. S., SYKES, B. D. and RICHARDS, F. M. (1992). *The chemical shift index: A fast and simple method for the assignment of protein secondary structure through NMR spectroscopy* Biochemistry **31**: 1647-1651.

WÜTHRICH, K. (1990). *Protein structure determination in solution by nmr spectroscopy*. J. Biol. Chem. **265**: 22059-22062.

XU, T. and FORGAC, M. (2001). *Microtubules are involved in glucose-dependent dissociation of the yeast V-ATPase in vivo*. J. Biol. Chem. **276**: 24855-24861.

XU, T., VASILYEVA, E. and FORGAC. M. (1999). *Subunit interactions in the clathrin-coated Vesicle vacuolar (H^+)-ATPase complex*. J. Biol. Chem. **274**: 28909-28915.

YAVER, D., NELSON, H., NELSON, N. and KLIONSKY, D. (1993). *Vacuolar ATPase mutants accumulate precursor proteins in a pre-Vacuolar compartment*. J. Biol Chem. **268**: 10564-10572.

ZHANG, Z., INOUE, T., FORGAC, M. and WILKENS. S. (2006). *Localization of subunit C (vma5p) in the yeast Vacuolar ATPase by immuno electron microscopy*. FEBS Lett. **580**: 2006-2010.

Author's publication during Ph.D period

January 2007 to May 2011

1. **RISHIKESAN, S**., THAKER, Y. R., PRIYA, R., GAYEN, S., MANIMEKALAI, M. S. S., HUNKE, C. and GRÜBER, G. (2008). *Spectroscopical identification of residues of subunit G of the yeast V-ATPase in its connection with subunit E*. Mol. Memb. Biol. **25**: 400-410.

2. **RISHIKESAN, S**., GAYEN, S., THAKER, Y. R., VIVEKANANDAN, S., MANIMEKALAI, M. S. S., YAU, Y. H., SHOCHAT, S. G. and GRÜBER. G. (2009). *Assembly of subunit d (Vma6p) and G (Vma10p) and the NMR solution structure of subunit G (G_{1-59}) of the Saccharomyces cerevisiae V_1V_O ATPase*. Biochim. Biophys. Acta - Bioenergetics **(4)**: 242-251.

3. **RISHIKESAN, S**., MANIMEKALAI, M. S. S. and GRÜBER, G. (2010). *The NMR solution structure of subunit G (G_{61-101}) of the eukaryotic V_1V_O ATPase from Saccharomyces cerevisiae*. Biochim. Biophys. Acta - Biomembranes **1798**: 1961-1968.

4. **RISHIKESAN, S**., THAKER, Y. R. and GRÜBER, G. (2011). *NMR solution structure of subunit E (fragment$_{1-69}$) of the Saccharomyces cerevisiaeV_1V_O-ATPase*. J. Bioenerg. Biomembr. **43**: 187-193.

5. **RISHIKESAN, S**. and GRÜBER, G. (2011). *Structural elements of the C-terminal domain of subunit E ($E_{133-222}$) from the Saccharomyces cerevisiae V_1V_O ATPase determined by solution NMR spectroscopy*. J. Bioenerg. Biomembr (PMID: 21826517)

Posters presented

1. 15th European Bioenergetics Conference (EBEC 2008) Dublin, Ireland from 19th – 24th July 2008.

   RISHIKESAN, S., THAKER, Y. R. and GERHARD. G.

   Low resolution structure of subunit d and NMR titration experiments, studying the interaction of subunits E and G of V-ATPase from yeast.

2. Joint 5th Structural Biology and Functional Genomics and 1st Biological Physics International Conference, NUS, Singapore from 9-11th Dec 2008.

   RISHIKESAN, S., GAYEN, S. and GERHARD. G.

   Title : NMR solution structure of subunit G (G_{1-59}) of the *Saccharomyces cerevisiae* V_1V_O ATPase

3. Joint 5th Structural Biology and Functional Genomics and 1st Biological Physics International Conference, NUS, Singapore from 6-8th Dec 2010

   RISHIKESAN, S., MANIMEKALAI, M. S. S. and GERHARD. G.

   Title : NMR Solution structure of subunit E (E_{1-69}) and ($E_{133-222}$) of the S*accharomyces cerevisiae* V-Atpase